

**FUNCTIONAL CHARACTERIZATION OF SYNAPTIC PROTEINS IN CALCIUM
TRIGGERED EXOCYTOSIS**

APPROVED BY SUPERVISORY COMMITTEE

Thomas C. Südhof, M.D., Advisor

Jose Rizo-Rey, Ph.D., Committee Chair

Stephen Cannon, Ph.D.

Jane Johnson, Ph.D.

DEDICATION

To my parents, my husband, and my brother

**FUNCTIONAL CHARACTERIZATION OF SYNAPTIC PROTEINS IN CALCIUM
TRIGGERED EXOCYTOSIS**

by

WEN-PIN CHANG

DISSERTATION

Presented to the Faculty of the Graduate School of Biomedical Sciences

The University of Texas Southwestern Medical Center at Dallas

In Partial Fulfillment of the Requirements

For the Degree of

DOCTOR OF PHILOSOPHY

The University of Texas Southwestern Medical Center at Dallas

Dallas, Texas

June, 2008

Copyright
by
Wen-Pin Chang, 2008

All Rights Reserved
Copyright

ACKNOWLEDGEMENTS

I would like to thank my mentor, Dr. Thomas C. Südhof, for giving me the opportunity to work along his side, and for giving me his invaluable suggestions, support, and encouragement in all the time of my graduate work. His stimulating ideas and insightful opinions, his enthusiasm and passion for science, and his perseverance have always inspired me, and his patience and guidance for me are indispensable to the completion of my thesis work.

I would also like to thank all the members in the Südhof's lab. Over the years, I had tremendous help from Drs. Anton Maximov, Pascal Kaeser, Zhiping Pang, Sang-Won Min, Ferenc Deák, and others. I specially want to thank the technical support team, including Iza Kornblum, Andre Roth, Jason Mitchell, Lin Fan and Ewa Borowicz for their continuous supports.

The Department of Neuroscience at UT Southwestern Medical Center provided me a great environment for my graduate work. The state-of-art facilities and the enthusiastic faculty members offered a supportive environment for my graduate training. Among all the faculties, I especially want to thank Drs. Ege Kavalali, Weichun Lin and their lab members.

At the end, I want to give thanks to my committee members, Drs. Jose Rizo-Rey, Jane Johnson, and Stephen Cannon, for their insightfulness and support in my projects. Completion of my graduate work will not be possible without their help.

**FUNCTIONAL CHARACTERIZATION OF SYNAPTIC PROTEINS IN CALCIUM
TRIGGERED EXOCYTOSIS**

Publication No. _____

Wen-Pin Chang Ph.D.

The University of Texas Southwestern Medical Center at Dallas, 2008

Supervising Professor: Thomas C. Südhof, M.D.

Release of neurotransmitter involves fusion of the membrane of synaptic vesicle with the presynaptic plasma membrane, a process that is tightly regulated by calcium. One of the central goals is to understand the molecular machinery underlying the fundamental fusion mechanism used at all synapses, thus it is important to characterize the physiological function of unknown synaptic proteins and to identify new members that might have functions in synaptic vesicle fusion. In this thesis, I first characterize the function of synaptic vesicle protein 2 (SV2), which is one of the first synaptic vesicle proteins identified. SV2 is essential for survival in mice; its deletion impairs neurotransmitter release, although the exact point at which step of release is affected remains unclear. Using electrophysiological approaches, our data demonstrate that SV2 acts downstream of the priming, but upstream of the Ca^{2+} -triggering of vesicle fusion. By using rescue experiments, we also demonstrate that

mutations of charged residues within the transmembrane regions or of the intravesicular glycosylation sequences of SV2 block its function, probably by impairing the folding and trafficking of SV2. In contrast, deletion of the conserved N-terminal putative synaptotagmin-binding sequence of SV2 did not abolish SV2 function, nor did mutation of another conserved cytoplasmic sequence. These observations suggest that SV2 functions in a maturation step of primed vesicles that converts the vesicles into a Ca^{2+} - and synaptotagmin-responsive state. Second, SNAREs and Sec1/Munc18 (SM) proteins are critical for intracellular membrane fusion. The neuronal SM protein Munc18-1 binds to SNARE complexes and syntaxin-1. The interaction to SNARE complex likely represents the general mode of SMARE/SM protein coupling, but the understanding of its physiological relevance to vesicle fusion and precise point of its function during the process is hindered by the duality of Munc18-1/SNARE binding modes. Here we designed three mutations that preserve Munc18-1/syntaxin-1 binding but differentially impairs the Munc18-1/SNARE complex binding. By utilizing rescue experiments, we showed that the impairment correlates with disruption of vesicle priming and evoked release, and suggest that Munc18-1/SNARE complex assemblies generally govern membrane traffic. Third, we reported the primary structure and biochemical properties of a family of evolutionarily conserved mammalian proteins, E-Syts, which contain multiple C_2 domains, a common Ca^{2+} binding module, and a transmembrane region. Our findings suggest that E-Syts function as Ca^{2+} -regulated intrinsic membrane proteins and expand the repertoire of multiple C_2 domains proteins to a fourth class beyond synaptotagmins, ferlins, and MTCPs (multiple C_2 domain and transmembrane region proteins).

TABLE OF CONTENTS

COMMITTEE SIGNATURE	i
DEDICATION.....	ii
TITLE PAGE.....	iii
ACKNOWLEDGEMENTS.....	v
ABSTRACTS	vi
TABLE OF CONTENTS.....	viii
PRIOR PUBLICATIONS.....	xiii
LIST OF FIGURES	xiv
LIST OF TABLES.....	xvii
LIST OF ABBREVIATIONS	xviii
CHAPTER I: INTRODUCTIONS	
1.1 Central Nervous System and Nerve Cells.....	1
1.2 Synapses.....	3
1.3 Synaptic Vesicles	4
1.3.1 Synaptic Vesicle Composition.....	4
1.3.2 Synaptic Vesicle Proteins	5
1.3.3 Synaptic Vesicle Cycle	7
1.3.4 Synaptic Vesicle Pools.....	8
1.4 Ca ²⁺ -triggered Exocytosis.....	9
1.5 Essential Proteins for Membrane Fusion	11
1.5.1 SNARE Proteins	11

1.5.2 SNARE Core Complex	13
1.6 SM Proteins.....	15
1.7 Synaptic Vesicle Protein 2.....	18
1.8 C ₂ Domains and E-Syts.....	20
1.9 Questions to Ask.....	23
 CHAPTER II: SV2 RENDERS PRIMED VESICLES COMPETENT FOR CA ²⁺ -INDUCED EXOCYTOSIS	
2.1 Introductions	25
2.2 Material and Methods	
2.2.1 Plasmid construction.....	27
2.2.2 Mouse breedings	27
2.2.3 Cortical primary neuronal cultures	28
2.2.4 Electrophysiology	28
2.2.5 Immunocytochemistry	30
2.3.6 Miscellaneous	30
2.3 Results	
2.3.1 Analysis of the effect of deleting SV2 on inhibitory synaptic transmission.....	31
2.3.2 Synaptic response to a 10 Hz stimulus train in SV2-deficient neurons	35
2.3.3 EGTA-AM reverses facilitation induced by deletion of SV2 but does not abolish phenotype.....	37
2.3.4 SV2 KO phenotype can be rescued by viral expression of wild-type SV2	39
2.3.5 Structure-function analysis of SV2A	41

2.3.6 The N-terminal synaptotagmin-binding sequence is not essential for SV2 function	43
2.3.7 Lysine 694 is dispensable for SV2 function	44
2.3.8 Mutation of charged residues in TMR1 blocks SV2 function	47
2.3.9 Blocking SV2 glycosylation abolishes SV2 function	49
2.4 Discussions	51
2.4.1 Dissection of the SV2 KO phenotype	51
2.4.2 Structure-function analysis of SV2A	54
2.4.3 The function of SV2	55
CHAPTER III: MUNC18-1 BINDING TO THE NEURONAL SNARE COMPLEX	
CONTROLS SYNAPTIC VESICLE PRIMING	
3.1 Introductions	57
3.2 Material and Methods	
3.2.1 Constructs	59
3.2.2 Preparation of recombinant proteins and SNARE complex	59
3.2.3 ITC	60
3.2.4 NMR experiments	60
3.2.5 Cortical cultures	61
3.2.6 Lentiviral infection	61
3.2.7 Immunocytochemistry	62
3.2.8 Fluorescence imaging	62
3.2.9 Electrophysiology	63

3.2.10 Data analysis	64
3.3 Results	
3.3.1 Design of mutations to distinguish Munc18-1/SNARE interactions.....	64
3.3.2 Rescue of survival and neurotransmitter release in Munc18-1 KO neurons ..	71
3.3.3 Mutations in Munc18-1 impair neurotransmitter release.....	75
3.3.4 Mutations in Munc18-1 decrease the readily-releasable pool size	76
3.4 Discussions	78
 CHAPTER IV: E-SYTS, A FAMILY OF MEMBRANOUS CA ²⁺ -SENSOR PROTEINS WITH MULTIPLE C ₂ DOMAINS	
4.1 Introductions	82
4.2 Material and Methods	
4.2.1 Cloning, sequence analyses, and data bank search.....	83
4.2.2 Expression and purification of recombinant GST fusion proteins.....	83
4.2.3 Construction and expression of vectors encoding various myc-tagged E-Syt fusion proteins.....	83
4.2.4 Immunostaining and confocal imaging.....	84
4.2.5 Miscellaneous procedures.....	85
4.3 Results	
4.3.1 Phospholipid binding by E-Syt2	85
4.3.2 Subcellular localization of E-Syt2	87
4.3.3 Plasma membrane targeting of E-Syt2 and E-Syt3 is mediated by its C-terminal C ₂ domain.....	90

4.4 Discussions	92
BIBLIOGRAPHY	95

PRIOR PUBLICATIONS

1. Min SW, Chang WP & Südhof TC. E-Syts, a family of membranous Ca^{2+} -sensor proteins with multiple C2 domains. *Proc Natl Acad Sci U S A*. 2007 Mar 6; 104(10):3823-8.
2. Deák F, Xu Y, Chang WP, Khvotchev M, Dulubova I, Liu X, Südhof TC & Rizo J.
Munc18-1 Binding to the Neuronal SNARE complex Controls Synaptic Vesicle Priming.
In Preparation.
3. Chang WP & Südhof TC. SV2 functions in rendering primed vesicles competent for Ca^{2+} -induced exocytosis. In Revision of Journal of Neuroscience.

LIST OF FIGURES

Figure 1.1 Golgi stained neurons in the dentate gyrus.....	2
Figure 1.2 Structures, proposed interactions, and putative functions of synaptic vesicle trafficking proteins.....	6
Figure 1.3 The synaptic vesicle cycle.....	8
Figure 1.4 Reaction sequence and timing of synaptic transmission.....	10
Figure 1.5 Structures of the neuronal SNARE proteins.....	12
Figure 1.6 Model of the neuronal SNAREs assembling.....	15
Figure 1.7 Transmembrane domain structure of SV2s and location of conserved residues..	19
Figure 1.8 Domain structures of E-Syts.....	23
Figure 2.1 Spontaneous synaptic transmission is not altered in SV2-deficient neurons	32
Figure 2.2 SV2 deletion selectively impairs Ca ²⁺ -triggering of release without decreasing the RRP size.....	34-35
Figure 2.3 SV2 deletion decreases release but increases facilitation during 10 Hz stimulus trains.....	36
Figure 2.4 Effect of EGTA-AM on synaptic responses in SV2-deficient neurons	38-39
Figure 2.5 Rescue of the phenotype in SV2-deficient neurons by lentiviral expression of EGFP-tagged SV2A.....	40-41
Figure 2.6 Structure and mutants of SV2A.....	42
Figure 2.7 Rescue of the SV2 KO phenotype by mutant SV2A lacking the N-terminal 107 residues implicated in synaptotagmin-binding	45-46

Figure 2.8 Rescue of the SV2 KO phenotype by mutant SV2A with the K694A substitution	46-47
Figure 2.9 Lack of rescue of the SV2 KO phenotype by DA-mutant SV2A containing a double amino-acid substitution in TMR1 (D179A/E182A)	48-49
Figure 2.10 Lack of rescue of the SV2 KO phenotype by NQ-mutant SV2A in which the N-glycosylation sites in the intravesicular loop were substituted (N498Q/N548Q /N573Q)	50-51
Figure 3.1 Design of mutations to disrupt Munc18-1/SNARE interactions.....	66-67
Figure 3.2 ITC analysis of binding of WT and mutant Munc18-1 to syntaxin-1	67
Figure 3.3 Differential disruption of Munc18-1 binding to the SNARE complex by Munc18-1 point mutations.....	69-70
Figure 3.4 E59K mutant of Munc18-1 retains binding to the syntaxin-1	70
Figure 3.5 Rescue of neuronal survival in cortical cultures by Munc18-1 expression.....	72
Figure 3.6 Synaptic release depends on Munc18-1 binding to the SNARE complex	74-75
Figure 3.7 Munc18-1 binding to the SNARE complex is critical for release readiness of synaptic vesicles.....	75
Figure 3.8 Munc18-1 mutations in SNARE binding reduce the size of readily releasable pool	77
Figure 4.1 Ca^{2+} - and phospholipids-dependent membrane binding by E-Syt2 C ₂ domain .	86
Figure 4.2 Phospholipid dependence of Ca^{2+} -dependent membrane binding of the E-Syt2 C ₂ AB domains	87
Figure 4.3 Subcellular localization of E-Syts in HEK293 cells.....	88

Figure 4.4 Transmembrane Region of E-Syt2 does not mediate plasma membrane targeting..
..... 90-91

Figure 4.5 The C-terminal C2 domain of E-Syt2 and E-Syt3 but not E-Syt1 direct plasma
membrane localization..... 91-92

LIST OF ABBREVIATIONS

1D	One dimensional
AMPA	alpha-amino-3-hydroxy-5-methyl-4-isoxazolepropionic acid
ANOVA	Analysis of variance
AP	Action potential
APV	(2 <i>R</i>)-amino-5-phosphonovaleric acid
BSA	Bovine serum albumin
BKO	SV2B Knock-out
CASK	Calmodulin-associated serine/threonine kinase
CL	Cerulean
CNS	Central nervous system
CNQX	6-cyano-7-nitroquinoxaline-2,3-dione
CSP	Cysteine-string protein
DAPI	4',6-diamidino-2-phenylindole
DIV	Days <i>in vitro</i>
DKO	SV2A/SV2B Knock-out
DMEM	Dulbecco's modified eagle medium
EGFP	Enhanced Green Fluorescent Proteins
EGTA	Ethyleneglycol-bis(β -aminoethyl ether)-N,N,N',N'-tetraacetic acid
EGTA-AM	Ethyleneglycol-bis(β -aminoethyl)-N,N,N',N'-tetraacetoxy-methyl Ester

EPSC	Excitatory postsynaptic current
ER	Endoplasmic Reticulum
E-Syts	Extended synaptotagmins
FM dye	Fei Mao dye
FRET	Förster resonance energy transfer
GABA	γ -aminobutyric acid
GDI	Guanine nucleotide dissociation inhibitor
GST	Glutathione-S-transferase
IPSC	Inhibitory postsynaptic current
ITC	Isothermal titration calorimetry
KO	Knock-out
MAP2	Microtubule associated protein 2
MEM	Minimum Essential Medium
mEPSC	Miniature excitatory postsynaptic current
mIPSC	Miniature inhibitory postsynaptic current
MTCPs	C ₂ domain and transmembrane region proteins
Munc18-1	Mouse uncoordinated 18-1
NMDA	N-methyl-D-aspartic acid
NMJ	Neuromuscular junction
NMR	Nuclear magnetic resonance
NSF	N-ethylmaleimide-sensitive factor
PAGE	Polyacrylamide gel electrophoresis

PBS	Phosphate Buffered Saline
PC	Phosphocholine
PE	Phosphatidylethanolamine
PIP	Phosphatidylinositolphosphate
PIP ₂	Phosphatidylinositol bisphosphate
PKC	Protein kinas C
PS	Phosphoserine
PTEN	Phosphatase and tensin homolog
Rop	Repressor of primer
RP	Reserve Pool
RRP	Readily-releasable pool
RT-PCR	Reverse transcription polymerase chain reaction
SCAMP	Secretory carrier membrane proteins
SDS	Sodium dodecyl sulfat
SEM	Standard error of the mean
SM proteins	Sec1/Munc-18 related proteins
SMR	Strongest methyl resonance
SNAP	Soluble NSF attachment protein
SNAP-25	Synaptosome-associated protein of 25 kda
SNARE	Soluble NSF attachment receptor element
SNARE core complex	SNARE complex containing only SNARE motifs
SV	Synaptic Vesicle

SV2	Synaptic Vesicle Protein 2
SVOP	<u>SVtwo</u> -related protein
Syt-7	Synaptotagmin-7
TMR	Transmembrane region
TTX	Tetrodotoxin
VAMP	Vesicle associated membrane protein
WT	Wild-type

CHAPTER I: INTRODUCTIONS

1.1 Central Nervous System and Nerve Cells

The nervous system is divided into central and peripheral parts. The central nervous system (CNS) is a bilateral and essentially symmetrical structure that is composed of the brain and the spinal cord. The brain is the control center of CNS; it receives sensory inputs via the spinal cord as well as from its own nerves. Most parts of the brain are devoted to processing its various sensory inputs and initiating and coordinating appropriate motor outputs. The function of the spinal cord is to conduct sensory information from the peripheral system to the brain and to conduct motor information from the brain to muscles and glands. The spinal cord also serves as a minor reflex center.

Nervous tissues are composed of two broad classes of cells, termed neurons and glial cells (or glia, Greek for “glue”). In the vertebrate nervous system, glial cells are about 10 to 50 times outnumbering neurons; however, unlike neurons which have at least thousands of different cell types, glial cells are mainly consist of four types of groups: microglia, astrocytes, oligodendrocytes, and schwann cells. Although, historically, glial cells have been afforded far less attention than neurons, they are imperative for providing support, nutrition, and insulation for the central nervous system.

The functional unit of the nervous system, the neuron, was first recognized through the work of the Spanish anatomist Santiago Ramón y Cajal, using a silver staining method developed by Camillo Golgi in the early 20th century (S. Ramón y Cajal, 1937) (Figure 1-1). Cajal claimed that neurons were discrete cells that communicated with each

other via specialized junctions, or spaces, between cells, called “synapses”. This theory is now known as the fundamental neuron doctrine, which states that neurons are the basic structural and functional units of the nervous system (S. Ramón y Cajal, 1937).

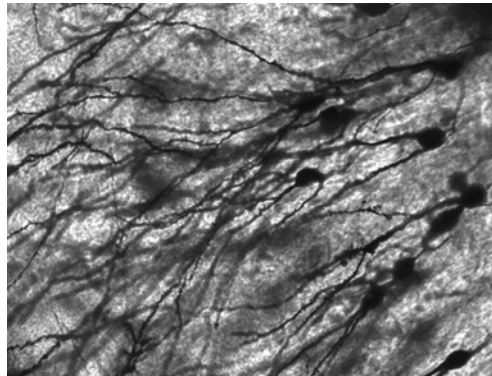


Figure 1-1 Golgi stained neurons in the dentate gyrus.
(http://en.wikipedia.org/wiki/Image:Gyrus_Dentatus_40x.jpg)

There are more than 100 billion neurons in human brain. For the diversity of functions performed by neurons in different parts of the nervous system, there is, as expected, a wide variety in the shape, size, and electrochemical properties of neurons. However, neurons can be commonly polarized to three morphologically defined parts: soma or cell body, dendrites and axons. The soma is the central part of a neuron and contains the nucleus and other organelles. The dendrites are cellular extensions with many branches; they receive inputs from other neurons. Axons are cable-like projections that carry and thus send nerve signals.

As suggested by Cajal and Sherrington, neurons communicate with one another via synapses, where the axon terminal of one cell impinges upon another neuron's dendrite, soma or, less commonly, axon. It is estimated that, in the human brain, the 100 billion neurons form more than 100 trillion synaptic connections.

1.2 Synapses

Neuronal synapses can be divided into two types depending on how they function, chemical synapses and electrical synapses.

An Electrical synapse is a mechanical and electrically conductive link formed between two adjacent neurons. This narrow gap formed between the pre- and postsynaptic cells is also known as a gap junction. At gap junctions, cells are about 3.5 nm apart (E. R. Kandel, Schwartz. J.H., and Jessell, T.M., 2000), a substantially shorter distance than the 20 to 40 nm distance between neuron cells at chemical synapses (B. W. Connors and M. A. Long, 2004).

Chemical synapses are specialized junctions through which the cells of the nervous system communicate to each other and to non-neuronal cells such as those in muscles or glands. Chemical synapses provide the means through which the nervous system connects to and controls the other systems of the body. For example, neuromuscular junction (NMJ), a type of synapse that is well studied, is a chemical synapse between a motor neuron and a muscle cell. Chemical synapses allow the neurons of the central nervous system to form interconnected neural circuits. Thus, they are crucial to the biological computations that underlie perception and thought.

By using traditional Golgi staining, or more advanced technology, such as Fei Mao (FM) dye staining or cell-filling fluorophore in combination with fluorescence microscopy, the synaptic bouton can be exposed at the light microscopy level. Synaptic endings can be found on dendrites, the cell body, and in more rare cases, on axons (E. R. Kandel, Schwartz. J.H., and Jessell, T.M., 2000).

At the ultrastructure level, the synapse consists of three elements: the presynaptic membrane formed by the terminal button of an axon; the postsynaptic membrane that is composed of a segment of dendrite or cell body; and the space between these two structures called the synaptic cleft. Images taken by electron microscopy have revealed the highly asymmetric structure of the synapse. The presynaptic terminal contains hundreds of synaptic vesicles in addition to early endosomal structures (T. C. Südhof, 2004). An electron-dense projection on the presynaptic membrane called the active zone is the vesicle release site, and can be seen using special staining. The synaptic cleft probably contains cell adhesion molecules and extracellular matrix proteins, and is about 20 nm in distance. The postsynaptic membrane also has electron-dense structures, most likely clustered scaffolding proteins that are important for postsynaptic receptor positioning.

1.3 Synaptic Vesicle

1.3.1 Synaptic Vesicle Composition

Synaptic vesicles, also called neurotransmitter vesicles, are relatively small and simple organelles located at the presynaptic terminal of synapses. Synaptic vesicles are about 35 nm in diameter as measured by electric microscopy and may be slightly larger under native conditions (T. C. Südhof, and Scheller, R.H. , 2000). Purified vesicles have a protein:phospholipid ratio of 1:3 with an unremarkable lipid composition (40% phosphatidylcholine, 32% phosphatidylethanolamine, 12% phosphatidylserine, 5% phosphatidylinositol, 10% cholesterol, wt/wt; (F. Benfenati et al., 1989); (T. C. Südhof, 2004)). Because they are relatively small, only a limited number of lipids and proteins can

be accommodated into the sphere. Calculations suggest that each synaptic vesicle is composed of about 10,000 molecules of phospholipids and of protein with a combined molecular weight of approximately $5-10 \times 10^3$ kDa (R. Jahn and T. C. Südhof, 1993). Taking an average molecular weight of a protein to be ~ 50 kDa, there are only approximately 200 protein molecules per synaptic vesicle. Synaptic vesicles are also functionally relatively simple considering that their only known function is their role in neurotransmitter release. Because of its limited functions and associated proteins, the molecular aspect of the organelle has been relatively well dissected by extensive biochemical studies (T. C. Südhof, and Scheller, R.H. , 2000).

1.3.2 Synaptic Vesicle Proteins

There are two classes of essential components on the synaptic vesicle: transporter proteins, which participate in neurotransmitter uptake, and trafficking proteins, which implement synaptic vesicle exo- and endocytosis and recycling. Transporter proteins are composed of a vacuolar-type proton pump that generates the electrochemical gradient, which provide energy for neurotransmitter transporter and the process of neurotransmitter uptake (T. C. Südhof, 2004). Transporter proteins are inserted in the lipid bilayer membrane of synaptic vesicles with specificity to each type of neurotransmitter. Vesicular glutamate transporters, for example, sequester glutamate into vesicles by this process. Thus, the class of neurotransmitter transporter present in the vesicle is one of the determinants of classifying the transmitter type that is used by a particular synapse.

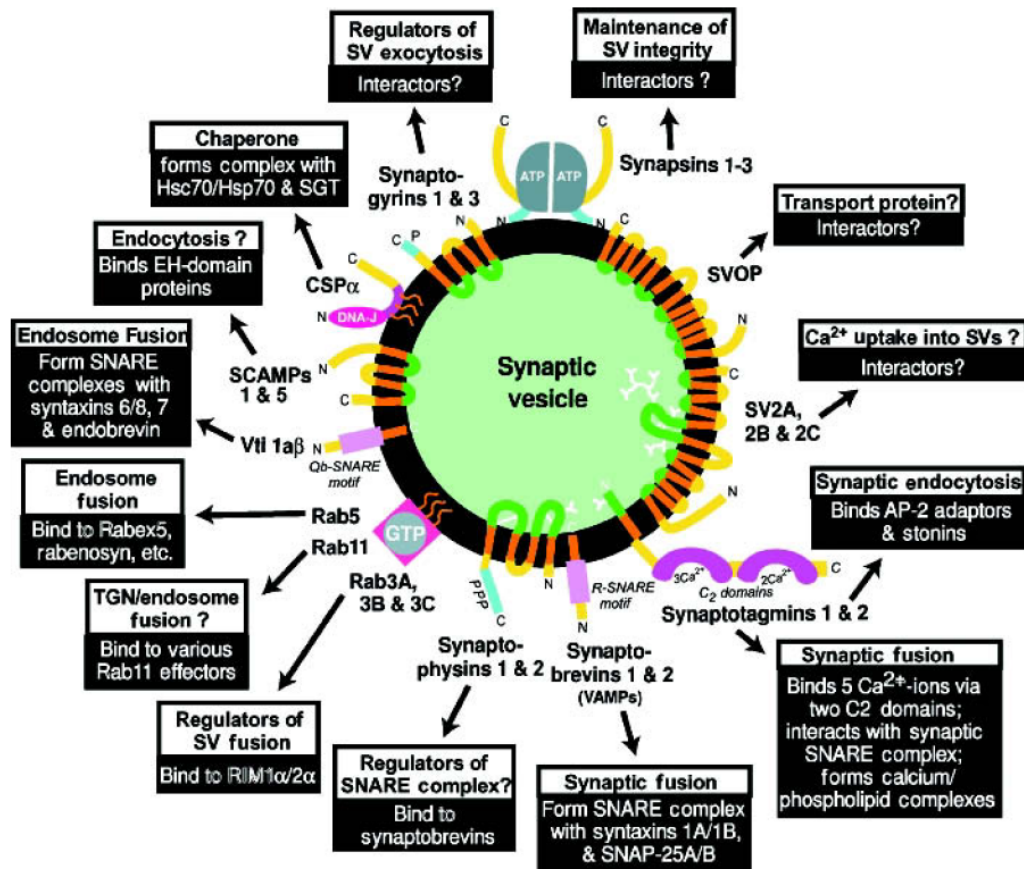


Figure 1-2 Structures, proposed interactions, and putative functions of synaptic vesicle trafficking proteins.

Proteins are shown schematically (green, intravesicular sequences; orange, transmembrane regions; blue, phosphorylation domains; pink, SNARE motifs; red and gray, folded domains; yellow, other sequences) the white connecting lines in the intravesicular space identify disulfide bonds, and the branched white lines indicate sugar residues. In the boxes corresponding to the individual proteins, proposed functions are shown on a white background and purported interactions on a black background (T. C. Südhof, 2004).

The trafficking proteome of synaptic vesicles includes intrinsic membrane proteins (synaptotagmins, VAMP/synaptobrevins with single transmembrane region (TMR), synaptophysins, synaptogyrins, and SCAMPs with four TMRs, and SV2s and SVOPs with twelve TMRs), proteins associated via posttranslational lipid modifications (CSP and rab proteins), and peripherally bound proteins (e.g., synapsin) (Figure 1-2). The putative functions and interacting partners of known synaptic vesicle proteins are

summarized in Figure 1-2, as you can see, many but not all of these proteins interact with non-vesicular proteins and are linked to specific functions. The proteome is more complicated since they do not share a characteristic that would make them identifiable as synaptic vesicle proteins, and little is known about how these proteins are specifically deposited into synaptic vesicles (T. C. Südhof, 2004). More work is required for many of synaptic vesicle proteins to further characterize their physiological role in vesicle cycle.

1.3.3 Synaptic Vesicle Cycle

Synaptic vesicle cycle starts with the uptake of neurotransmitters into the synaptic vesicle by an energy-dependent transport activity that is mediated by specialized transporter protein in the vesicle membrane (Step 1). The filled synaptic vesicles move and cluster in front of the active zone of the presynaptic plasma membrane (Step 2). At the active zone, vesicles become attached (or docked) to the plasma membrane (Step 3). The docking process requires specific interactions between active zones and vesicles, since vesicles do not attach to other parts of the plasma membrane. Attached vesicles then undergo an ATP-dependent perfusion reaction that primes them to the plasma membrane (priming) and convert them into the readily releasable pool (RRP) of vesicles, which will be elucidated in more detail later. Finally, primed vesicles are triggered for exocytosis by Ca^{2+} (Step 5) (T. C. Südhof, 2004).

After Ca^{2+} -triggered exocytosis, synaptic vesicles undergo three alternative ways of endocytosis and recycling: (1) kiss-and-stay: vesicles remain at the readily release pool, refill with neurotransmitter without undocking (Step 6). (2) Kiss-and-run: vesicles undock and refill with neurotransmitter but are still recycled locally (Step 7). (3) Vesicles

undergo endocytosis via clathrin-coated pits (Step 8) and refill the neurotransmitter through an endosomal intermediate (Step 9) (T. C. Südhof, 2004) (Figure 1-3).

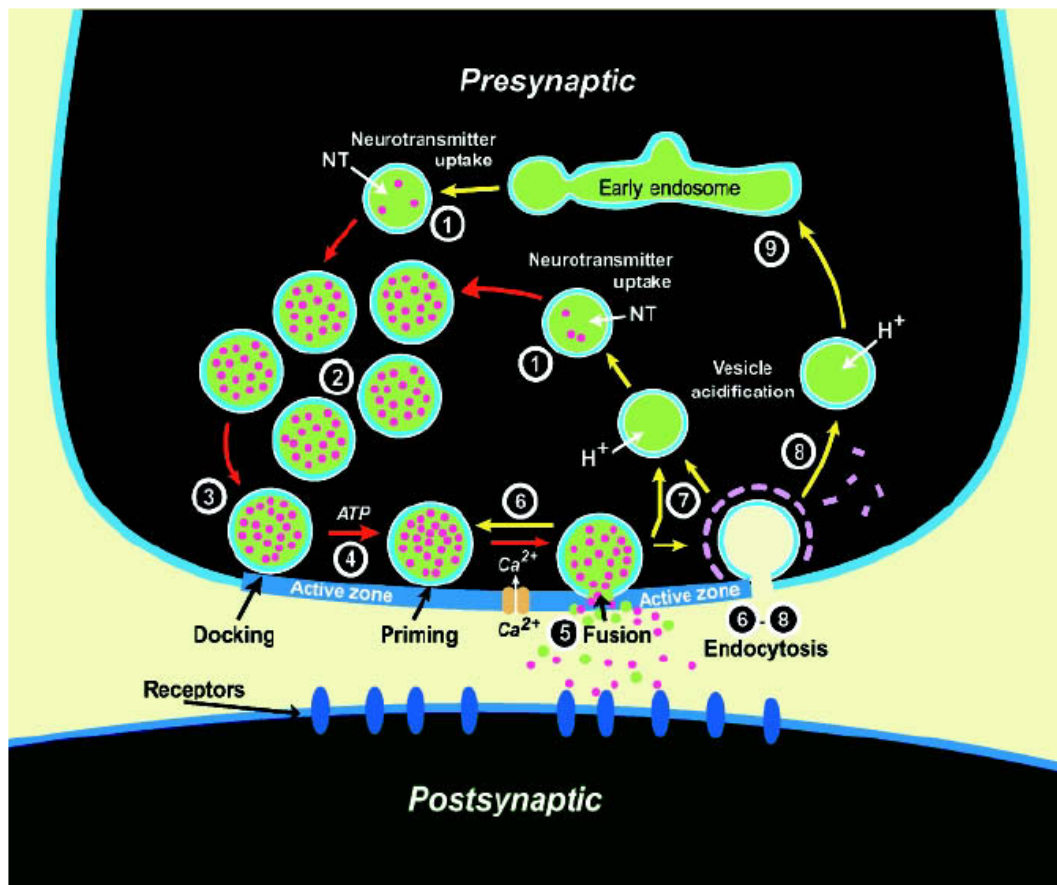


Figure 1-3 The synaptic vesicle cycle.

Synaptic vesicles are filled with neurotransmitters by active transport (step 1) and form vesicle clusters that may represent the reserve pool (step 2). Filled vesicles dock at the active zone (step 3), where they undergo a priming reaction (step 4) that makes them competent for Ca^{2+} triggered release (step 5). After fusion-pore opening, synaptic vesicles undergo endocytosis and recycle *via* several routes: local reuse (step 6), fast recycling without an endosomal intermediate (step 7), or clathrin-mediated endocytosis (step 8) with recycling *via* endosomes (step 9). Steps in exocytosis are indicated by red arrows and steps in endocytosis and recycling by yellow arrows (T. C. Südhof, 2004).

1.3.4 Synaptic Vesicle Pools

The total numbers of vesicles that participate in exo- and endocytosis during prolonged stimulation are defined as the recycling pool. The recycling pool of vesicles

has been subdivided into readily releasable pool (RRP) and reserve pool (RP), which replenish the RRP upon its depletion (T. C. Südhof, 2004). Typically, the size of RRP that is measured by the set of secretory vesicles exocytosed by high-frequency stimulation (C. Heinemann et al., 1994; R. Schneggenburger et al., 1999) generally agrees with the amount of vesicle release upon application of hypertonic sucrose as a mechanical stimuli (C. F. Stevens and T. Tsujimoto, 1995; C. Rosenmund and C. F. Stevens, 1996), or with the number of morphologically docked vesicles revealed by electron microscopy (T. Schikorski and C. F. Stevens, 2001; K. Satzler et al., 2002).

The number and the size of vesicle pools vary in different synapses. At the neuromuscular junctions, about 20% of vesicles are in RRP, and 80% in RP, with no resting vesicles (D. A. Richards et al., 2003). In cultured hippocampal neurons, high-frequency stimulation in the presence of FM dye, which is taken up with endocytosed vesicles, suggest an estimation of only 21-25 vesicles per synapse at recycling pool, with ~4-8 vesicles at RRP, and ~17-20 at RP (V. N. Murthy and C. F. Stevens, 1999). Thus, implying a surprisingly small recycling pool compared to total vesicles (>200 vesicles) in the terminal (T. C. Südhof, 2000).

1.4 Ca²⁺-triggered Exocytosis

In 1960s, by insertion of electrodes to both presynaptic terminal and postsynaptic cell and recording from the giant synapse of the squid, Sir Bernard Katz and Ricardo Miledi demonstrated that the transmitter release is initiated by the presynaptic depolarization (B. Katz and R. Miledi, 1967b). Their other contribution was the finding of the requirement for calcium ions in synaptic transmission (B. Katz and R. Miledi,

1967a, c).

We now know that when an action potential invades an axon terminal, it causes the opening of voltage-gated calcium channels located at the active zone, and extracellular calcium ions influx into presynaptic terminal. Calcium entry evokes synaptic vesicle fusion and thus neurotransmitter release. Binding of released neurotransmitter to postsynaptic receptors induces conformational change and the opening of ligand-gated channels, followed by generation of postsynaptic potential. The whole process occurs within the time range of milliseconds (Figure 1-4).

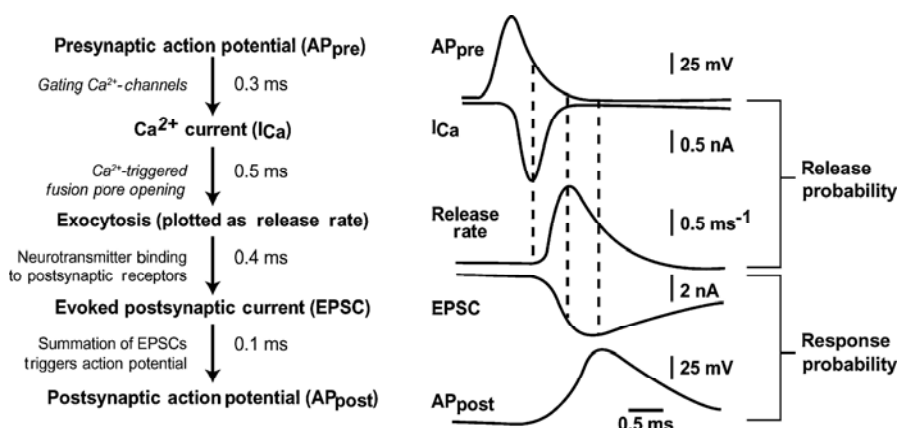


Figure 1-4 Reaction sequence and timing of synaptic transmission.

The principal reactions with the associated time constants are shown on the left, and traces from the corresponding reactions in the calyx of Held synapses are illustrated on the right. The time calibration bar at the bottom applies to all traces. (C. J. Meinrenken et al., 2003; T. C. Südhof, 2004)

A Ca^{2+} influx triggered vesicle release exhibits at least two mechanically distinct components: A fast, synchronous component, which dominates at low-frequency stimulation, is induced as fast as $50 \mu\text{s}$ after a Ca^{2+} transient develops (B. L. Sabatini and W. G. Regehr, 1996), and a slower asynchronous component, which dominates at high-frequency stimulation, and continues to release more than 1 s after the action potential (E. F. Barrett and C. F. Stevens, 1972; M. Geppert et al., 1994; Y. Goda and C. F.

Stevens, 1994; P. P. Atluri and W. G. Regehr, 1998). Both release components are Ca^{2+} -dependent with similar apparent Ca^{2+} cooperativities, but different apparent Ca^{2+} affinities (Y. Goda and C. F. Stevens, 1994).

1.5 Essential Proteins for Membrane Fusion

Several key proteins have been identified as essential for Ca^{2+} triggered exocytosis. Among them are soluble N-ethylmaleimide-sensitive factor attachment protein receptor (SNARE) proteins (VAMP/synaptobrevin, syntaxin, and SNAP25), Sec1/Munc-18 related (SM) protein Munc18, active zone proteins Munc13 and RIM, and the major calcium sensor, synaptotagmin 1.

1.5.1 SNARE Proteins

SNARE proteins are characterized by a homologous 70 residue sequence called the SNARE motif, which has a high propensity to form coiled coil domains (R. Jahn and T. C. Südhof, 1999; J. Rizo and T. C. Südhof, 2002). The traditional classification based on cellular localization divided SNAREs into two categories: vesicle or v-SNAREs, which are incorporated into the membranes of vesicle donors, including synaptic vesicles; and target or t-SNAREs, which are located on the target plasma membrane acceptors.

In the central nervous system, major SNAREs for vesicle fusion include: synaptobrevin/VAMP (vesicle associated membrane protein, a v-SNARE); the plasma membrane protein syntaxin (a t-SNARE), and membrane associated protein SNAP-25 (synaptosomal-associated protein of 25kD, a t-SNAREs). The four SNARE motifs (two from SNAP-25) from these three proteins form a very tight SNARE core complex (Figure

1-5).

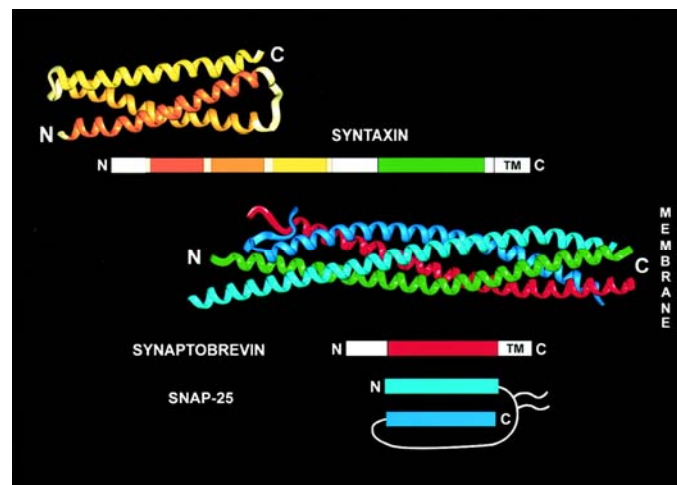


Figure 1-5 Structures of the neuronal SNARE proteins.

Syntaxin has three N-terminal H_{abc} domains that can fold automatically (depicted in the upper left corner) and a C terminal SNARE motif (green). Middle panel, ribbon diagram of core complex composed of all four SNARE motifs from syntaxin, SNAP-25 and Synaptobrevin. Bottom cartoon shows the domain structure and relative position of the SNARE motif within synaptobrevin (red) and SNAP-25 (dark and light blue). For comparison, the linear arrangement of the domains is shown for each protein in like colors. (R. Jahn and T. C. Südhof, 1999)

Synaptobrevin/VAMP: synaptobrevin is a short (~120 residues) and very abundant synaptic vesicle protein composed of a flanking C-terminal TMR, a 30 residue N-terminal proline-rich sequence that is not well conserved between species, and a central SNARE motif (W. S. Trimble et al., 1988; T. C. Südhof et al., 1989).

Syntaxin: The SNARE motif of syntaxin is located at the C-terminus followed by the TMR that anchors it to the membrane. The N-terminal sequence of syntaxin is relatively long (~180 residues) and forms an independently folded three-helical bundle called the H_{abc} domain. H_{abc} domain is conserved among different species from *C. elegans* to mammals (I. Fernandez et al., 1998). In isolated syntaxin, the H_{abc} domain folds back onto the C-terminal SNARE motif, forming a "closed" conformation that is distinct from

the “open conformation” of syntaxin in the core complex. Neuronal SM protein *sec1/Munc18-1* (mouse uncoordinated 18-1) tightly binds to closed syntaxin-1 by embracing the four helical bundles in its horseshoe shaped cavity. When binding with *Munc18-1*, syntaxin-1 is locked at the closed state, and is incompatible with SMARE complex formation, thus must undertake a conformational switch between its complex with *Munc18-1* and core complex. One potential candidate that takes on this role is *Munc13* (A. Betz et al., 1997).

SNAP-25 has two SNARE motifs (the N-terminal and the C-terminal SNARE motifs designated as SNN and SNC, respectively) that are connected by a linker region containing multiple cysteine residues. The linker region is long enough to ensure the parallel alignment of two SNARE motifs while SNARE complex assembly. Since *SNAP-25* lacks a TMR, it is attached to the membrane through multiple palmitoyl residues bound to the cysteine residues in the linker region (G. A. Oyler et al., 1989; S. H. Gerber and T. C. Sudhof, 2002).

1.5.2 SNARE Core Complex

The synaptic core complex is formed by two SNARE motifs from *SNAP25* and one of each from syntaxin and synaptobrevin. Although together they form a tight parallel four-helix bundle assembly, none of these proteins appear to have a defined structure upon isolation (R. B. Sutton et al., 1998). Crystal structure study has revealed that the core complex is highly twisted and has several salt bridges on the surface, as well as highly conserved interior leucine-zipper-like layers (R. B. Sutton et al., 1998). In addition, embedded in the center of the complex, there is a polar layer consisting of three

glutamines and one arginine (Q from syntaxin and SNAP25, and R from synaptobrevin) contributed from the four alpha-helix. This observation led to the classification of Q- and R- SNAREs (D. Fasshauer et al., 1998; R. B. Sutton et al., 1998) and the proposal that all core complexes consist of four-helix bundles are formed by three Q-SNAREs and one R-SNARE. Both reconstitution studies (K. L. Nicholson et al., 1998; K. M. Fiebig et al., 1999; J. A. McNew et al., 2000; F. Paumet et al., 2001; W. Antonin et al., 2002; F. Parlati et al., 2002) and crystal structure of the endosomal SNARE complex, which is remarkably similar to that of the neuronal complex (W. Antonin et al., 2002), have supported this proposal.

The functional importance of SNAREs in synaptic transmission was first shown by the discovery that they are the specific targets of clostridial neurotoxins, which inhibit synaptic transmission by cleavage of SNARE proteins. Null mutation of these SNARE genes invariably produces strong fusion and/or secretion defects (J. Rizo and T. C. Südhof, 2002; R. Jahn and R. H. Scheller, 2006; J. Rizo et al., 2006). Based on the stability of the core complex, it has been postulated that energy released during the assembly serves as a means to overcome the repulsive force between membrane structures (R. Jahn et al., 2003) (Figure 1-6). *In vitro* reconstitution experiments with SNAREs incorporated into separate liposomes showed that the SNARE complex itself is able to drive vesicles fusion (T. Weber et al., 1998). However, the low efficiency and long time scale indicate that this minimal fusion machinery itself cannot fully perform the fusion event of synaptic vesicle and other factors might be required to facilitate its physiological functions.

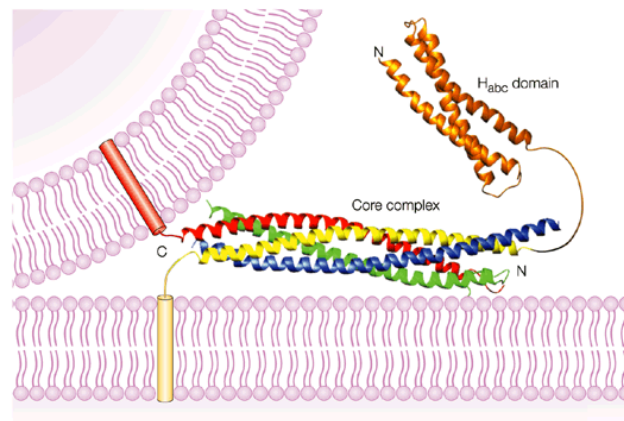


Figure 1-6 Model of the neuronal SNAREs assembling.

SNARE assembled into the core complex and positions of a synaptic vesicle in close proximity to the plasma membrane. The ribbon diagrams depict the crystal structure of the core complex and the NMR structure of the N-terminal H_{abc} domain of syntaxin-1. The H_{abc} domain is colored in orange and the SNARE motifs are color coded as follows: synaptobrevin, red; syntaxin-1, yellow; SNAP-25 amino terminus, blue; SNAP-25 carboxyl terminus, green. The cylinders represent the transmembrane regions of synaptobrevin and syntaxin-1, which are inserted into the synaptic vesicle and plasma membrane, respectively. (J. Rizo and T. C. Südhof, 2002)

1.6 SM Proteins

Sec1/Munc-18 related (SM) proteins are hydrophilic proteins of 60-70 kDa that are devoid of recognizable domains that are associated with their primary function. Unc-18 was the first SM protein discovered in *C. elegans* in genetic screens for uncoordinated phenotype (S. Brenner, 1974). Later, *sec1* in yeast was identified in screening for genes involved in secretory pathway (P. Novick et al., 1980), and the mammalian homologue of *unc-18*, Munc18-1, was isolated by its binding with syntaxin (Y. Hata et al., 1993). Since then, SM proteins have been identified in all types of membrane traffic studies, similar to SNAREs (R. Jahn and T. C. Südhof, 1999).

Electrophysiological analyses of Munc18-1 depleted mammalian synapse revealed that Munc18-1 is absolutely required for synaptic transmission. In Munc18-1 knockout mice, Ca^{2+} -triggered evoked release, miniatures, and vesicle release evoked by hypertonic

sucrose and latrotoxin were all abolished (M. Verhage et al., 2000). In the Munc18-1 deficient mice, however, normal brain assembly and morphologically defined synapses including unaltered docked synaptic vesicles were observed (M. Verhage et al., 2000).

There are seven Munc18 homologues in mammalian, among which three (Munc18-1, -2, and -3) are involved in exocytosis. Munc18-1, a 67 kDa neuronal protein, binds to closed conformation of syntaxin-1 with high affinity to form a complex that blocks the Q-SNARE motif from entering the SNARE core complex (I. Dulubova et al., 1999). The syntaxin level was reduced by 70% in Munc18-1 knockout mice (M. Verhage et al., 2000). Initially, the fact that Munc18-1 tightly bind to syntaxin suggests that Munc18-1 could potentially function by interacting with syntaxin. In addition, the observation that Munc18-1 only binds to closed conformation of syntaxin and competes with core complex formation indicates that the interaction is inhibitory. This idea is supported by an observation that a mutation on Rop, the *Drosophila* Munc18-1, that decreases binding affinity to syntaxin, increases neurotransmitter release (M. N. Wu et al., 1999). However, it is difficult to reconcile that Munc18-1 is simply an inhibitor of SNARE formation and thus of exocytosis for the evidences that show the positive requirements of SM proteins found in chromaffin cells (T. Voets et al., 2001) and many other systems (P. Novick and R. Schekman, 1979; P. Novick et al., 1980; C. Dascher et al., 1991; R. Hosono et al., 1992; S. D. Harrison et al., 1994) Moreover, the inhibitory interaction does not reconcile with the finding that in Munc18-1 depleted mice that neurotransmitter release is completely eliminated.

The understanding of the function of Munc18-1 has been complicated by the discrepancy between the requirement of Munc18-1 for vesicle fusion and the negative

function that Munc18-1 clinches closed form of syntaxin-1 preventing SNARE complex formation (K. M. Misura et al., 2000). Recent findings from *in vitro* binding assays and structure studies, however, reconciled the positive and negative roles of Munc18-1 by providing convincing evidence that Munc18-1, like most other SM proteins, also binds assembled SNARE complexes (E. Connell et al., 2007; I. Dulubova et al., 2007; C. F. Latham et al., 2007; C. Rickman et al., 2007; J. Shen et al., 2007). Moreover, besides binding to the SNARE motif of syntaxin-1, Munc18-1 also interacts with the N-terminal of syntaxin-1, which was not resolved in the crystal structure. The interaction is compatible with SNARE formation and even essential because either deletion of the first 6-24 amino acids of the L8A mutation in syntaxin-1 abolishes the interaction between Munc18-1 and the SNARE complex (C. Rickman et al., 2007; J. Shen et al., 2007). Therefore, Munc18-1 can be viewed as a recognized component of SNARE complex. In addition, SNARE binding with SM proteins, which first reported for yeast ortholog Sec1p (C. M. Carr et al., 1999), is now a general phenomenon (M. Khvotchev et al., 2007) contrary to binding of Munc18-1 to syntaxin-1, which appear to be an atypical feature that might have involved in meeting specific requirements of neuronal exocytosis (R. F. Toonen and M. Verhage, 2007).

Munc18-1 is expressed through out the brain and, besides syntaxin and SNARE complex, interacts with other protein partners including Mint proteins (M. Okamoto and T. C. Sudhof, 1997), Doc2 proteins (M. Verhage et al., 1997), granophilin (T. Coppola et al., 2002; M. Fukuda et al., 2002; T. Tsuboi and M. Fukuda, 2006), phospholipase D (H. Y. Lee et al., 2004), and Munc13 (T. Sassa et al., 1999). Mint1 and Mint2 were detected in a complex with Munc18-1 and syntaxin in the brain and may recruit Munc18-1 to

neurexin-containing regions of the plasma membrane through an association with CASK (T. Biederer and T. C. Südhof, 2000). Doc2 proteins were co-purified with synaptic vesicles and have been suggested to act as adaptors to regulate the Munc18-1-syntaxin interaction during vesicle docking (M. Verhage et al., 1997). Granuphilin has been shown to bind to Munc18-1, Rab3, and Rab27A, thus provide a potential pathway for the modulation of Munc18-1 function through Rab activity (T. Coppola et al., 2002; M. Fukuda et al., 2002). It is possible that further functions of the Munc18-1 may depend on these interactions (L. F. Ciufo et al., 2005).

1.7 Synaptic Vesicle Protein 2

Synaptic vesicle protein 2 (SV2), initially identified by a monoclonal antibody screen for synaptic vesicle proteins, is a component of all synaptic vesicles in vertebrates (K. Buckley and R. B. Kelly, 1985). Three highly homologous SV2 isoforms, SV2A, SV2B and SV2C, were identified (S. M. Bajjalieh et al., 1992; M. B. Feany et al., 1992; J. A. Gingrich et al., 1992; S. M. Bajjalieh et al., 1993; R. Janz and T. C. Südhof, 1999). All SV2 proteins contain 12 TMRs with N- and C-terminal cytoplasmic sequences and a large intravesicular loop that is N-glycosylated. Comparison of different SV2 isoforms shows that the TMRs and cytoplasmic loops are highly conserved, while the intravesicular loop – although N-glycosylated in all SV2 isoforms – exhibits little homology (Figure 1-7) (R. Janz and T. C. Südhof, 1999).

The three SV2 proteins are differentially distributed in brain. SV2A is expressed ubiquitously in almost all neurons, while SV2B is present in a more restricted forebrain pattern (S. M. Bajjalieh et al., 1994), and SV2C is primarily present in caudal brain

regions (R. Janz and T. C. Südhof, 1999). A distantly related synaptic vesicle protein called SVOP contains a similar transmembrane structure as SV2, but lacks its long cytoplasmic loop and highly glycosylated intravesicular sequence (R. Janz et al., 1998). Interestingly, although no SV2 homolog was identified in invertebrates, SVOP is highly conserved, suggesting that SVOP may be the evolutionary precursor of SV2.

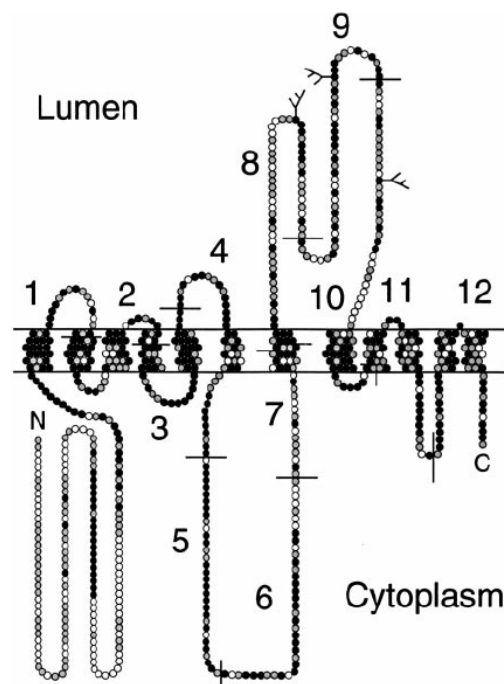


Figure 1-7 Transmembrane domain structure of SV2s and location of conserved residues.

Amino Acids in the primary sequence of SV2s are indicated by circles, with 12 potential TMRs predicted by sequence analyses. Residues that are conserved in SV2A, SV2B, and SV2C are shown in black, residues that are identified in at least two of the three isoforms in gray, and nonconserved residues in white. Coding exons are numbered 1 through 12, and positions of introns are indicated by lines crossing the peptide chain. Branched lines show positions of N-linked carbohydrates. N and C termini are identified by letters. (R. Janz et al., 1999)

Several potential functions of SV2 have been postulated based on its structure and protein interactions. The significant homology between SV2 (and SVOP) and bacterial and eukaryotic sugar transporter proteins (S. M. Bajjalieh et al., 1992; M. B. Feany et al., 1992; J. A. Gingrich et al., 1992), indicating that SV2 and SVOP may serve as transporter

proteins. The enormous glycosylation of SV2 proteins indicates that they could function as chemiosmotic stabilizers of synaptic vesicles (T. W. Scranton et al., 1993; R. Janz et al., 1998). SV2 interacts *in vitro* with synaptotagmin, the primary Ca^{2+} -sensor for synaptic vesicle exocytosis, suggesting that SV2 acts by binding to synaptotagmin (A. E. Schivell et al., 1996). SV2C is the protein receptor for botulinum neurotoxin A, which blocks neurotransmitter release by cleaving SNAP-25 (M. Dong et al., 2006; S. Mahrhold et al., 2006). Finally, SV2 attracted attention when it was identified as the target of the anti-epileptic drug levetiracetam (B. A. Lynch et al., 2004). However, the actual role of SV2 in synaptic transmission is still ambiguous.

1.8 C₂ Domains and E-Syts

C₂ domains are common Ca^{2+} -binding modules that were identified as conserved sequence motifs in protein kinase C isoforms (L. Coussens et al., 1986), and were shown to portray autonomously folded Ca^{2+} -binding domains in synaptotagmin-1 (B. A. Davletov and T. C. Südhof, 1993; E. R. Chapman and R. Jahn, 1994). C₂ domain is composed of 8 β -sheets, forming a β -sandwich motif that contains flexible loops at the top and bottom, with “top” and “bottom” defined by reference to the synaptotagmin-1 C₂A domain whose structures under native state and Ca^{2+} -binding mode have been determined (R. B. Sutton et al., 1995; J. Rizo and T. C. Südhof, 1998). In all C₂ domains that bind to Ca^{2+} , Ca^{2+} ions bind exclusively to the top loops where five conserved aspartate or asparagine residues are required to coordinate the binding (J. Ubach et al., 1998).

Ca^{2+} -binding properties differ in different C₂ domains. C₂ domains, like such of

synaptotagmin-1, display a low intrinsic Ca^{2+} -binding affinity that is boosted by the presence of phospholipids (B. A. Davletov and T. C. Sudhof, 1993; J. Ubach et al., 1998). Other C_2 domains, such as those of rabphilin, exhibit high intrinsic Ca^{2+} -binding affinity (J. Ubach et al., 1999). In addition, some C_2 domains lack Ca^{2+} -binding ability, due to the fact that they are deficient in essential binding residues (J. O. Lee et al., 1999; H. Dai et al., 2005). More strikingly, some C_2 domains, like the C_2B domains of synaptotagmins 4 and 11, canonical Ca^{2+} -binding residues are intact, however, the domains does not bind to Ca^{2+} because a subtle change in the orientation of the β -sheets disables the top loops to coordinate Ca^{2+} ions (H. Dai et al., 2004).

Most, but not all, Ca^{2+} -dependent C_2 domains, like synaptotagmin-1 C_2A domain (B. A. Davletov and T. C. Sudhof, 1993; E. R. Chapman and R. Jahn, 1994), and some of Ca^{2+} -independent C_2 domains, like the PTEN (phosphatase and tensin homolog) C_2 domain (J. O. Lee et al., 1999), bind to phospholipids. Several Ca^{2+} -independent C_2 domains comprise protein interacting motifs, for example, C_2A domain of muc13-1 forms complex with the RIM zinc finger domain (J. Lu et al., 2006). In synaptotagmin-1 C_2A domain, Ca^{2+} -binding triggers both interactions to phospholipids and to SNARE complexes, suggesting that C_2 domains can perform multiple functions and bind to proteins and phospholipids simultaneously (Z. P. Pang et al., 2006; J. Tang et al., 2006).

C_2 domains are primarily found in membrane trafficking or signal transduction proteins. In membrane trafficking proteins, C_2 domains are commonly present in multiple copies (e.g., synaptotagmin-1) and functions as effector domains, while proteins being attached to membrane either by a TMR or by binding to other membrane proteins (e.g., rabphilin that binds to Rab3) (B. Stahl et al., 1996). On the contrary, in signal

transduction proteins, C₂ domains are usually present in single copy (e.g., protein kinase C and Pten) (J. O. Lee et al., 1999; J. R. Giorgione et al., 2006) and responsible for the membrane localization of the respective protein.

Three families of putative trafficking proteins comprising a single TMR and multiple C₂ domains have been identified: synaptotagmins, ferlins, and multiple C₂ domain and transmembrane region proteins (MTCPs) (T. C. Südhof, 2002; D. Bansal and K. P. Campbell, 2004; O. H. Shin et al., 2005). In addition, a fourth type of protein with multiple C₂ domains and a single TMR has been reported from rat adipocytes (N. J. Morris et al., 1999). The type of proteins is defined by *Min et al.* and was referred as E-Syts, for extended synaptotagmins, owing to their similarity to synaptotagmins (S. W. Min et al., 2007). E-Syts are distantly homologous to a family of yeast membrane proteins containing three C₂ domains that were called tricalbins (C. E. Creutz et al., 2004). However, they are different from tricalbin in that they are Ca²⁺-binding proteins. Analyses of vertebrate sequences revealed three evolutionarily related E-Syt proteins, E-Syt1, E-Syt2, and E-Syt3 (S. W. Min et al., 2007).

The domain structure of E-Syts is consist of a short, non-conserved N-terminal sequence, a single N-terminal TMR, a conserved X domain unique to E-Syts, and either five (E-Syt-1) or three (E-Syt2 and E-Syt3) C₂ domains (Figure 1-8) (S. W. Min et al., 2007). In E-Syt1, C₂C and C₂D are highly homologous to C₂A and C₂B domains, and thus suggested as duplicates of the first two C₂ domains (Figure 1-8). In mammalian, worm, and insect E-Syts, only the C₂A domain contains the complete Ca²⁺-binding motifs in the top loop. For the tissue distribution, RT-PCR analyses revealed that all E-Syts are ubiquitously expressed, while E-Syt2 and E-Syt3 are more enriched in cerebellum (S. W.

Min et al., 2007).

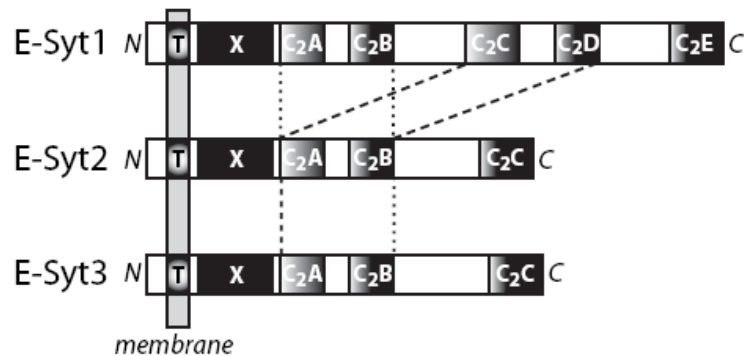


Figure 1-8 Domain structures of E-Syts.

T, TMR; X, X domain unique to E-Syts; C₂A to C₂E, C₂ domains (note that the C₂C and C₂D domains of E-Syt1 are highly homologous to the C₂A and C₂B domains of all E-Syts) (S. W. Min et al., 2007).

1.9 Questions to Ask

Questions remain for the functions or properties of the synaptic proteins. First, as I discussed above, although the functions of SV2 have been proposed based on its structure and protein interactions, the actual role of this protein in synaptic transmission is still ambiguous. Physiological phenotypes of SV2 KO mice reported from several groups seem to be controversial, although this could be caused by recording from different systems or various conditions of neurons. The postnatal death revealed by genetic studies implicated that SV2 should have a physiologically important role that is universal and should not be affected by comparatively trivial variations in experimental conditions. In addition, there seems to be a gap between our knowledge in structure and protein interactions of SV2 and its physiological functions. To address these questions, we developed a lentiviral infection system that allows us to express SV2 proteins in cultured SV2 deficient neurons. The system allows us to rescue physiological phenotypes we

found in SV2 deficient neurons; this further confirms the phenotypes were indeed arisen for the deletion of SV2A. Furthermore, it allows us to conduct structure-function studies of the SV2A protein (see Chapter II).

Second, recent data of *in vitro* binding assay and/or structure study revealed new interactions of Munc18-1 to neuronal SNARE assemblies and syntaxin-1 by its N-terminus. These observations seem to solve the discrepancy of the roles of Munc18-1 in vesicle fusion suggested by genetic study and its binding to closed conformation of syntaxin-1. However, direct evidence is still lacking in physiological relevance of Munc18-1/SNARE complex binding and Munc18-1/syntaxin-1 binding and needs to be addressed. In our study, we utilized the lentiviral infection system and tested mutations that display differential disruption on Munc18-1/SNARE complex binding, but are intact in Munc18-1/syntaxin-1 binding. Our findings suggested Munc18-1/SNARE complex binding is essential for vesicle fusion, and is likely important for vesicle priming (Chapter III).

Third, one way to further our understanding of the molecular mechanism of synaptic transmission is to identify new proteins that are involved in membrane fusion. Thus, by databank search for C₂ domain proteins that contain a TMR, we identified a new group of proteins referred as E-Syts. We investigated the phospholipid binding property and subcellular localization of E-Syt proteins. In addition, we also recovered an unusual membrane targeting mechanism of this family of protein. Our findings suggest E-Syts represent a family of Ca²⁺-binding membrane proteins that expand multiple C₂ domains trafficking proteins to a fourth class beyond synaptotagmins, ferlins, and MCTPs (Chapter IV)

CHAPTER II: SV2 RENDERS PRIMED VESICLES COMPETENT FOR Ca^{2+} -INDUCED EXOCYTOSIS

2.1 Introductions

The structure and protein interactions of SV2 suggest multiple functions. SV2 (and SVOP) exhibits significant homology to bacterial and eukaryotic sugar transporter proteins (S. M. Bajjalieh et al., 1992; M. B. Feany et al., 1992; J. A. Gingrich et al., 1992), indicating that SV2 and SVOP may serve as transporter proteins. This hypothesis is supported by the conservation in all SV2 isoforms of two negatively-charged residues in TMR1 that are three amino acids apart, placing them to the same face of an α -helix. Moreover, the enormous glycosylation of SV2 proteins suggested that they could function as chemiosmotic stabilizers of synaptic vesicles (T. W. Scranton et al., 1993; R. Janz et al., 1998). Furthermore, SV2 interacts *in vitro* with synaptotagmin, the primary Ca^{2+} -sensor for synaptic vesicle exocytosis, suggesting that SV2 acts by binding to synaptotagmin (A. E. Schivell et al., 1996), although the mode of interaction remains unclear (R. A. Pyle et al., 2000; D. R. Lazzell et al., 2004; A. E. Schivell et al., 2005). SV2C is the protein receptor for botulinum neurotoxin A, which blocks neurotransmitter release by cleaving SNAP-25 (M. Dong et al., 2006; S. Mahrhold et al., 2006). Finally, SV2 attracted attention when it was identified as the target of the anti-epileptic drug levetiracetam (B. A. Lynch et al., 2004).

SV2B KO mice are phenotypically normal, whereas SV2A KO mice and SV2A/SV2B double KO mice exhibit severe seizures and die postnatally, without developmental changes in brain structure (R. Janz et al., 1999). Electrophysiologically,

cultured hippocampal SV2A- or SV2B-deficient neurons exhibit no detectable abnormalities, whereas neurons that lack both isoforms experience sustained synaptic facilitation during high-frequency stimulus trains (R. Janz et al., 1999). The increased facilitation was reversed by a membrane-permeable EGTA-analog that chelates intracellular free Ca^{2+} , suggesting that the SV2 deletion causes increased facilitation by enhancing the accumulation of residual presynaptic Ca^{2+} during high-frequency stimulus trains (R. Janz et al., 1999). Moreover, acute slices of SV2A-deficient mice exhibit abnormal GABAergic synaptic transmission (K. M. Crowder et al., 1999). In SV2A-deficient chromaffin cells, the size of the pool of release-ready chromaffin secretory vesicles was decreased, and SNARE-complex assembly in brain was impaired, suggesting that SV2A may function upstream of Ca^{2+} -triggering in priming synaptic vesicles (T. Xu and S. M. Bajjalieh, 2001). These results were supported by studies in cultured hippocampal neurons suggesting that SV2 primes vesicles in quiescent neurons, and that this function can be bypassed by an activity-dependent priming mechanism (K. L. Custer et al., 2006).

Although the currently available data thus establish that SV2 is important for neurotransmitter release, they do not clarify at what step during exocytosis SV2 functions. Whereas the binding of SV2 to synaptotagmin indicates a role in Ca^{2+} -triggering, some of the physiological experiments suggested a function in vesicle priming, possibly in an activity-dependent manner as indicated by the synaptic facilitation. Moreover, it is unknown how the physiological role of SV2 relates to its properties, i.e. its massive intravesicular glycosylation and its transmembrane architecture resembling a transporter protein. In the present study, I have investigated these issues using an

electrophysiological analysis of SV2-deficient cultured neurons, either without further treatment or after rescue with wild-type (WT) or mutant SV2A delivered by lentiviral infection. My results indicate that SV2 acts as a booster of synaptic exocytosis upstream of Ca^{2+} -triggering, but downstream of priming, in a function that is independent of its possible binding to synaptotagmin, but requires a normal transmembrane structure and intravesicular glycosylation.

2.2 Materials and Methods

2.2.1 Plasmid construction

The wild-type rat SV2A cDNA was replicated by PCR and cloned into pFUW lentivirus expression vector (with multiple cloning sites: XbaI- EcoRI- BstBI- NheI- BamHI- HpaI) using EcoRI and BamHI. EGFP was inserted in frame at the N-terminal of SV2A between the XbaI and EcoRI sites. Mutations were generated by PCR and subcloned into pFUGW (G=EGFP) vector. DA-mutant contains alterations of an aspartic acid to alanine at 179aa and a glutamic acid to alanine at 182aa. NQ-mutant contains three asparagines to glutamines mutations at 498aa, 548aa, and 573aa on glycosylated residues. KA-mutant includes a lysine to alanine mutation at 694aa. Mutant d107 was generated by deleting first 107 amino acid residues, which was denoted as the N-terminal synaptotagmin binding region of SV2A (A. E. Schivell et al., 1996; D. R. Lazzell et al., 2004; A. E. Schivell et al., 2005). Sequences are verified by DNA sequencing.

2.2.2 Mouse breedings

All analyses were performed on littermate offspring of breedings between SV2A

heterozygotes/SV2B knockout (KO) homozygotes (SV2A (+/-)/SV2B (-/-)). Cultured cortical neurons from SV2A WT/SV2B homozygous (SV2A (++)/SV2B (-/-)) pups and SV2A/SV2B homozygous (SV2A (-/-)/SV2B (-/-)) pups were used in the experiments in this study. All genotyping was performed as described (R. Janz et al., 1999), except primers A1*: GAGTTAGGGATGAGTGTTCTGG, A2*: GTTGACTGAGAGTGAGATGAGC, and N: GAGCGCGCGCGGCGGAGTTGTTGAC were used for SV2A.

2.2.3 Cortical primary neuronal cultures

The cortexes were dissected from the brains of postnatal day 1 (P1) mice, dissociated by trypsin digestion, and plated on circle glass coverslips coated with Matrigel. The cortical neurons were maintained in MEM medium (Invitrogen, San Diego, CA) supplemented with B-27 (Invitrogen), L-glutamine, 0.5% glucose, 5% fetal bovine serum, and Ara-C (Sigma-Aldrich, Louis, MO). The cultures were used for experiments at 14–17 days *in vitro* (DIV). For the tests of the effect of neuronal silencing on the SV2 KO phenotype, I incubated the cultured neurons for 24 hrs in the regular medium containing 1 μ M tetrodotoxin (TTX) before performing the analyses.

2.2.4 Electrophysiology

Synaptic responses were triggered by 1 ms current injection (900 μ A) through a local extracellular electrode (FHC concentric bipolar electrode; catalog #CBAEC75) and recorded in whole-cell mode using Multiclamp 700A amplifier (Molecular Devices, Union City, CA). Model 2100 Isolated Pulse Stimulator (A-M Systems, Carlsborg, WA)

was used to control the frequency, duration, and magnitude of extracellular stimulus. The whole-cell pipette solution contained 135 mM CsCl₂, 10 mM Hepes, 1 mM EGTA, 1 mM Na-GTP, 4 mM Mg-ATP, and 10 mM QX-314, pH 7.4. The bath solution contained 140 mM NaCl, 5 mM KCl, 2 mM MgCl₂, 10 mM Hepes-NaOH pH 7.4, 10 mM glucose, and in 1 mM Ca²⁺ if not indicated otherwise. Signals were digitized at 10 kHz, filtered at 2 kHz, and stored using pClamp9 (Axon Instruments, Inc.) software. Spontaneous synaptic responses (mIPSCs and mEPSCs) were monitored in the presence of 1 μM TTX to block action potentials. Spontaneous mEPSCs were recorded with additional 100 μM picrotoxin in the bath solution. IPSCs were pharmacologically isolated by adding 50 μM APV and 20 μM CNQX to suppress the excitatory AMPA and NMDA currents. Synaptic responses were recorded at least 1 min after obtaining whole-cell patch before recording of evoked synaptic responses, allowing the internal pipette solution to diffuse into the patched neuron. Series resistance was compensated to 60–70%. For EGTA-AM (EGTA, ethylene glycol tetraacetic acid) experiments, cultured neurons were pre-treated with EGTA-AM at 0.1 mM for at least 10 min. Hypertonic sucrose (0.5 M) was applied for 30 s, or 20 s for the tests of the effect of neuronal silencing on the SV2 KO phenotype, through perfusion system at speed of 1 ml/min. All experiments were performed at room temperature. Data were analyzed using Clampfit 9.0 (Molecular Devices). mIPSCs and mEPSCs events detection were performed manually to collect individual mIPSCs and mEPSCs. Statistical analysis was performed with *t* test (*, $p \leq 0.05$, **, $p \leq 0.01$, and ***, $p \leq 0.001$). All data are shown as means \pm the SEM. Cortical neurons were infected with lentiviruses encoding EGFP fusion of WT SV2A, or SV2A mutants. The cultures were infected before 7 DIV and analyzed at 14–17 DIV. As determined by EGFP fluorescence,

the efficiency of lentiviral infections exceeded 95%, therefore, I randomly selected the neurons for whole-cell recording assuming that most presynaptic inputs in infected cultures were formed by neurons expressing recombinant protein of interest.

2.2.5 Immunocytochemistry

Neurons attached to the glass coverslips were rinsed once with PBS, fixed for 15 min on ice in 4% of formaldehyde and 4% of sucrose in PBS. After fixation, the neurons were washed with PBS twice, and then incubated for 30 min in blocking solution, PBSS, containing 3% milk, 0.1% saponin, and in PBS, followed by 1-h incubation with primary and rhodamine- and FITC-conjugated secondary antibodies diluted in blocking solution. The coverslips were then mounted on glass slides with Aqua-Poly/Mount medium (Polysciences, Inc.) and analyzed at room temperature using a confocal microscope (DMIRE2; Leica) and 63x/1.32–0.6 oil immersion objective. The images were collected using confocal software (Leica) and processed using Photoshop software (Adobe). All digital manipulations were equally applied to the entire image.

2.2.6 Miscellaneous

Samples of EGFP-SV2 recombinant proteins were collected by adding 1x sample buffer (U. K. Laemmli, 1970) to cultured cortical neurons, boiled for 10 min, then stored at -80 °C until used. Samples were analyzed by SDS-PAGE and electroblotted to nitrocellulose membranes (Amersham). The membranes were probed using antibodies against SV2A (P915), EGFP (JL-8, Clontech), and GDI (CL81.2). SDS-PAGE and immunoblotting were performed as standard procedure described (U. K. Laemmli, 1970; R. Janz et al.,

1999).

2.3 Results

2.3.1 Analysis of the effect of deleting SV2 on inhibitory synaptic transmission.

I prepared high-density cultures of cortical neurons from double KO mice that lack both SV2A and SV2B, and from littermate control mice that lack only SV2B but contain at least one WT allele of SV2A (R. Janz et al., 1999). SV2B KO neurons were used as a control for SV2A/2B double KO neurons because previous studies showed that SV2B-deficient mice exhibit no detectable phenotype compared to WT controls, whereas SV2A/2B double KO neurons exhibit a significant phenotype (R. Janz et al., 1999). The cultured neurons were analyzed electrophysiologically using postsynaptic whole-cell recordings as described (A. Maximov et al., 2007). Spontaneous miniature and evoked inhibitory post-synaptic currents (mIPSCs and IPSCs, respectively) were recorded in the presence of AMPA- and NMDA-receptor blockers (20 μ M CNQX and 50 μ M AP-5), whereas spontaneous miniature and evoked excitatory postsynaptic currents (mEPSCs and EPSCs, respectively) were monitored in the presence of the GABA-receptor blocker picrotoxin (100 μ M).

I first examined action potential-independent, spontaneous ‘miniature’ neurotransmitter release events in the presence of 1 μ M TTX. Consistent with the results of *Custer et al.* (K. L. Custer et al., 2006), the frequency and amplitude of spontaneous mIPSCs and mEPSCs were not significantly different between synapses lacking either only SV2B or both SV2A and SV2B, although the mEPSCs frequency in the double KO neurons tended to be slightly higher (Figures 2-1, A-D).

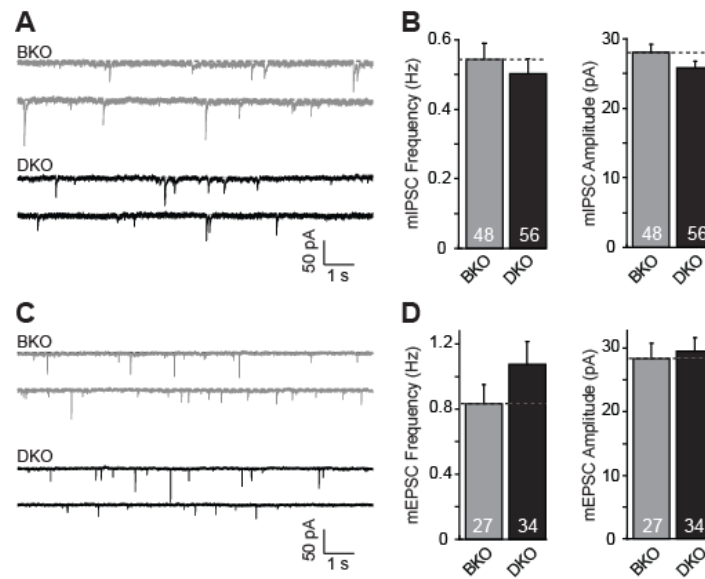


Figure 2-1 Spontaneous synaptic transmission is not altered in SV2-deficient neurons.

Representative traces (left panels, A and C) and the frequency and amplitudes (right panels, B and D) of mIPSCs (A and B) and mEPSCs (C and D) recorded in neurons from SV2B KO mice (BKO) or from SV2A/SV2B double KO mice (DKO). Spontaneous events were recorded in a bath solution containing 2 mM Ca^{2+} and 0.5 mM Mg^{2+} at a -70 mV holding potential in the presence of 1 μM TTX and 20 μM CNQX/ 50 μM AP-5 (for mIPSCs) or 100 μM picrotoxin (for mEPSCs). All data shown are means \pm SEMs (n=numbers shown in bar diagrams from at least 3 independent cultures).

I next investigated whether deletion of SV2A and SV2B impaired evoked IPSCs (Figure 2-2, A). In these experiments, IPSCs were measured instead of EPSCs because in our recording system, IPSCs can be more accurately and reliably monitored than EPSCs (A. Maximov et al., 2007). I detected a highly significant $\sim 30\text{-}40\%$ decrease in the peak amplitudes and the synaptic charge transfer (integrated over 1.5 sec) of IPSCs in neurons lacking SV2A and SV2B compared to control neurons lacking only SV2B (Figure 2-2, B). Kinetic analyses did not uncover a difference in the IPSC kinetics between SV2A/2B double KO and SV2B single KO neurons, indicating that the change in release is not due to a selective loss of synchronous or asynchronous release (data not shown).

The observation that the SV2 double KO decreases action-potential evoked release (Figure 2-2, B) and binds to synaptotagmin (A. E. Schivell et al., 1996) suggests that SV2

may act during Ca^{2+} -triggering of release mediated by synaptotagmin, and may alter the Ca^{2+} -affinity of release. To test this hypothesis, I measured the amplitude of IPSCs evoked in the presence of different concentration of extracellular Ca^{2+} . Plots of the absolute IPSC amplitudes showed that at all except the lowest Ca^{2+} -concentration, synapses lacking SV2 proteins exhibited a uniform ~30-40% decrease in the peak amplitude (Figure 2-2, C). This relationship indicates that the SV2-deletion does not alter the apparent Ca^{2+} -affinity of release, as confirmed by plots of the normalized IPSC amplitudes which revealed an identical Ca^{2+} -concentration dependence of release in SV2-deficient and control synapses (Figure 2-2, D).

To determine whether the decrease in inhibitory neurotransmitter release in SV2-deficient neurons is due to a decrease in the RRP, we applied hypertonic sucrose to cultured neurons for 30 s, and estimated the size of the RRP as the integrated charge transfer over the first 10 s (Figure 2-2, E). Hypertonic sucrose is thought to stimulate release of the entire RRP in cultured neurons, thereby allowing measurement of the RRP (C. Rosenmund and C. F. Stevens, 1997). Surprisingly, I detected no significant change in the size of the RRP in double KO synapses (Figure 2-2, F). This result differs from observations obtained with SV2-deficient hippocampal neurons that had formed autapses in which a large decrease in the RRP was observed as a function of the SV2 deletion (K. L. Custer et al., 2006). This difference could be due to differences between autapses and synapses, for example the presence of constant network activity in our high-density cultures of neurons that is not observed in autaptic neurons. Thus, to test whether such network activity may have induced a compensatory occlusion of an RRP phenotype in the SV2-deficient neurons, I also measured the size of the RRP after a 24 hr treatment with

TTX, but again did not detect a difference (Figure 2-2, G and H).

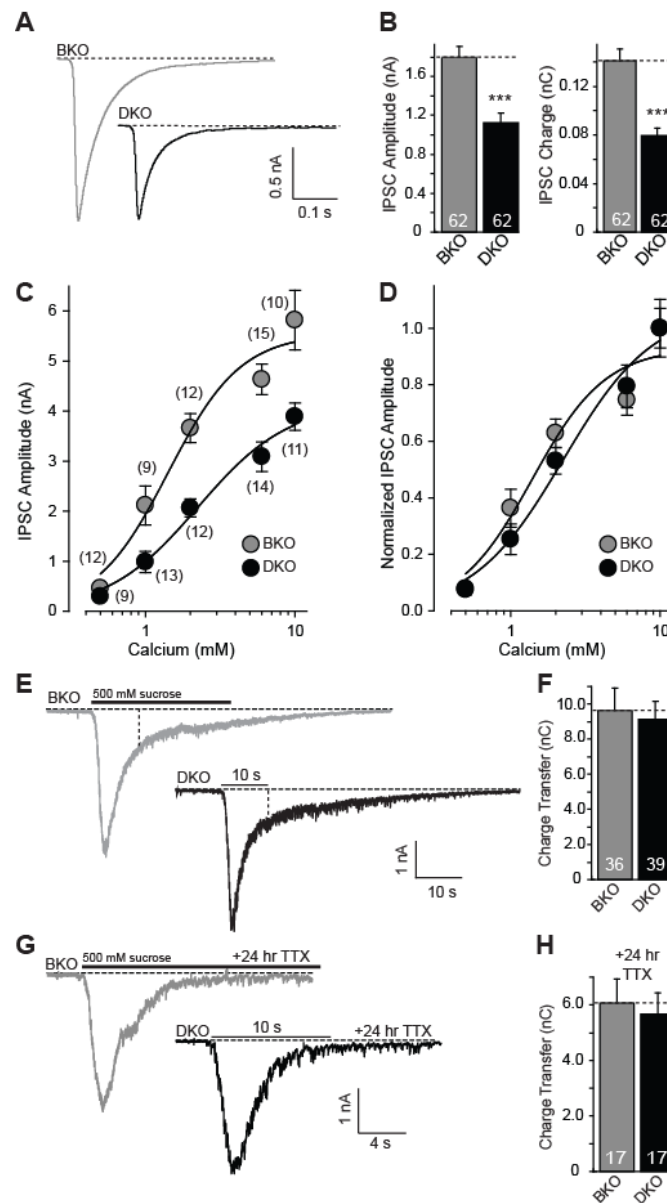


Figure 2-2 SV2 deletion selectively impairs Ca²⁺-triggering of release without decreasing the RRP size.

(A, B) Representative traces (A) and mean amplitude and charge transfer (B) of IPSCs evoked by extracellular stimulation at 0.1 Hz frequency in cultured cortical neurons from littermate SV2B KO (BKO) and SV2A/SV2B double KO mice (DKO). Action potentials were evoked with a focal electrode in a bath solution containing 1 mM Ca²⁺ and 2 mM Mg²⁺.

(C, D) Ca²⁺-titration of IPSC amplitudes in BKO and DKO neurons plotted in absolute terms (C) or normalized to the maximal Ca²⁺-concentration (D). Recordings were performed in bath solutions containing

the indicated Ca^{2+} -concentrations with a constant 2 mM Mg^{2+} -concentration.

(E-H) Measurements of the RRP size by application of 0.5 M sucrose to either naïve neurons (E and F) or neurons that were treated with 1 μM TTX for 24 hrs (G and H). Panels show representative traces (E and G) and summary graphs depicting the integrated charge transfer during the first 10 sec of the response (F and H).

All data shown are means \pm SEMs (n=numbers shown in bar diagrams from at least 3 independent cultures; *** = $p < 0.001$ by Student's t-test; in C and D, n= numbers shown above or under data points; the absolute values are significantly different between BKO and DKO neurons at the $p < 0.0001$ level as tested by 2-way ANOVA).

2.3.2 Synaptic responses to a 10 Hz stimulus train in SV2-deficient neurons.

To test the role of SV2 in Ca^{2+} -triggered release evoked by a high-frequency stimulus train, I evoked IPSCs by 10 action potentials applied at 10 Hz in 1 mM Ca^{2+} and 2 mM Mg^{2+} (Figure 2-3, A). Measurements of the amount of total release during the train ('train release'), after the train ('delayed release'), or both ('total charge transfer') were obtained by integrating the synaptic charge transfer over the respective time periods. Train release calculate by integrating charges from the beginning of the train till 0.1 sec after last stimulus; total charge transfer was calculated by integrating over 5 sec of the train; and delayed release is the difference between total charge transfer and train release. These measurements revealed the same ~40% decrease in release in SV2-deficient synapses compared to control synapses as detected for isolated IPSCs (Figure 2-3, B-D). All measures of release induced by the 10 Hz stimulus train (train release, delayed release, total charge transfer) were decreased similarly. Much of the release during the train, and all of it during the 'delayed release' period after the train, is asynchronous, whereas release induced by isolated action potentials is largely synchronous (A. Maximov and T. C. Sudhof, 2005). Thus, as observed for IPSCs triggered by isolated action potentials, deletion of SV2 equally impairs synchronous and asynchronous release.

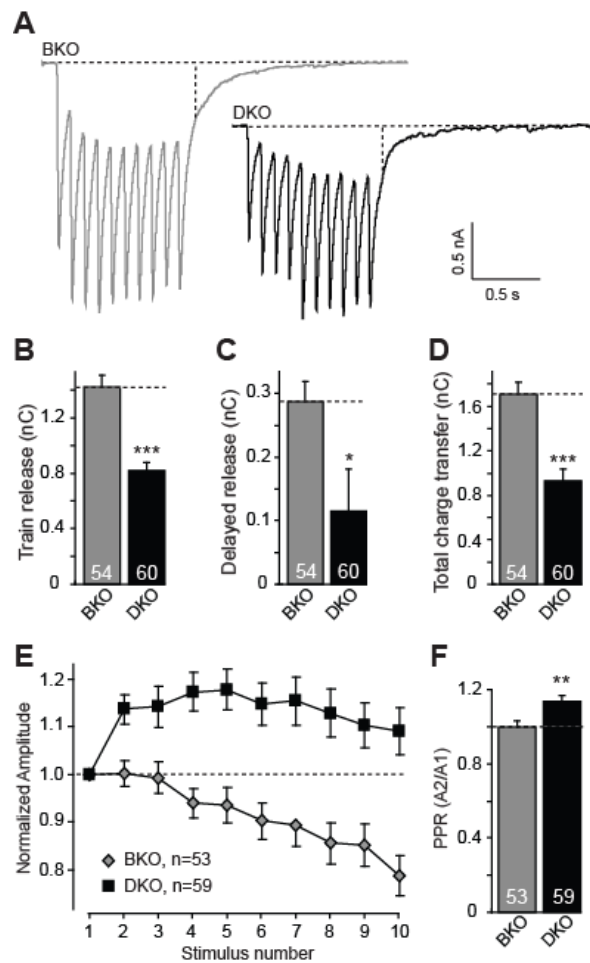


Figure 2-3 SV2 deletion decreases release but increases facilitation during 10 Hz stimulus trains.

(A) Representative traces of IPSCs induced by a 1 sec, 10 Hz stimulus train in cultured neurons from SV2B KO (BKO) and SV2A/SV2B double KO mice (DKO) (bath solution contains 1 mM Ca^{2+} and 2 mM Mg^{2+}). (B-D) Summary graphs of the charge transfer during the stimulus train (train release, B), after the train (delayed release, C, a measure of asynchronous release), and over the entire experiment (total charge transfer, D) in BKO and DKO neurons.

(E) Plot of the normalized amplitude as a function of the stimulus number during the 10 Hz stimulus train (F) Paired-pulse ratio (PPR) of synaptic responses.

All data shown are means \pm SEMs (n=numbers shown in bar diagrams from at least 3 independent cultures; *= $p < 0.05$, **= $p < 0.01$, and ***= $p < 0.001$ by Student's t-test; in E, n=53 for BKO neurons and n=59 for DKO neurons; values are significantly different between BKO and DKO neurons at the $p < 0.0001$ level as tested by 2-way ANOVA).

I next plotted the synchronous components of release during the 10 Hz stimulus train as normalized responses as a function of the stimulus number (Figure 2-3, E). In control neurons lacking only SV2B, the 10 Hz stimulus train induced a progressive reduction in

synaptic responses (referred to as short-term synaptic depression). In SV2-deficient neurons, however, the 10 Hz stimulus train induced an increase in synaptic responses (i.e., synaptic facilitation; Figure 2-3, E). Since the relative decrease in the total amount of release during a stimulus train and an isolated action potential induced by the SV2 deletion is similar, the facilitation of synchronous responses observed in SV2-deficient synapses likely represents a Ca^{2+} -dependent shift from asynchronous to synchronous release during the stimulus train. This behavior is consistent with the notion that with an unchanged RRP but decreased ability of Ca^{2+} to trigger release, the accumulating Ca^{2+} during the stimulus train causes facilitation of synaptic responses in the SV2A/2B double KO neurons since the RRP does not become depleted.

2.3.3 EGTA-AM reverses facilitation induced by deletion of SV2 but does not abolish phenotype.

We previously hypothesized that SV2 functions as a Ca^{2+} -uptake system that clears Ca^{2+} from nerve terminals after a pulse of Ca^{2+} has entered the terminals during an action potential (R. Janz et al., 1999). This hypothesis was based on the observation that the synaptic facilitation phenotype in SV2-deficient synapses was reversed by EGTA-AM which sequesters intracellular Ca^{2+} . However, the decrease in total release observed in the current study (which we could not measure in previous studies due to technical limitations) strongly argues against this hypothesis because an impairment in Ca^{2+} -uptake into synaptic vesicles should not lead to a decrease in the synaptic response during an isolated action potential or stimulus train. To confirm this, I tested the effect of EGTA-AM on release induced by isolated action potentials (Figure 2-4, A-C) or action

potential trains (Figure 2-4, D-G). I pre-treated cultured neurons with EGTA-AM for at least 10 minutes before recording synaptic responses. EGTA-AM treatment suppressed release in SV2-deficient and control synapses to an almost identical relative amount (Figure 2-4, B), even though the absolute amount of release was decreased ~40% in the SV2-deficient synapses. This observation was true for release induced by isolated action potentials (~60% EGTA-induced decrease) or release induced by action potential trains (~70% EGTA-induced decrease).

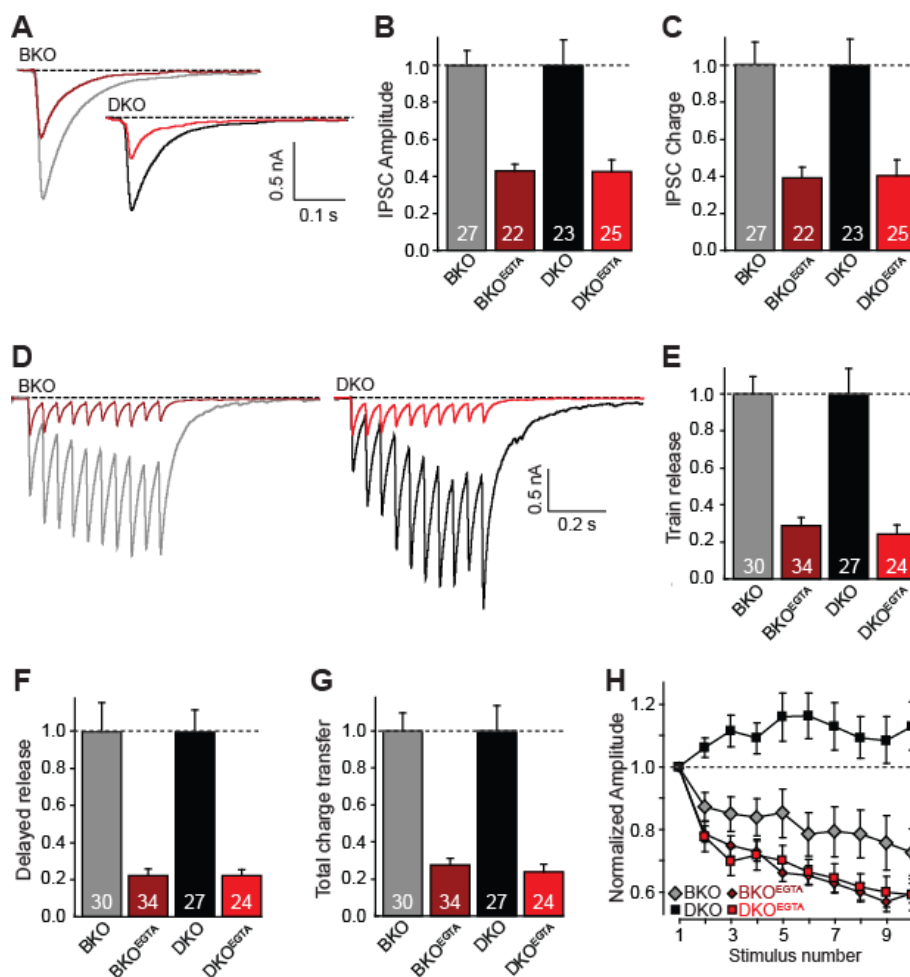


Figure 2-4 Effect of EGTA-AM on synaptic responses in SV2-deficient neurons.

(A-C) Representative traces (A) and summary graphs of the amplitudes (B) and synaptic charge transfers (C) of evoked IPSCs in neurons from SV2B KO mice (BKO) and SV2A/B double KO mice (DKO), recorded before or after pretreatment with 0.1 mM EGTA-AM (>10 min). Data are normalized for the response before the EGTA-AM treatment; no statistically significant difference in the relative effect of

EGTA-AM on the response size was detected.

(D-G) Effect of EGTA-AM on synaptic responses evoked during a 10 Hz stimulus train (1 sec). Data shown are representative traces (D) and summary graphs of the train release (E), the delayed release (F) and the total release (G). In E-G, responses are normalized for the naïve condition.

(H) Effect of EGTA-AM on the facilitation induced by deletion of SV2. The graph depicts a plot of the relative amplitude of synaptic responses as a function of the stimulus number during a 10 Hz stimulus train observed in BKO and DKO neurons.

All data shown are means \pm SEMs (n=numbers shown in bar diagrams from at least 3 independent cultures; the effect of EGTA-AM is not statistically significantly different between neurons from BKO and DKO mice; in H, n=29 for BKO synapses; n=33 for BKO synapses treated with EGTA-AM; n=26 for DKO synapse; and n=25 for DKO synapses treated with EGTA-AM; values are significantly different between naïve vs. EGTA-AM treated neurons from DKO mice at the $p < 0.0001$ level as tested by 2-way ANOVA, whereas the responses from BKO vs. DKO mice are not significantly different after EGTA-AM treatment).

However, when I examined synaptic facilitation/depression during the 10 Hz stimulus train, we found that EGTA-AM reversed the facilitation in SV2-deficient synapses which now became depressing synapses indistinguishable from control synapses (Figure 2-4, H). This observation confirms our earlier result (R. Janz et al., 1999), suggesting that EGTA-AM selectively reverses the short-term synaptic plasticity phenotype induced by deletion of SV2. Viewed together with the data in Figure 3, these results suggest that the synaptic facilitation of synaptic responses during the 10 Hz stimulus train in SV2-deficient synapses is due to accumulating Ca^{2+} triggering a larger remaining RRP.

2.3.4 The SV2 KO phenotype can be rescued by viral expression of wild-type SV2.

To investigate whether the phenotype of SV2-deficient synapses may reflect a developmental change or is related to an acute action of SV2 in synaptic transmission, I tested whether the phenotype could be rescued by expression of WT SV2A in SV2-deficient neurons. I produced lentivirus expressing an EGFP fusion protein of rat SV2A, and infected SV2-deficient neurons with this lentivirus within 7 days *in vitro* (DIV). The neurons were then analyzed at 14–17 DIV.

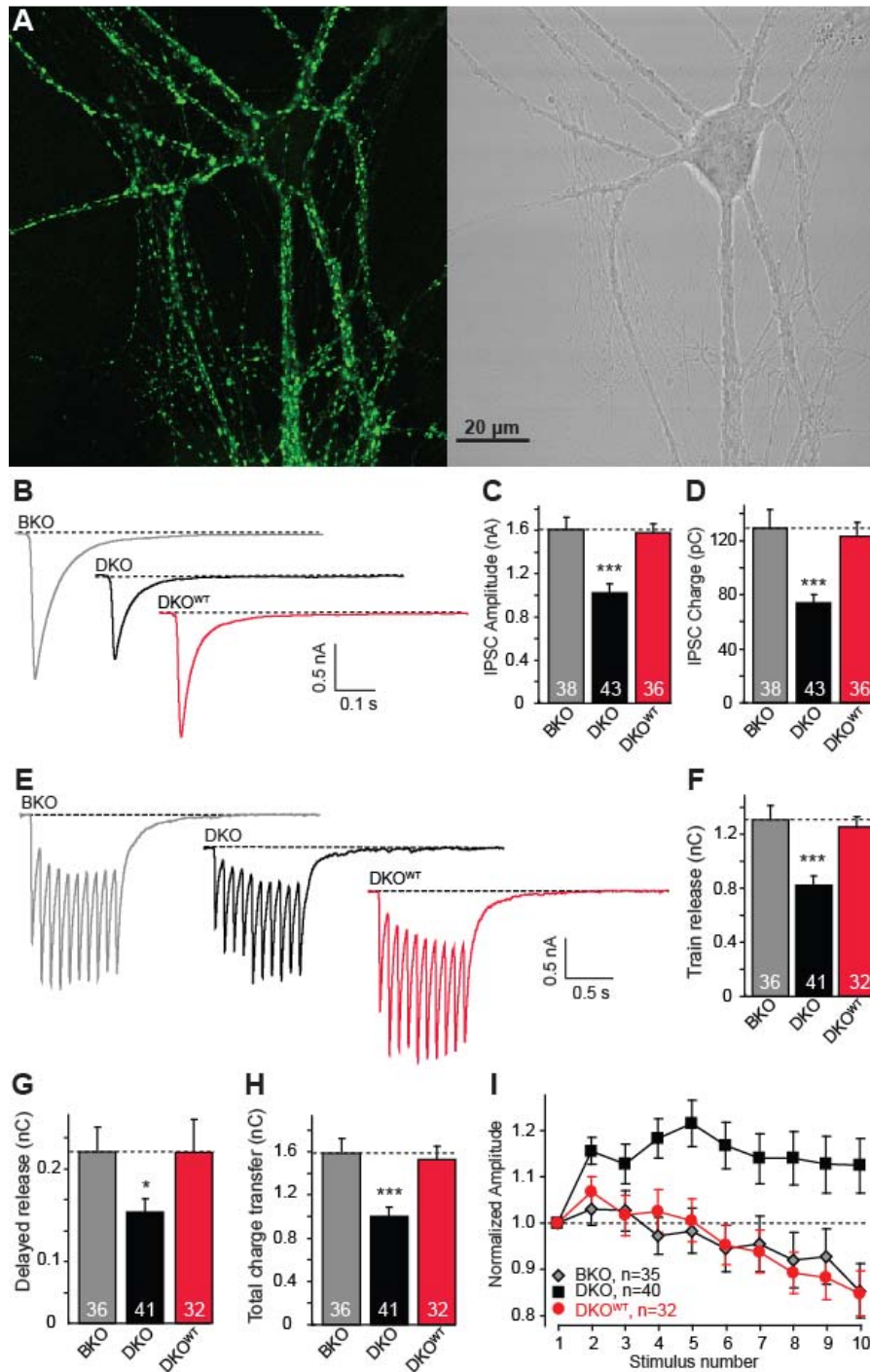


Figure 2-5 Rescue of the phenotype in SV2-deficient neurons by lentiviral expression of EGFP-tagged SV2A.

(A) Fluorescence (left) and phase contrast images (right) of neurons infected with lentivirus expressing EGFP-SV2A.

(B-D) Representative traces (B) and mean amplitudes (C) and charge transfers (D) of IPSCs evoked by extracellular stimulation at 0.1 Hz. Responses were monitored in cultured cortical neurons from littermate SV2B KO (BKO) and SV2A/SV2B double KO mice, the latter either as naïve neurons (DKO) or after

infection with wild-type EGFP-SV2A expressing lentivirus (DKO^{WT}). Action potentials were evoked with a focal electrode in a bath solution containing 1 mM Ca²⁺ and 2 mM Mg²⁺.

(E-H) Representative traces (E) and summary graphs of the charge transfer during the stimulus train (train release, F), after the train (delayed release, G), and over the entire experiment (total charge transfer, H) in the same neurons described for panel B above.

(I) Plot of the normalized amplitude as a function of the stimulus number during the 10 Hz stimulus train in BKO and DKO neurons without or with rescue

All data shown are means \pm SEMs (n=numbers shown in bar diagrams from at least 3 independent cultures; *= $p < 0.05$ and ***= $p < 0.001$ by Student's t-test; in I, n=35 for BKO neurons; n=40 for DKO neurons; and n=32 for DKO^{WT} neurons; values are significantly different between BKO and DKO neurons at the $p < 0.0001$ level as tested by 2-way ANOVA).

Fluorescence microscopy revealed that the exogenous EGFP-fusion protein of SV2 was expressed in a punctate pattern, consistent with a synaptic localization (Figure 2-5, A). Measurements of synaptic responses induced by isolated action potentials (Figure 2-5, B-D) or 10 Hz stimulus trains (Figure 2-5, E-I) demonstrated that the SV2 EGFP-fusion protein rescued all aspects of the SV2-deficiency phenotype, i.e. both the release and the short-term plasticity impairments. Thus, the EGFP-SV2 fusion protein introduced into the neurons after synapse development had been initiated was clearly fully functional, suggesting that SV2 acts acutely during release.

2.3.5 Structure-function analysis of SV2A.

Since lentivirally expressed SV2A rescues the electrophysiological SV2 deficiency phenotype, I am now in a position to investigate the structure- function relations of SV2. I employed four mutations in conserved sequences that were previously implicated in functional hypotheses about SV2 action (Figure 2-6, A).

1. In SV2A^{d107}, I deleted 107 N-terminal residues that include the conserved cytoplasmic sequence that binds to synaptotagmin (Schivell et al., 1996 and 2005; however, see Lazzell et al., 2004 for an alternative view), and coincidentally includes the epitope for the canonical SV2 antibody (S. M. Bajjalieh et al., 1992).

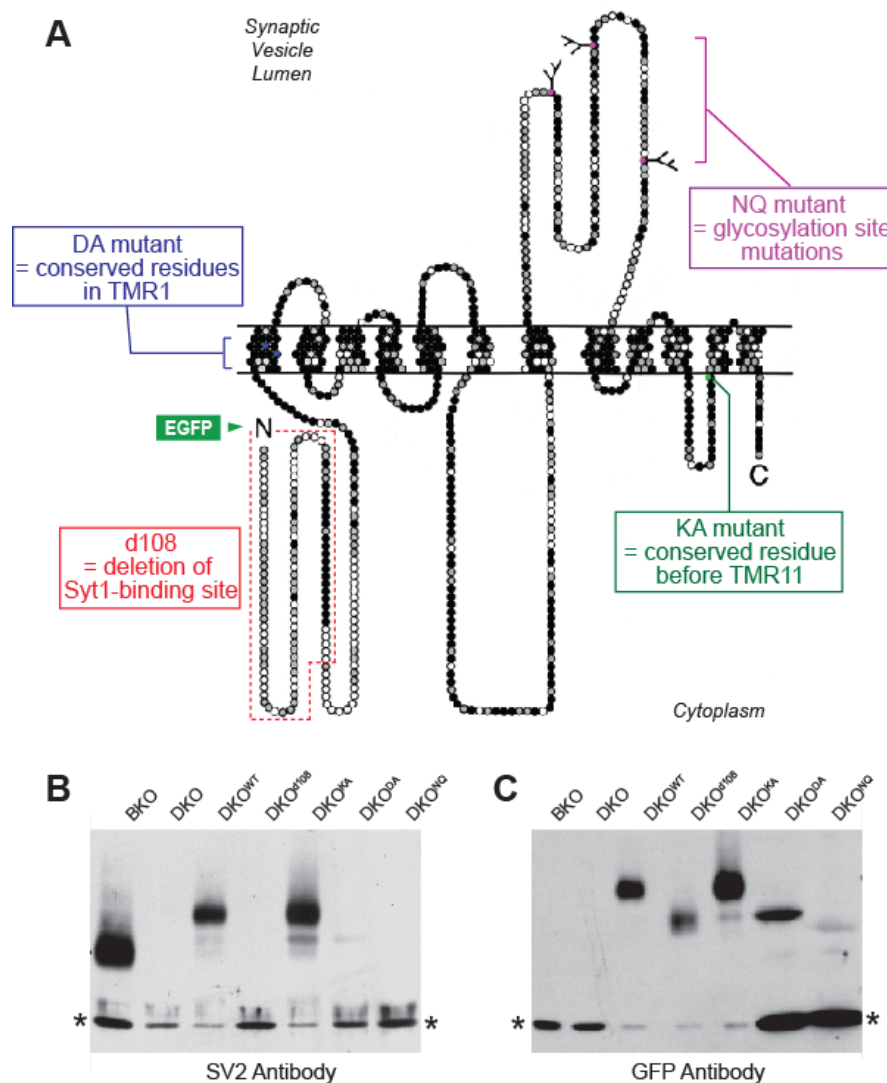


Figure 2-6 Structure and mutants of SV2A.

(A) Schematic diagram of the structure of SV2 proteins, and location of mutants analyzed in Figures 7-10. Amino acids residues in the primary sequence of SV2A are indicated by circles, with 12 potential transmembrane regions (TMRs) predicted by sequence analyses. Residues that are conserved in SV2A, SV2B, and SV2C are shown in black, residues that are identical in at least two of the three isoforms in gray and nonconserved residues in white. Branched lines show positions of N-linked carbohydrates. N- and C-termini are identified by letters (R. Janz et al., 1999). The positions of mutations are indicated with different colors: DA-mutant (D179A/E182A), blue; NQ-mutant (N498Q/N548Q/N573Q), purple; KA-mutant (K694A), green; d107-mutant (deletion of residues 1-107), red. Fluorescent protein EGFP was fused to the N-terminal of full-length or deletion of SV2A protein as indicated by green arrow.

(B, C) Immunoblot analysis of the expression of wild-type EGFP-SV2A and of various EGFP-SV2A mutants in lentiviral infected cultured neurons using antibodies to SV2 (B) and to GFP (C). All blots were additionally blotted for GDI as a loading control (bottom bands shown in the blot, indicated by asterisks); note that depending on expression levels, different amounts of protein were loaded on each lane, as is evident from the loading control.

2. In SV2A^{KA}, I substituted a highly conserved lysine residue in the fifth cytoplasmic loop of SV2 (lysine 694) for alanine.

3. In SV2A^{DA}, I substituted two conserved charged residues in TMR1 that are also present in SVOP (aspartate 179 and glutamate 182) (R. Janz et al., 1999) for alanines.

4. In SV2A^{NQ}, I substituted three asparagines that represent the conserved N-glycosylation sites in the large intravesicular loop of SV2 for glutamines (asparagine 498, asparagine 548, and asparagine 573).

All of these mutants were analyzed as EGFP-fusion proteins since EGFP-fused WT SV2A fully rescued the KO phenotype (Figure 2-5). The EGFP allowed me to directly visualize the localization of the expressed protein.

Initial tests of the expression of the various SV2 mutants in cultured neurons confirmed that all of them were produced at the expected molecular weight (Figure 2-6, B and C). However, the relative expression levels of the mutants in which the glycosylation site (SV2A^{NQ}) or the charged residues in TMR1 were substituted (SV2A^{DA}) were very low compared to WT SV2A or the other two mutant SV2A variants. This observation suggests that the mutations in the glycosylation site and in TMR1 may potentially destabilize the protein.

2.3.6 The N-terminal synaptotagmin-binding sequence is not essential for SV2 function.

I first focused on our observation that SV2 is required for Ca²⁺-triggering of vesicle exocytosis without being essential for normal priming of vesicles, which suggests an action for SV2 coincident with that of synaptotagmin, the Ca²⁺-sensor for release. Since

SV2A was reported to directly bind to synaptotagmin via a conserved N-terminal sequence (A. E. Schivell et al., 1996; A. E. Schivell et al., 2005), I tested whether this N-terminal sequence was in fact essential for rescue. We found that mutant SV2A lacking its N-terminal 107 residues (referred to as the d107-mutant) was localized to a punctate ‘synaptic’ pattern in cultured SV2-deficient neurons (Figure 2-7, A), and was fully capable of reversing the SV2 deficiency phenotype, including the decrease in release evoked by single action potentials (Figure 2-7, B and C) and by 10 Hz stimulus trains (Figure 2-7, D-G). These findings indicate that binding of the N-terminal conserved SV2 sequence to synaptotagmin is not essential for its function.

2.3.7 Lysine 694 is dispensable for SV2 function.

I next investigated the lysine 694 residue in SV2A that we mutated to alanine (referred to as the KA-mutation). Lysine 694 is located N-terminal to the 11th TMR and is conserved in all SV2 isoforms (Figure 2-6, A). Again, the KA-mutation did not abolish rescue, i.e. had no effect on either the localization of SV2A or its ability to restore normal release elicited by isolated action potentials, or 10 Hz stimulus trains of action potentials (Figure 2-8). Moreover, the short-term plasticity phenotype of the SV2 deletion was also fully rescued.

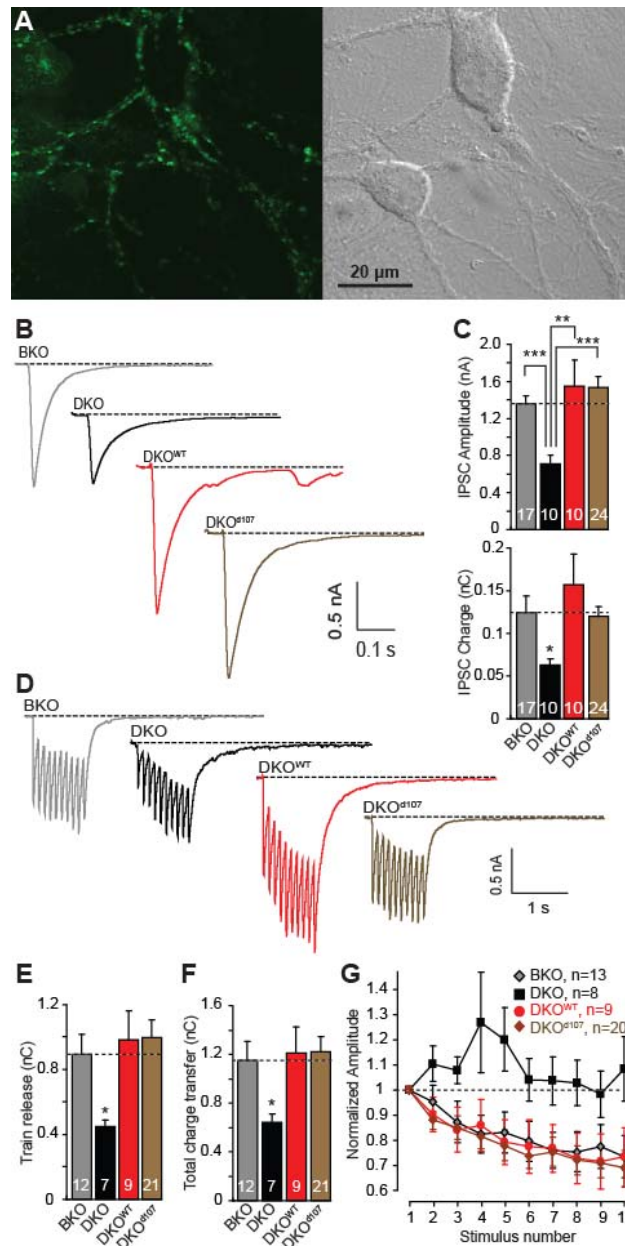


Figure 2-7 Rescue of the SV2 KO phenotype by mutant SV2A lacking the N-terminal 107 residues implicated in synaptotagmin-binding.

(A) Fluorescence (left) and phase contrast images (right) of neurons infected with lentivirus expressing d107-mutant EGFP-SV2A.

(B, C) Representative traces (B) and summary graphs (C) of IPSCs evoked by isolated action potentials in SV2B KO neurons (BKO), SV2A/B double KO neurons without rescue (DKO) or after rescue with wild-type SV2A (DKO^{WT}) or d107-mutant SV2A (DKO^{d107}).

(D-F) Representative traces (D) and summary graphs of train release (E) and total release (F) of BKO neurons and naïve and rescued DKO neurons stimulated at 10 Hz for 1 sec.

(G) Plot of the relative amplitude of synaptic responses during a 10 Hz stimulus train as a function of stimulus number in BKO neurons and naïve and rescued DKO neurons.

All data shown are means \pm SEMs (n=numbers shown in bar diagrams from at least 3 independent cultures;

*= $p < 0.05$, **= $p < 0.01$, and ***= $p < 0.001$ by Student's t-test; in G, $n=13$ for BKO synapses; $n=8$ for DKO synapses; $n=9$ for rescued DKO^{WT} synapses; and $n=20$ for DKO^{d107} neurons; values are significantly different between BKO and DKO neurons, but not between BKO and rescued DKO neurons, at the $p < 0.0001$ level as tested by 2-way ANOVA).

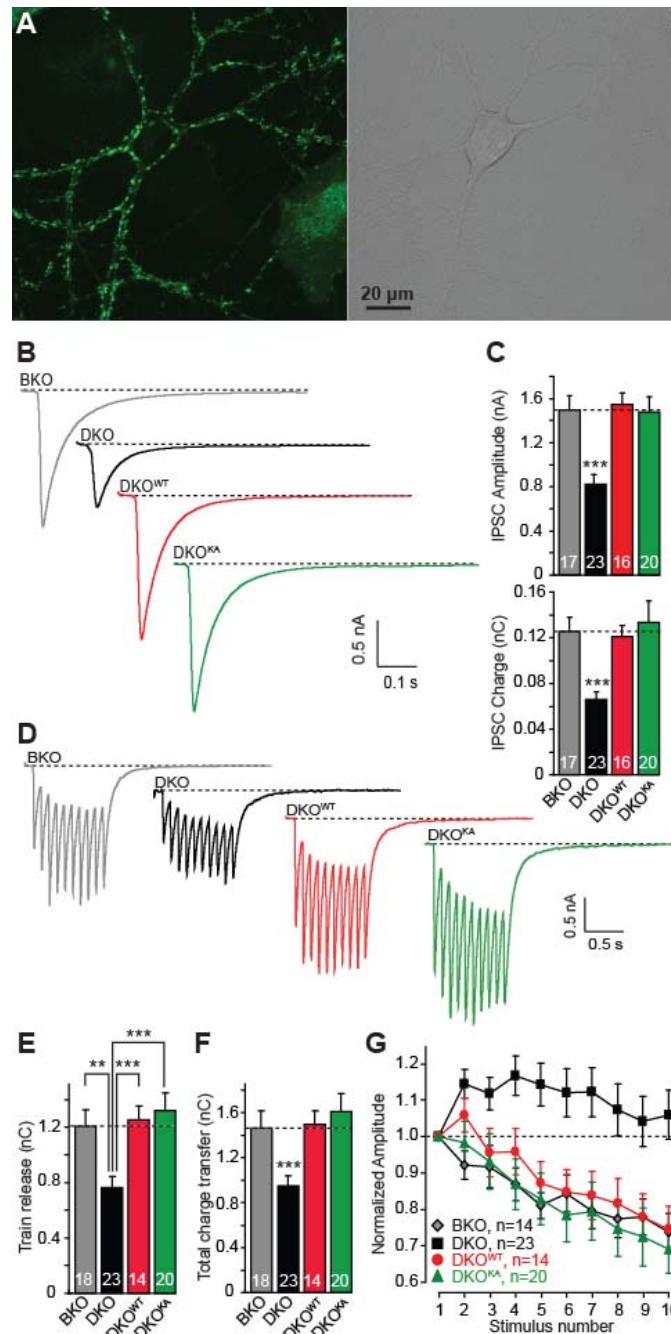


Figure 2-8 Rescue of the SV2 KO phenotype by mutant SV2A with the K694A substitution.

(A) Fluorescence (left) and phase contrast image (right) of neurons infected with lentivirus expressing KA-mutant EGFP-SV2A.

(B, C) Representative traces (B) and summary graphs (C) of IPSCs evoked by isolated action potentials in SV2B KO neurons (BKO), SV2A/B double KO neurons without rescue (DKO) or after rescue with wild-type SV2A (DKO^{WT}) or KA-mutant SV2A (DKO^{KA}).

(D-F) Representative traces (D) and summary graphs of train release (E) and total release (F) of BKO neurons and naïve and rescued DKO neurons stimulated at 10 Hz for 1 sec.

(G) Plot of the relative amplitude of synaptic responses during a 10 Hz stimulus train as a function of stimulus number in BKO neurons and naïve and rescued DKO neurons.

All data shown are means \pm SEMs (n=numbers shown in bar diagrams from at least 3 independent cultures; **= $p < 0.01$, and ***= $p < 0.001$ by Student's t-test; in G, n=14 for BKO synapses; n=23 for DKO synapses; n=14 for DKO^{WT} synapses; and n= 20 for DKO^{KA} synapses; values are significantly different between BKO and DKO neurons, but not between BKO and rescued DKO neurons, at the $p < 0.0001$ level as tested by 2-way ANOVA).

2.3.8 Mutation of charged residues in TMR1 blocks SV2 function.

Sequence analysis of the TMRs of SV2 isoforms and SVOP identified two negatively charged residues in TMR1 of these proteins (R. Janz et al., 1998; R. Janz and T. C. Südhof, 1999). The presence of charged residues in the middle of TMR1 and of multiple conserved glycine and proline residues in other TMRs fits the notion that SV2s could be transporters (R. Janz et al., 1999). Therefore, I mutated the two most conserved charged residues in a TMR1, namely aspartate 179 and glutamate 182, to alanine (D179A/E182A; referred to as the DA-mutation). Immunoblotting of cultured neurons infected with lentivirus encoding SV2A with the mutant TMR1 revealed lower levels of expression (Figure 2-6, B-D), as long as with fluorescence image demonstrated that the mutant SV2A protein failed to go into synapses, but instead exhibited a diffuse pattern that filled the entire neuron (Figure 2-9, A). These observations indicate that the charged residues in TMR1 of SV2A may be required for the normal folding and targeting of SV2A. Not surprisingly, electrophysiological analyses revealed that the mutant TMR1 SV2A was unable to rescue responses evoked by single or repeated action potentials, and did not correct the short-term plasticity phenotype (Figure 2-9, B-G). Thus the two charged residues in TMR1 are essential for the normal structure and function of SV2A.

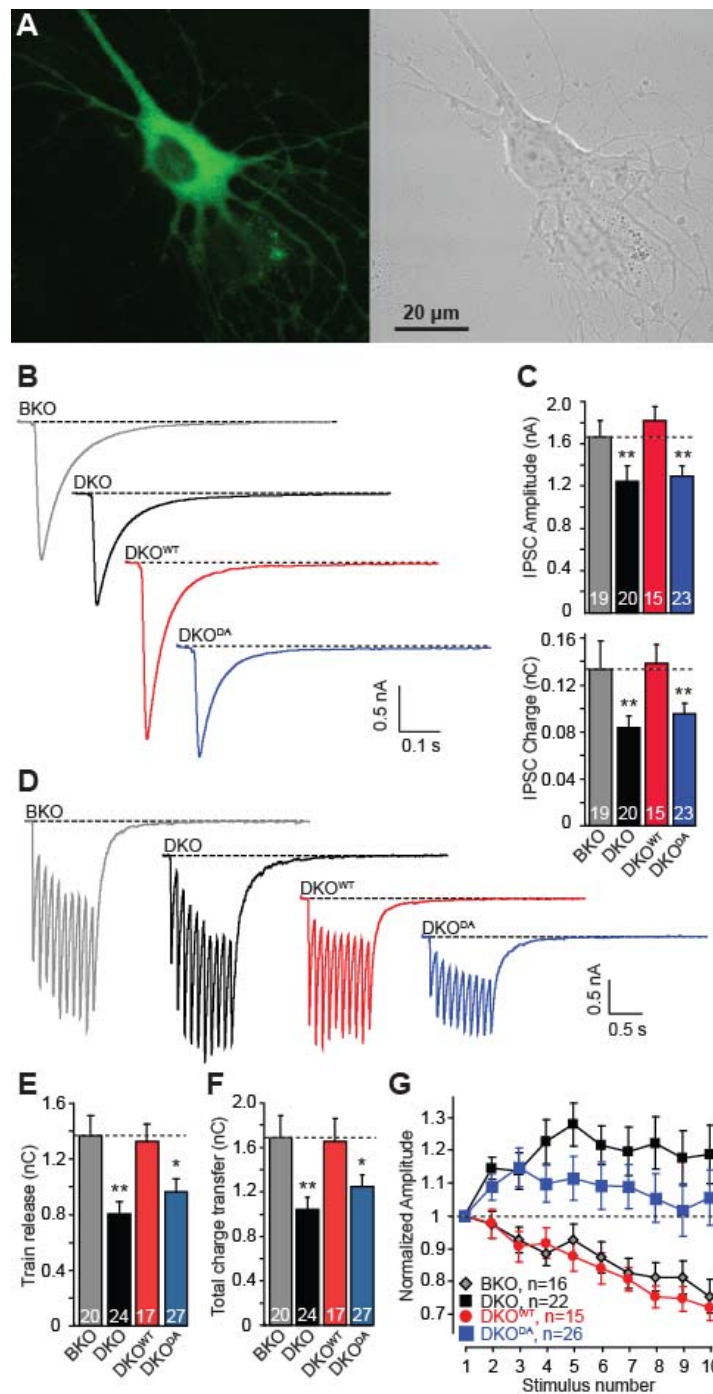


Figure 2-9 Lack of rescue of the SV2 KO phenotype by DA-mutant SV2A containing a double amino-acid substitution in TMR1 (D179A/E182A).

(A) Fluorescence (left) and phase contrast images (right) of neurons infected with lentivirus expressing DA-mutant EGFP-SV2A.

(B, C) Representative traces (B) and summary graphs (C) of IPSCs evoked by isolated action potentials in

SV2B KO neurons (BKO), SV2A/B double KO neurons without rescue (DKO) or after rescue with wild-type SV2A (DKO^{WT}) or DA-mutant SV2A (DKO^{DA}). (D-F) Representative traces (D) and summary graphs of train release (E) and total release (F) of BKO neurons and naïve and rescued DKO neurons stimulated at 10 Hz for 1 sec. (G) Plot of the relative amplitude of synaptic responses during a 10 Hz stimulus train as a function of stimulus number in BKO neurons and naïve and rescued DKO neurons. All data shown are means \pm SEMs (n=numbers shown in bar diagrams from at least 3 independent cultures; *= $p < 0.05$, and **= $p < 0.01$ by Student's t-test; in G, n=16 for BKO neurons; n=22 for DKO neurons; n=15 for DKO^{WT} neurons; and n=26 for DKO^{DA} neurons; values are significantly different between BKO and DKO neurons, but not between DKO and DKO^{DA} rescued neurons, at the $p < 0.0001$ level as tested by 2-way ANOVA).

2.3.9 Blocking SV2 glycosylation abolishes SV2 function.

It was proposed that the three N-glycosylation consensus sequences in the large intravesicular loop of SV2 serve as glycosaminoglycan attachment sequences in SV2 (R. Janz et al., 1999), but the importance of this N-glycosylation, even its very dependence on the putative N-glycosylation sequences, was never examined. To test this question, and to probe the functional significance of SV2 glycosylation, I mutated the three asparagines in these consensus sequences to glutamines (Figure 2-6, A; N498Q/N548Q/N573Q; referred to as the NQ-mutation). Immunoblotting of the expressed intravesicular loop mutant of SV2A (SV2A^{NQ}) showed that the levels of the mutant protein were dramatically decreased, suggesting that without N-glycosylation, SV2 may not be targeted correctly and be unstable. Consistent with this notion, the localization of the mutant SV2A in neurons was strikingly abnormal: this mutant SV2A variant was not synaptic like WT SV2A, nor was it uniformly distributed throughout the cytoplasm like the TMR1 mutant, but present in larger concentrations, possibly aggresomes, throughout the neuron (Figure 2-10, A). As expected from this mislocalization, I observed no rescue of SV2 function in neurons lacking SV2A and SV2B that expressed this mutant of SV2A (Figure 2-10, B-G). Thus N-glycosylation of SV2A is essential for its normal processing and possibly folding.

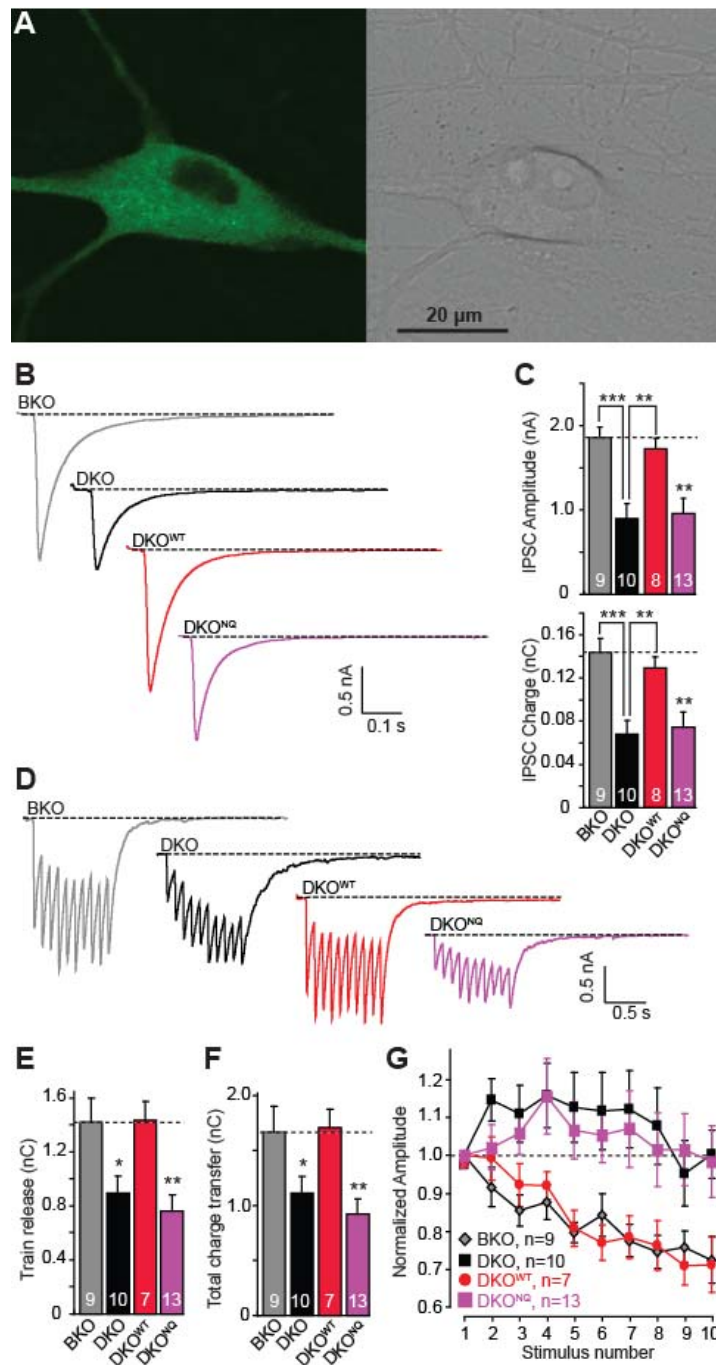


Figure 2-10 Lack of rescue of the SV2 KO phenotype by NQ-mutant SV2A in which the N-glycosylation sites in the intravesicular loop were substituted (N498Q/N548Q/N573Q).

(A) Fluorescence (left) and phase contrast images (right) of neurons infected with lentivirus expressing NQ-mutant EGFP-SV2A.

(B, C) Representative traces (B) and summary graphs (C) of IPSCs evoked by isolated action potentials in SV2B KO neurons (BKO), SV2A/B double KO neurons without rescue (DKO) or after rescue with

wild-type SV2A (DKO^{WT}) or NQ-mutant SV2A (DKO^{NQ}).

(D-F) Representative traces (D) and summary graphs of train release (E) and total release (F) of BKO neurons and naïve and rescued DKO neurons stimulated at 10 Hz for 1 sec.

(G) Plot of the relative amplitude of synaptic responses during a 10 Hz stimulus train as a function of stimulus number in BKO neurons and naïve and rescued DKO neurons.

All data shown are means \pm SEMs (n=numbers shown in bar diagrams from at least 3 independent cultures; *= $p<0.05$, **= $p<0.01$, and ***= $p<0.001$ by Student's t-test; in G, n=9 for BKO synapses; n=10 for DKO synapses; n=7 for DKO^{WT} synapses; and n=13 for DKO^{NQ} synapses; values are significantly different between BKO and DKO neurons, but not between DKO and DKO^{NQ} rescued DKO neurons, at the $p<0.0001$ level as tested by 2-way ANOVA).

2.4 Discussion

SV2 is one of the most interesting and enigmatic synaptic vesicle proteins.

Interesting, because its structure suggests a sugar transporter that introduces into the synaptic vesicle lumen a large glycosaminoglycan, and because its deletion induces epilepsy whereas leviracetam, a drug binding to SV2, is therapeutically active against epilepsy (K. Buckley and R. B. Kelly, 1985; S. M. Bajjalieh et al., 1992; M. B. Feany et al., 1992; J. A. Gingrich et al., 1992; S. M. Bajjalieh et al., 1993; K. M. Crowder et al., 1999; R. Janz et al., 1999; R. Janz and T. C. Südhof, 1999; B. A. Lynch et al., 2004; K. L. Custer et al., 2006). Enigmatic, because it is not conserved in invertebrates, has no identified transporter function, and produces a severe KO phenotype that is difficult to interpret. In the present study, I aimed towards a better understanding of SV2 by studying its KO phenotype, and to gain further insight into its function by analysis of four mutants in previously identified functionally important sequences.

2.4.1 Dissection of the SV2 KO phenotype.

Consistent with earlier studies studying excitatory synapses (Janz et al., 1999; Crowder et al., 1999; Custer et al., 2006), I observed that deletion of SV2 causes a large loss of evoked neurotransmitter release (Figures 2-2 and 2-3), and a change in short-term

synaptic plasticity as manifested by the facilitation observed during 10 Hz stimulus trains (Figure 3). Specifically, five principal observations were made:

1. SV2 performs similar essential functions in both inhibitory synapses (this work) and excitatory synapses (previous studies)
2. Deletion of SV2 decreases the size of synaptic responses evoked by isolated and by repeated action potentials (Figures 2-2 and 2-3). It equally decreases synchronous and asynchronous release, with the facilitation observed during high-frequency stimulus trains resulting from the accumulation of residual Ca^{2+} acting on a relatively larger residual RRP.
3. The SV2 deletion did not change the size of the RRP, either when measured with neurons that were constitutively active in a high-density cellular network, or after neuronal activity was blocked for 24 hrs with TTX (Figure 2-2). This lack of a change is consistent with the lack of a change in mini frequency in the SV2-deficient synapses (Figure 2-1).
4. The SV2 deletion also did not cause a change in apparent Ca^{2+} -affinity of synapses. This is surprising because an overall decrease in release is usually caused by a change in either the size of the RRP and/or the efficacy of Ca^{2+} -triggering which in turn usually manifests as a change in apparent Ca^{2+} -affinity (see discussion below).
5. EGTA-AM, a drug that lowers the bulk cytoplasmic Ca^{2+} -concentration, strongly suppressed both isolated responses and responses induced by the stimulus train, and acted equally in SV2-deficient and control synapses (Figure 2-4). Strikingly, EGTA-AM reversed the facilitation of synaptic responses observed during 10 Hz stimulus trains in SV2-deficient synapses, consistent with the notion that the facilitation is due to

accumulation of residual Ca^{2+} .

These results generally agree with previous studies on SV2-deficient synapses analyzed in autapses (R. Janz et al., 1999; K. L. Custer et al., 2006). Different from *Custer et al.* (K. L. Custer et al., 2006), however, I do not observe a decrease in the RRP or a rescue of the release phenotype by accumulating Ca^{2+} during stimulus trains. The lack of a change in the RRP by deletion of SV2 is supported by the finding that the mini frequency is unchanged (Figure 2-1), as also previously reported by *Custer et al.* (K. L. Custer et al., 2006). A possible explanation for the lack of a change in RRP could have been that the continuous network activity in our cultures creates a permanent state of ‘accumulating Ca^{2+} ’ that might rescue the phenotype. However, chronic treatment of our cultures with TTX which blocks continuous network activity did not alter the lack of an RRP phenotype (Figure 2-2). Another possible explanation for the differences between our and *Custer et al.* (K. L. Custer et al., 2006) results is that I analyzed inhibitory synapses but *Custer et al.* (K. L. Custer et al., 2006) studied excitatory synapses. However, the decrease in release I observed in inhibitory synapses precisely matches that detected by *Custer et al.* (K. L. Custer et al., 2006) in excitatory synapses, suggesting that the SV2 KO phenotype is the same between the two types of synapses. A third possible explanation for the discrepancy in the phenotype I observed vs. that reported by *Custer et al.* (K. L. Custer et al., 2006) is that I study interneuronal synapses, whereas *Custer et al.* (K. L. Custer et al., 2006) examined autapses. This hypothesis is consistent with the fact that the dynamics of accumulating Ca^{2+} during a stimulus train is likely to differ between autapses and interneuronal synapses because in the former, pre- and postsynaptic neurons are one and the same, whereas in the latter, only the presynaptic neuron is excited. Lastly,

the difference in results may be due to the fact that I studied dissociated cortical neuron whereas *Custer et al.* (K. L. Custer et al., 2006) analyzed hippocampal neurons. Although SV2A is ubiquitously expressed in all neurons, recording from different types of neurons may be another possibility for different observations.

2.4.2 Structure-function analysis of SV2A.

The three SV2 isoforms are extremely similar, and can be thought of containing four conserved elements: the N-terminal sequence bearing the epitope of the original SV2 monoclonal antibody that reacts with all isoforms; the membrane-associated sequences with the 12 TMRs and the small loops connecting them; the large intravesicular loop that is N-glycosylated but otherwise exhibits major variations between the different isoforms; and the large cytoplasmic loop (R. Janz et al., 1999). Three of these four conserved elements were previously associated with functional hypotheses that were tested in the present experiments: the N-terminal sequence was shown to bind synaptotagmin (Schivell et al., 1996 and 2005; Pyle et al., 2000; but see Lazell et al., 2004), the transmembrane sequence were hypothesized to function as transporters due to their homology to sugar transporter proteins (S. M. Bajjalieh et al., 1992; M. B. Feany et al., 1992; J. A. Gingrich et al., 1992; S. M. Bajjalieh et al., 1993; R. Janz and T. C. Südhof, 1999), and the glycosylated intravesicular sequence was thought to mediate vesicle stability and neurotransmitter storage (T. W. Scranton et al., 1993; R. Janz and T. C. Südhof, 1999; D. Reigada et al., 2003). My data reveal that the N-terminal synaptotagmin-binding sequence containing the SV2-antibody epitope is dispensable for the ability of the SV2A to rescue the SV2 KO phenotype (Figure 2-7), but that mutations

of conserved charged residues in the TMR1 that are likely to be central for a presumed transporter function or of the N-glycosylation sites in the intravesicular sequence loop of SV2A abolished its function (Figures 2-9 and 2-10). Both of these mutations destabilized SV2A as indicated by decreased expression levels in infected culture neurons, and abolished the targeting of SV2 to synapses as indicated by imaging in neurons expressing the mutant SV2A. Thus, it is likely that these mutations inactivated SV2A by impairing the folding and targeting of SV2A, suggesting that one of the functions of the sequences involved is to allow the correct conformation of SV2A required for its normal transport into synaptic vesicles.

2.4.3 The function of SV2.

My data clarify old hypotheses regarding SV2 function, but also raise new questions. Specifically, the lack of rescue of the neurotransmitter release phenotype by the intracellular Ca^{2+} -buffer EGTA-AM (Figure 2-4), manifested in the identical relative suppression of synaptic transmission by EGTA-AM in control and SV2-deficient synapses, suggests that SV2 does not primarily function as a Ca^{2+} -transporter during stimulus trains as we hypothesized earlier (R. Janz et al., 1999), but acts even at resting Ca^{2+} -concentrations. The fact that the phenotype can be rescued by expression of EGFP-tagged SV2A demonstrates that it is a functional and not a developmental change that causes the phenotype (Figure 2-5). The lack of an effect of the SV2 deletion on the apparent Ca^{2+} -affinity of release and the full rescue of release upon expression of the N-terminally deleted SV2 indicate that synaptotagmin-binding by SV2 is not functionally essential. Similarly, the lack of an effect of the SV2 deletion on the RRP size indicates

that SV2 is not yet another priming factor.

In view of all these actions that SV2 does not do, the question arises what it actually does do. The selective nature of the release phenotype I observed in SV2-deficient synapses is surprising in that it does not conform to our current models of release. I show that the SV2 deletion causes a substantial loss of release that operates downstream of synaptic vesicle priming (since the size of the RRP, and the amplitude and frequency of mEPSCs and mIPSCs were unchanged (Figures 2-1 and 2-2), but upstream of Ca^{2+} -triggering of release (since the Ca^{2+} -sensitivity and kinetics of release were also unchanged (Figure 2-2), and since the relative loss of release was not altered by accumulating Ca^{2+} during stimulus trains (Figure 2-4)). Moreover, both synchronous and asynchronous releases are impaired (Figure 2-3). The most parsimonious and plausible hypothesis to account for this phenotype is that the SV2 KO impairs the transition of synaptic vesicles from a primed but relatively Ca^{2+} -insensitive state into a Ca^{2+} -competent state. According to this hypothesis, SV2 normally functions to render primed synaptic vesicles responsive to triggering by both the synchronous Ca^{2+} -sensor (i.e., synaptotagmin) (R. Fernandez-Chacon et al., 2001), and the asynchronous Ca^{2+} -sensor (which is unknown – see *Sun et al.*) (J. Sun et al., 2007). As such an ‘efficiency factor’, SV2 may not be required in invertebrate synapses, accounting for its relatively recent evolutionary appearance. Among others, such a role would also indicate that the RRP as measured by stimulation with hypertonic sucrose and continuous increases in the intracellular Ca^{2+} -concentration are not necessarily identical, since they are separated by an SV2-dependent step.

CHAPTER III: MUNC18-1 BINDING TO THE NEURONAL SNARE COMPLEX CONTROLS SYNAPTIC VESICLE PRIMING

3.1 Introductions

Genetic study has demonstrated that Munc18-1 is absolutely required for vesicle fusion (M. Verhage et al., 2000). Meanwhile, biochemical studies of Munc18-1 also revealed protein interactions that are important for its biological function. Munc18-1 has been shown to bind to the closed conformation of syntaxin-1 (K. M. Misura et al., 2000), as well as to the N-terminal sequence of syntaxin-1 (A. Bracher and W. Weissenhorn, 2002; I. Dulubova et al., 2002; T. Yamaguchi et al., 2002; L. N. Carpp et al., 2006; S. H. Hu et al., 2007), the later, unlike the former binding, is compatible and even essential for Munc18-1-SNARE interaction and thus SNARE complex formation (C. Rickman et al., 2007; J. Shen et al., 2007). Recently, *in vitro* binding assay and structure studies have provided compelling evidence that Munc18-1, similar to other SM proteins, binds to assembled SNARE complex (E. Connell et al., 2007; I. Dulubova et al., 2007; C. F. Latham et al., 2007; C. Rickman et al., 2007; J. Shen et al., 2007). However, although many studies have given more insight implications of physiological relevance of Munc18-1/syntaxin-1 binary complex and Munc18-1/SNARE complex assembly in vesicle fusion, no direct evidence has been presented.

A key function for binding of Munc18-1 to SNARE complexes was suggested by the observation that Munc18-1 enhances SNARE-induced liposome fusion (J. Shen et al., 2007); however, in contrast to the *in vivo* situation (M. Verhage et al., 2000), no strict

requirement of Munc18-1 for fusion was observed, and no precise correlation between binding and fusion enhancement was established. Moreover, since *in vitro* liposome fusion assay does not represent some basic aspects of neurotransmitter release (J. Rizo et al., 2006; J. Shen et al., 2007), the results from this assay should be viewed with caution. Recently, we showed that the interaction of the syntaxin-1 N-terminal sequence with diverse Munc18 isoforms is critical for exocytosis, however, it was not clarified that when and how this interaction becomes crucial for fusion (M. Khvotchev et al., 2007). Therefore, it is currently unclear whether the binding of Munc18-1 to either syntaxin-1 alone and/or to SNARE complexes is required in vesicle fusion, and little is known about which, if any, steps of vesicle fusion is controlled by these interactions.

Perhaps the most definitive approach to prove the functional relevance of a protein-protein interaction is to correlate the effects of point mutations on the interaction with their physiological consequences in living cells. Application of this approach to Munc18-1/SNARE interactions has been hindered because Munc18-1 deficient neurons die early (M. Verhage et al., 2000), and are thus difficult to analyze. In this study, we have overcome this problem by establishing a lentiviral infection system, through which we were able to express WT Munc18-1 in neurons from Munc18-1 knockout mice and rescue the neuron survival and phenotypes. We then designed mutations in WT Munc18-1 that differentially disrupt the Munc18-1/SNARE complex interaction while still retaining tight binding of Munc18-1 to syntaxin-1. All mutations were able to rescue neuronal survival while having different effects on neurotransmitter release. Our results show that the mutations cause differential impairments of release that clearly correlated with the disruption of Munc18-1/SNARE complex binding. Our data also show that

Munc18-1/SNARE complex interactions are critical for vesicle priming and support the general functional importance of SM protein/SNARE complex assemblies for membrane traffic.

3.2 Materials and Methods

3.2.1 Constructs

Bacterial expression vectors to express full-length rat Munc18-1 and fragments corresponding to the cytoplasmic region of rat syntaxin-1A (residues 2-253), and to the SNARE motifs of rat synaptobrevin-2 (29-93) and human SNAP-25B (11-82 and 141-203) as GST-fusion proteins were described previously (X. Chen et al., 2002; I. Dulubova et al., 2007). Analogous vectors to express full-length rat Munc18-1 point mutants (E59K, K63E and E66A), were generated from the WT construct using the QuickChange site-directed mutagenesis kit (Stratagene) and custom designed primers, and verified by sequencing. For the construction of Munc18-1-24-cerulean constructs, a Munc18-1 (aa 1-24) fragment was first generated by PCR to introduce EcoRI and SseI cloning sites at the N- and C- termini, and then a Munc18-1 (aa 25-601) fragment was produced by PCR to introduce BsrGI and XbaI cloning sites to at N- and C- terminus. These two PCR products were then inserted to the N-terminus and C-terminus of cerulean, respectively, on a PCMV5-cerulean vector. The cDNAs of WT and mutant Munc18-1-24-cerulean versions were subcloned between the EcoRI and BamHI sites into the pFUGW shuttle vector for virus production.

3.2.2 Preparation of recombinant proteins and SNARE complex

Syntaxin-1A (2-253), synaptobrevin-2 (29-93), SNAP-25 (11-82), SNAP-25 (141-203), and WT and mutant full-length Munc18-1 were expressed in bacteria as GST-fusion proteins, isolated by affinity chromatography, cleaved with thrombin and purified by ion exchange or gel filtration chromatography as described (I. Dulubova et al., 1999; X. Chen et al., 2002; I. Dulubova et al., 2007). Uniform ^{13}C -labeling of syntaxin-1A (2-253) was accomplished by expression in bacteria using $^{13}\text{C}_6$ -glucose as the sole carbon source. SNARE complexes were prepared by overnight incubation of the four purified SNARE fragments [with the syntaxin-1A (2-253) fragment ^{13}C -labeled] and further purification by gel filtration on a Superdex 200 column (Amersham Biosciences) in PBS (pH 7.4) containing 2mM TCEP (I. Dulubova et al., 2007).

3.2.3 ITC

isothermal titration calorimetry (ITC) experiments were performed using a VP-ITC system (MicroCal) at 20°C in PBS (pH 7.4) containing 2 mM TCEP with samples of 5-10 μM WT or mutant Munc 18-1s in the sample cell and successive injections of 100-150 μM syntaxin-1A (2-253). All proteins were purified by gel filtration on a Superdex 200 column (Amersham Biosciences) in the same buffer before the experiments. After polynomial baseline correction of the initial data points, the data were fitted with a nonlinear least squares routine using a single-site binding model with Origin for ITC v.5.0 (Microcal).

3.2.4 NMR experiments

1D ^{13}C -edited ^1H NMR spectra were acquired on a Varian INOV A600 spectrometer

at 25°C in 20 mM sodium phosphate pH 7.1, 150 mM NaCl and 2 mM DTT, acquiring the first trace of a ^1H - ^{13}C HSQC spectrum (1,500 scans; 30 min total acquisition time). For the titrations, samples contained 2 μM SNARE complex [with uniformly ^{13}C -labeled syntaxin-1A (2-253) or 2 μM ^{13}C -labeled syntaxin-1A (2-253) and the desired concentration of unlabeled WT or mutant Munc18-1s; a separate sample was prepared for each concentration. The data were fit to a single-site binding model using Sigma Plot (D. Arac et al., 2003).

3.2.5 Cortical cultures

Homozygote Munc18-1 KO mice were bred by crossing heterozygous mutant Munc18-1 KO mice (M. Verhage et al., 2000). Cortical neurons from littermate mice at embryonic day 16 (E16) were dissociated by trypsin (5 mg/ml for 5 min at 37°C), triturated with a siliconized Pasteur pipette, and plated onto 12 mm coverslips coated with Matrigel (~12 coverslips/cortex). Neurons were cultured at 37°C in a humidified incubator with 95%-air, 5%-CO₂ in Minimal Essential Media containing 5 g/l glucose, 0.1 g/l transferrin, 0.25 g/l insulin, 0.3 g/l glutamine, 5-10% heat inactivated FCS, 2% B-27 supplement and 1 μM cytosine arabinoside, and used after 5-22 days in vitro.

3.2.6 Lentiviral infection

Constructs were co-transfected with plasmids for viral envelop and enzymes into HEK 293 cells using of FuGENE6 transfection system (Roche Molecular Biochemicals) according to the manufacturer's specifications, and lentivirus containing culture medium was harvested two days later, filtered through 0.45 μm pores and immediately used for

infection or frozen in liquid nitrogen and stored at -80°C . Cortical cultures were infected at day one in vitro by adding 300 μl of viral suspension to each well.

3.2.7 Immunocytochemistry

Neurons attached to the glass coverslips were rinsed once in PBS, fixed for 15 min on ice in 4% formaldehyde, 4% sucrose in PBS. After fixation, the neurons were washed with PBS twice, and then incubated for 30 min in blocking solution, PBS containing 3% milk, 0.1% saponin, and in PBS, followed by 1-h incubation with primary and rhodamine- and FITC-conjugated secondary antibodies diluted in blocking solution. The coverslips were then mounted on glass slides with Aqua-Poly/Mount medium (Polysciences, Inc.) and analyzed at room temperature using a confocal microscope (DMIRE2; Leica) and 63x/1.32NA oil immersion objective. The images were collected using confocal software (Leica) and processed using Photoshop software (Adobe). All digital manipulations were equally applied to the entire image.

3.2.8 Fluorescence imaging

Modified Tyrode bath solution (in mM: 150 NaCl, 4 KCl, 2MgCl₂, 10 glucose, 10 HEPES-NaOH pH 7.4 0.01 CNQX, 0.05 AP-5, and 2 CaCl₂ ~310 mOsm) was used in all experiments. Synaptic boutons were loaded with FM2-10 (400 μM ; Molecular Probes, Eugene, OR) by a 90 s exposure to 47 mM K⁺/2 mM Ca²⁺; full destaining was triggered with a hyperkalemic bath solution containing 90 mM KCl substituted for NaCl. Images were taken after 10 min wash in dye-free, nominally Ca²⁺-free solution to minimize spontaneous release. In all experiments, isolated boutons ($\sim 1 \mu\text{m}^2$) were selected for

analysis. Synaptic vesicle fusion was induced by gravity perfusion of hyperkalemic solution onto the field of interest (1-2 ml/min) for 60 sec, followed by nominal Ca^{2+} -free Tyrode perfusion for 60 sec again. Images were acquired with a cooled CCD camera (Roper scientific, Trenton, NJ) during illumination (1 Hz and 200 msec) at 480 ± 20 nm (505 dichroic longpass and 534 ± 25 bandpass) via an optical switch (Sutter Instruments, Novato, CA), and analyzed using Metafluor Software (Universal Imaging, Downingtown, PA). Background staining levels determined after five consecutive rounds of high K^+ application were subtracted from all fluorescence images.

3.2.9 Electrophysiology

Synaptic responses were recorded from pyramidal cells in modified Tyrode bath solution in the whole-cell patch configuration. The solution routinely contained 50-100 μM picrotoxin to block inhibitory synaptic currents via GABA receptors. For spontaneous release experiments (F. Deak et al., 2006), 1 μM of tetrodotoxin to inhibit voltage gated sodium channels and action potential propagation. For evoked responses, tetrodotoxin was omitted from the bath. Data were acquired with an Axopatch 200B amplifier and Clampex 8.0 software (Molecular Devices, Union City, CA), filtered at 2 kHz, and sampled at 200 μsec . The internal pipette solution included (in mM): 115 Cs-MeSO₃, 10 CsCl, 5 NaCl, 0.1 CaCl₂, 10 HEPES, 4 Cs-BAPTA, 20 TEA-Cl, 4 Mg-ATP, 0.3 mM Na₂-guanosine-triphosphate, and 10 lidocaine *N*-ethylbromide, pH 7.35 (300 mOsm). A hypertonic solution, prepared by addition of 500 mM sucrose to the nominally Ca^{2+} -free Tyrode solution, was perfused directly into the close vicinity of the cell where the recording was made from. Field stimulations (24 mA pulses of 0.6 ms)

were applied with parallel platinum electrodes immersed into the perfusion chamber.

3.2.10 Data analysis

Evoked responses were adjusted with baseline subtraction for each stimulus. Synchronized responses were determined as those within 100 ms of stimulus; transferred charge was also calculated for this period. Normal distribution of data was analyzed with the Shapiro-Wilk's W test. Paired Student t-test or variance analysis followed with Tukey-test was used to determine significance, which is marked on the figures as asterisk: * equals to $p < 0.05$, ** to $p < 0.01$ and *** to $p < 0.005$ levels of significance.

3.3 Results

3.3.1 Design of mutations to distinguish Munc18-1/SNARE interactions.

The X-ray structure of the syntaxin-1/Munc18-1 complex revealed that Munc18-1 is an arch shape protein and in its cavity binds to the closed form of syntaxin-1 (K. M. Misura et al., 2000) (Figure 3-1, B). The N-terminal domain of Munc18-1 (in cyan in Figure 3-1, B) makes extensive interactions with the H_{abc} domain and the SNARE motif of syntaxin-1 (in orange and yellow, respectively, in Figure 3-1, B) and is essential for the interaction. The binding of Munc18-1 and the N-terminal of syntaxin-1 was not resolved in the crystal structure, but also participates in the binding (M. Khvotchev et al., 2007). Although high resolution structure of the Munc18-1/SNARE complex is not available, NMR data showed that formation of the complex involves the syntaxin-1 N-terminal sequence and H_{abc} domain, as well as the four-helix bundle formed by the SNARE motifs (I. Dulubova et al., 2007) (Figure 3-1, A, right), suggesting that the interactions of

Munc18-1 with the syntaxin-1 C-terminus must switch dramatically in the transition between the two complexes, whereas interactions with the N-terminal sequence and H_{abc} domain may involve similar residues in both complexes. Due to the rearrangement of syntaxin-1 C-terminal, the energetic contributions of individual interactions to binding are likely to be remodeled during the transition between the two complexes.

Based on these observations, we selected three residues (E59, K63 and E66) at the Munc18-1 N-terminal domain for mutagenesis study. These residues are located close to the binding interface, and make contacts with the syntaxin-1 H_{abc} domain (E59), the SNARE motif (K63) or both (E66), respectively (Figure 3-1, B). Modification of these residues may generate different effects on Munc18-1 binding to syntaxin-1 and/or the SNARE complex. Thus, we prepared WT Munc18-1 and three point mutants of Munc18-1 bearing substitutions of each of these three residues; among which E69K and K63E were reversed the charges of the residues to enhance their disruptive effects while the E66A mutation only neutralized the charge for a more moderate effect.

We tested the effects of the three Munc18-1 mutants on the affinity of the binary Munc18-1/syntaxin-1 complex using isothermal titration calorimetry (ITC). Tight binding in the nanomolar range was observed for WT Munc18-1 and the three mutants (Figure 3-2) with the following k_D values: WT, 2.4 nM; E59K, 25 nM; E66A, 3.0 nM; K63E, 10.5 nM. These values should be interpreted with caution because of the intrinsic difficulty of obtaining accurate measurements for such high affinities and because the WT Munc18-1 and the three mutants are rather unstable, and often partially precipitated, at the concentrations required for these experiments (5-10 μ M). This is likely the reason that a drift in the initial enthalpies per mol of injected syntaxin-1 in some of the ITC

experiments was observed. In order to remove this drift, we used polynomial baseline correction to obtain good fits of the data to a standard one-site binding model, without substantially altering the k_D values obtained without the baseline correction (exemplified for the E66A mutant in Figure 3-2, C). These problems led to variability in the k_D s measured in multiple experiments, and as a result, the poorer the quality of data, the weaker the affinities measured (the highest k_D s measured were 20 nM for WT, 88 nM for E59K, 60 nM for K63E, and 26 nM for E66A). Despite the variability of the data, it is still clear that all three Munc18-1 mutants retain tight binding to syntaxin-1, although the bindings of E59K and K63E appear to be weaker.

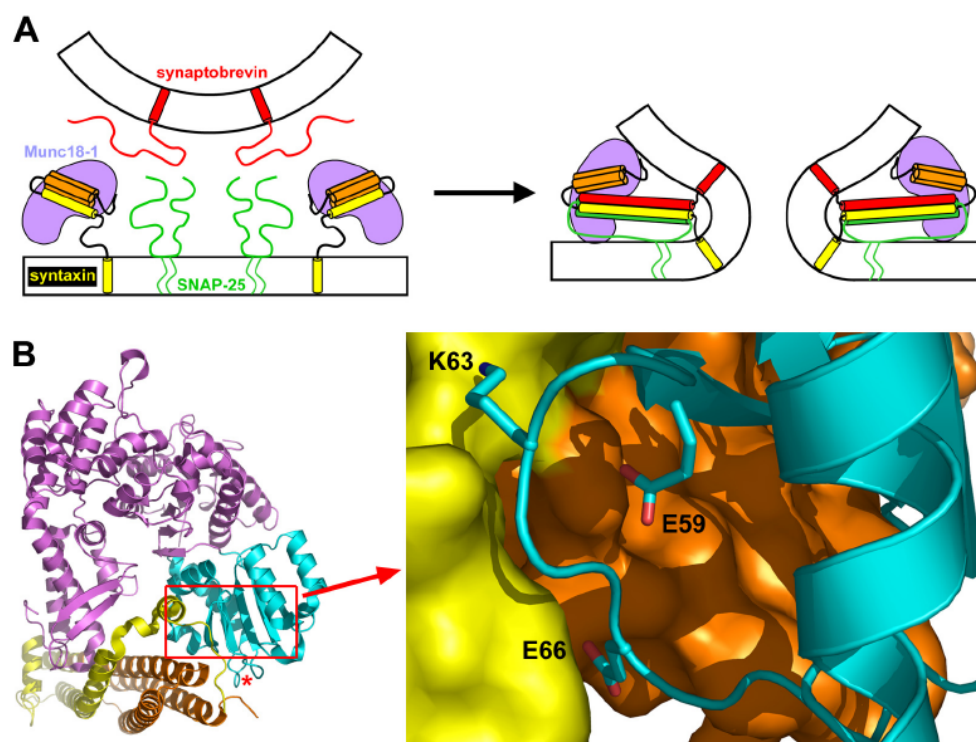


Figure 3-1 Design of mutations to disrupt Munc18-1/SNARE interactions.

(A) Models summarizing the two types of Munc18-1 SNARE interactions, with the binary Munc18-1/syntaxin-1 complex on the left and the Munc18-1/SNARE complex assembly on the right. Munc18-1 is colored in purple, synaptobrevin in red, SNAP-25 in green and syntaxin-1 in orange (H_{abc} domain) and yellow (SNARE motif and transmembrane region). The model of membrane fusion illustrated on the right is based on the hypothesis that binding of Munc18-1 to assembling SNARE complexes may prevent diffusion of these complexes to the center of the space between the membranes and thus plays a key role in application of mechanical force on the membranes (J. Rizo et al., 2006). (B) Ribbon diagram of

the binary Munc18-1/syntaxin-1 complex with Munc18-1 colored in purple except for the N-terminal domain, which is in cyan, and syntaxin-1 in orange (H_{abc} domain) and yellow (linker and SNARE motif). The red star indicates the position where cerulean was inserted for the rescue experiments. A close up of the interface showing the mutated residues is shown on the right. The diagrams in panels (A) and (B) were prepared with Pymol (DeLano Scientific, San Carlos, CA). (Figure from F. Deák et al., 2008, paper in preparation)

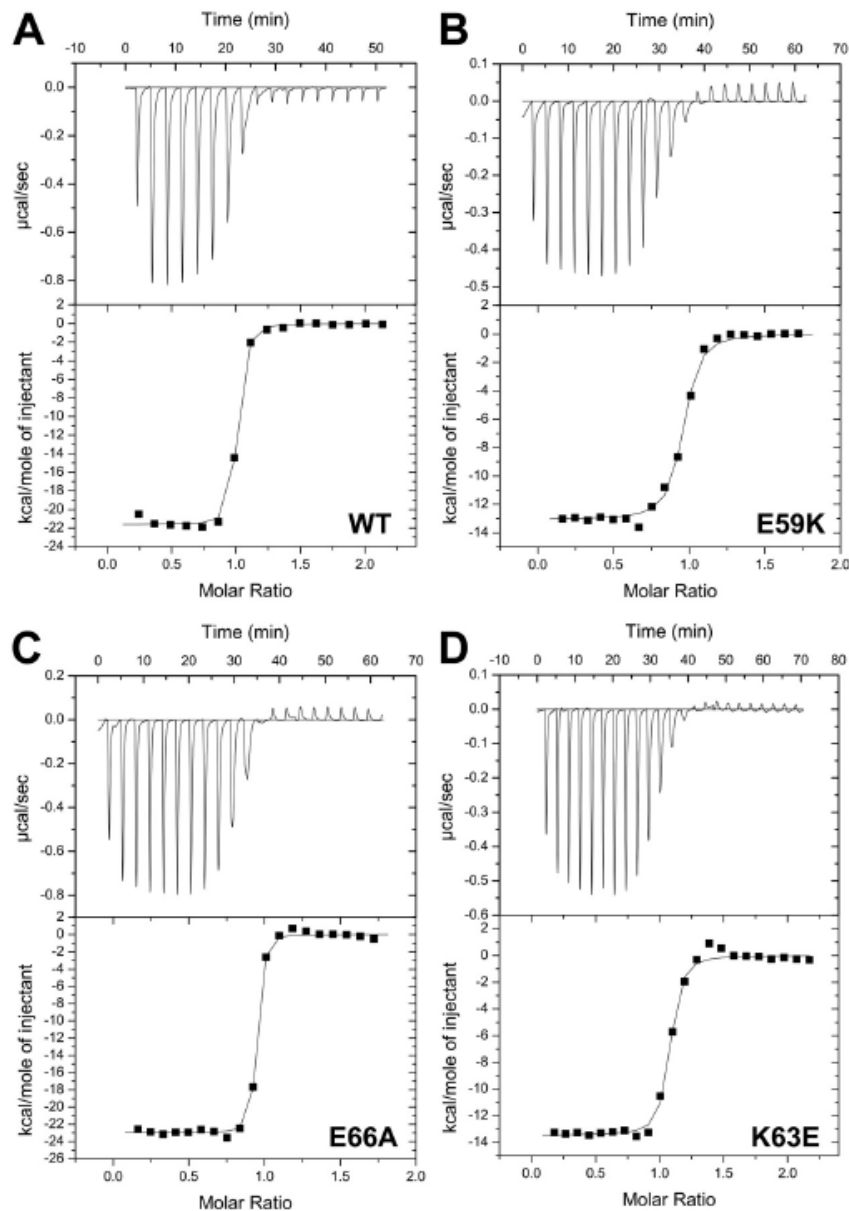


Figure 3-2 ITC analysis of binding of WT and mutant Munc18-1 to syntaxin-1. (Data by Yi Xu)
 (A)-(D) Illustrative examples of the ITC data obtained for WT Munc18-1 (A), E59K (B), E66A (C), and K63E (D) Munc18-1 mutants are shown. A polynomial baseline correction was applied to remove a systematic drift in the initial points of each titration before fitting the data to a single-site binding model. (Figure from F. Deák et al., 2008, paper in preparation)

ITC experiments for WT Munc18-1 and SNARE complex binding yields very small values for the measured enthalpies per mol of SNARE complex injected, which hinders the quantitative comparisons. Thus, we turned to the NMR method described by *Dulubova et al.* to measure the effects of the mutations in Munc-18-1 on its interaction with the SNARE complex (I. Dulubova et al., 2007). The principle of this method is that the intensity of the strongest methyl resonance (SMR) in one dimensional (1D) ^{13}C -edited ^1H -NMR spectra of a ^{13}C -labeled protein (or complex) decreases upon binding to an unlabeled protein due to the broadening caused by formation of a larger species (D. Arac et al., 2003). We prepared SNARE complexes containing ^{13}C -labeled syntaxin-1 (hereafter referred to as ^{13}C -labeled SNARE complex for simplicity) and added WT or mutant Munc18-1s. Addition of 2.5 μM WT Munc18-1 induced a moderate but reproducible decrease in the SMR intensity of 2 μM ^{13}C -labeled SNARE complex (Figure 3-3, A), which reflects formation of the Munc18-1/SNARE complex assembly. Interestingly, the K63E Munc18-1 mutant has a similar effect as WT Munc18-1, whereas no significant SMR intensity decrease of the ^{13}C -labeled SNARE complex was observed for the E59K mutant, and an intermediate effect for the E66A mutant was observed (Figure 3-3, A). Multiple titrations measuring the decrease in the SMR intensity of the ^{13}C -labeled SNARE complex as a function of WT Munc18-1 concentration (e.g. Figure 3-3, B) gave us a k_D value of 266 ± 41 nM, consistent with the value of 100-300 nM we estimated (I. Dulubova et al., 2007). Titrations of the Munc18-1 mutants yielded a k_D of 310 ± 82 nM for K63E, which has no significant difference from value of WT, and a k_D of 1.61 ± 0.35 μM for E66A which demonstrated a moderate but significant disruption of

Munc18-1 binding to the SNARE complex. Titrations of the E59K mutant consistently showed that this mutation strongly impairs SNARE complex binding, although some residual binding appeared at the higher concentrations (e.g. Figure 3-3, B); based on the sensitivity of the method, we estimate a k_D of $>30 \mu\text{M}$ for this mutant. As a summary, the three mutations in Munc18-1 have differential effects on binding to SNARE complex, among which E59K dramatically decrease the interaction (>100 fold), E66A causes a moderate disruption, and K63E has no significant effect (Figure 3-3).

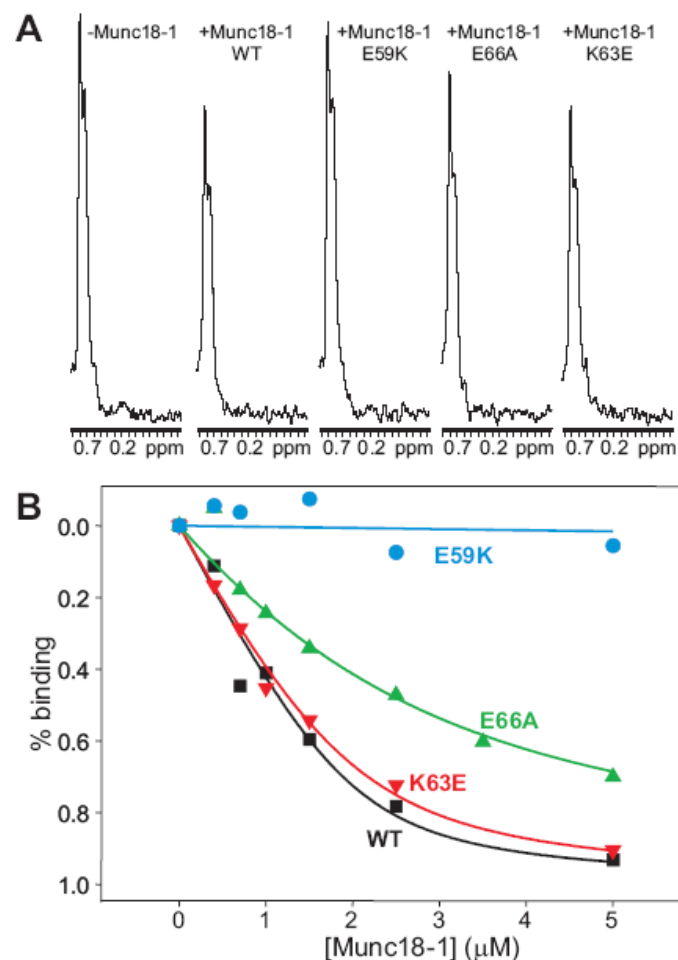


Figure 3-3 Differential disruption of Munc18-1 binding to the SNARE complex by Munc18-1 point mutations. (Data by Yi Xu)

(A) Sample traces of the regions of ^1D ^{13}C -edited ^1H -NMR spectra of $2 \mu\text{M}$ SNARE complex containing uniformly ^{13}C -labeled syntaxin-1 in the absence or presence of unlabeled WT or mutant Munc18-1s ($2.5 \mu\text{M}$). (B) Binding curves obtained from the SMR intensities observed in ^1D ^{13}C -edited ^1H -NMR spectra of

2 μM SNARE complex containing uniformly ^{13}C -labeled syntaxin-1 in the presence of increasing amounts of unlabeled WT or mutant Munc18-1s. The data were fit to a standard single-site binding model and normalized to % binding using as limit values the initial intensity in the absence of Munc18-1 (0% binding) and the intensity extrapolated to infinite munc18-1 concentration (100% binding). (Figure from F. Deák et al., 2008, paper in preparation)

Since the observed property that the E59K mutation strongly disrupts binding of Munc18-1 to the SNARE complex but retain tight binding to syntaxin-1 became important for the interpretation of results of the later electrophysiological study, we sought to confirm the effect of this mutation on Munc18-1 binding to syntaxin-1 by the same 1D NMR method that revealed the strong impairment of SNARE complex binding. At the concentrations of ^{13}C -labeled syntaxin-1 required to obtain reliable quantitative data (2 μM), titrations with either WT or E59K mutant Munc18-1 yielded indistinguishable saturation binding curves that plateaued above 2 μM Munc18-1 (Figure 3-4). Although these curves do not allow accurate affinity measurements, they do show that the k_{DS} for both the WT and the E59K mutant Munc18-1 are well below 100 nM, confirming that the mutant binds tightly to syntaxin-1.

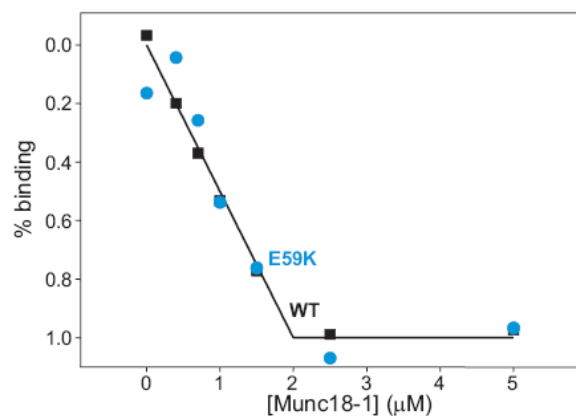


Figure 3-4 E59K mutant of Munc18-1 retains binding to the syntaxin-1. (Data by Yi Xu)

Binding curves obtained with the same methodology used in Figure 3-3, (B) for 2 μM ^{13}C -labeled syntaxin-1 and increasing amounts of WT or E59K mutant Munc18-1. The data were also fit to a standard single-site binding model but clearly yielded saturation binding curves and thus unreliable k_{d} values (<1 nM). (Figure from F. Deák et al., 2008, paper in preparation)

3.3.2 Rescue of survival and neurotransmitter release in Munc18-1 KO neurons.

Munc18-1 knockout mice die immediately at birth and exhibit a total abrogation of spontaneous, hypertonic sucrose-induced, and Ca^{2+} -triggered neurotransmitter releases (Verhage et al., 2000). Since Munc18-1 pups die immediately at birth, in this study, we used primary cortical cultures from mouse embryos at E16.5 day. During the first week *in vitro*, Munc18-1 deficient neurons exhibited apparently normal neurite outgrowth and synapse formation as revealed by immunocytochemistry staining and electron microscopy (data not shown). Subsequently, neurons from Munc18-1 knockout mice degenerate rapidly, and do not survive more than 10 DIV (Figure 3-5). To overcome this problem and to test whether the observed phenotype in Munc18-1 knockout neurons can be rescued by overexpression of WT or mutated Munc18-1s, we used lentiviral infection system to express Munc18-1 proteins in cultured neurons. In addition, we intended to visualize the Munc18-1 protein under the microscopy to monitor the level of WT and mutant Munc18-1 protein expressions. Therefore, we tagged Munc18-1 with the cerulean-variant of GFP.

Since it is essential that insertion of cerulean does not interrupt the normal functions of Munc18-1, we first tested four versions of cerulean-Munc18-1 fusion proteins, where ceruleans were engineered to different positions of Munc18-1: a C-terminal cerulean-fusion protein and three other fusion proteins where cerulean was inserted into loops of Munc18-1. The three loops were chosen based on the crystal structure of the Munc18-1/syntaxin-1 complex (K. M. Misura et al., 2000), and were located at the exposed surface of Munc18-1. These three loops were closed to syntaxin-1 (for future FRET studies *in vivo*) and were predicted to be able to harbor insertion of cerulean

without disrupting the folding of Munc18-1 and/or the binding to syntaxin-1. Although no systematic studies were performed, preliminary experiments indicated that insertion of cerulean between 24 and 23 amino acids (see red star in Figure 3-1, B) allowed most efficient rescue of the survival and the neurotransmitter release phenotypes in Munc18-1 deficient neurons among the four fusion proteins. Thus, here after, all of our functional experiments were performed with this version of cerulean-fusion protein of Munc18-1.

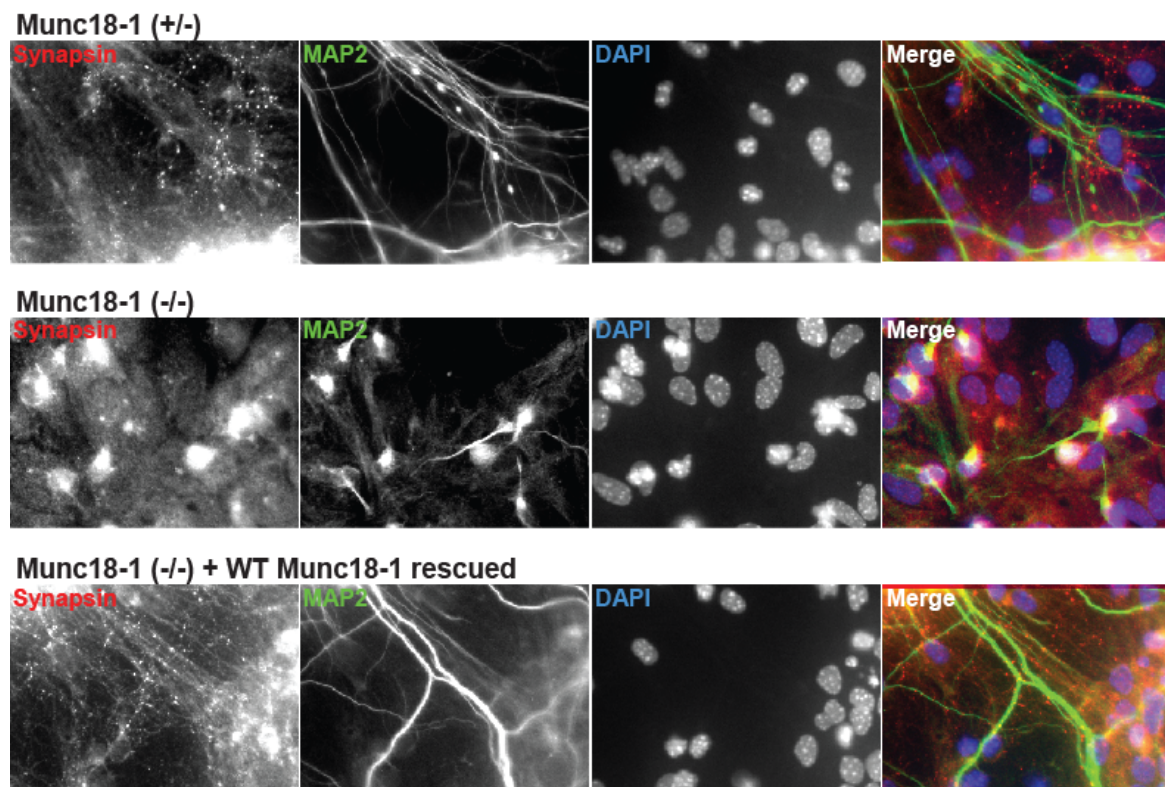


Figure 3-5 Rescue of neuronal survival in cortical cultures by Munc18-1 expression.

Representative images of cortical synapses from littermate heterozygotes (upper row), homozygote knockouts for Munc18-1 (middle row) or Munc18-1 knockouts infected with Munc18-1-containing lentivirus (lower row). Cells were maintained in culture for 11 days before labeled with antibodies against the presynaptic marker synapsin (first column from the left), the neurofilament marker MAP2 (second column) and the nuclear DAPI marker (third column.) The last column shows the combined image of the three labeling procedures, with colors that match the relevant labels in the other columns. (Figure from F. Deák et al., 2008, paper in preparation)

We infected cultured Munc18-1 deficient neurons at DIV 1 with lentivirus expressing cerulean fusion of WT, E59K-, E66A, or K63E-mutant Munc18-1s, and monitored the survival and morphology of the neurons and protein expression levels under the fluorescence microscopy at DIV 11. All Munc18-1 proteins rescued neuronal survival, and WT and all the mutants of Munc18-1 were detected in synapses (Figure 3-5 and data not shown). We next carried out patch-clamp recording to test whether the cerulean-tagged WT Munc18-1 rescues physiological phenotypes in Munc18-1 knockout neurons. In order to confirm previous findings (M. Verhage et al., 2000), we also recorded from untreated knockout cultures at DIV 6-7, when there are still surviving neurons, and as expected, no evoked or spontaneous activity was observed (data not shown). Lentiviral infection of WT Munc18-1 encoding virus rescued spontaneous neurotransmitter release (or minis) and fully restored evoked response by field stimulation at low frequency (0.4 Hz) (Figure 3-6), as well as the neurotransmitter release stimulated by high frequency (10 Hz) and by hyperosmotic sucrose (Figure 3-8, A-C), as monitored by recordings at DIV 12-18. These results suggest that overexpression of WT Munc18-1 by lentiviral infection is sufficient to confer WT electrophysiological responses on Munc18-1 deficient neurons. Moreover, both the synaptic release kinetics and the size of the recycling vesicle pools were indistinguishable among WT neurons, and KO neurons infected with either untagged or cerulean-tagged Munc18-1 in fluorescent FM dye experiments (Figure 3-7, A-C).

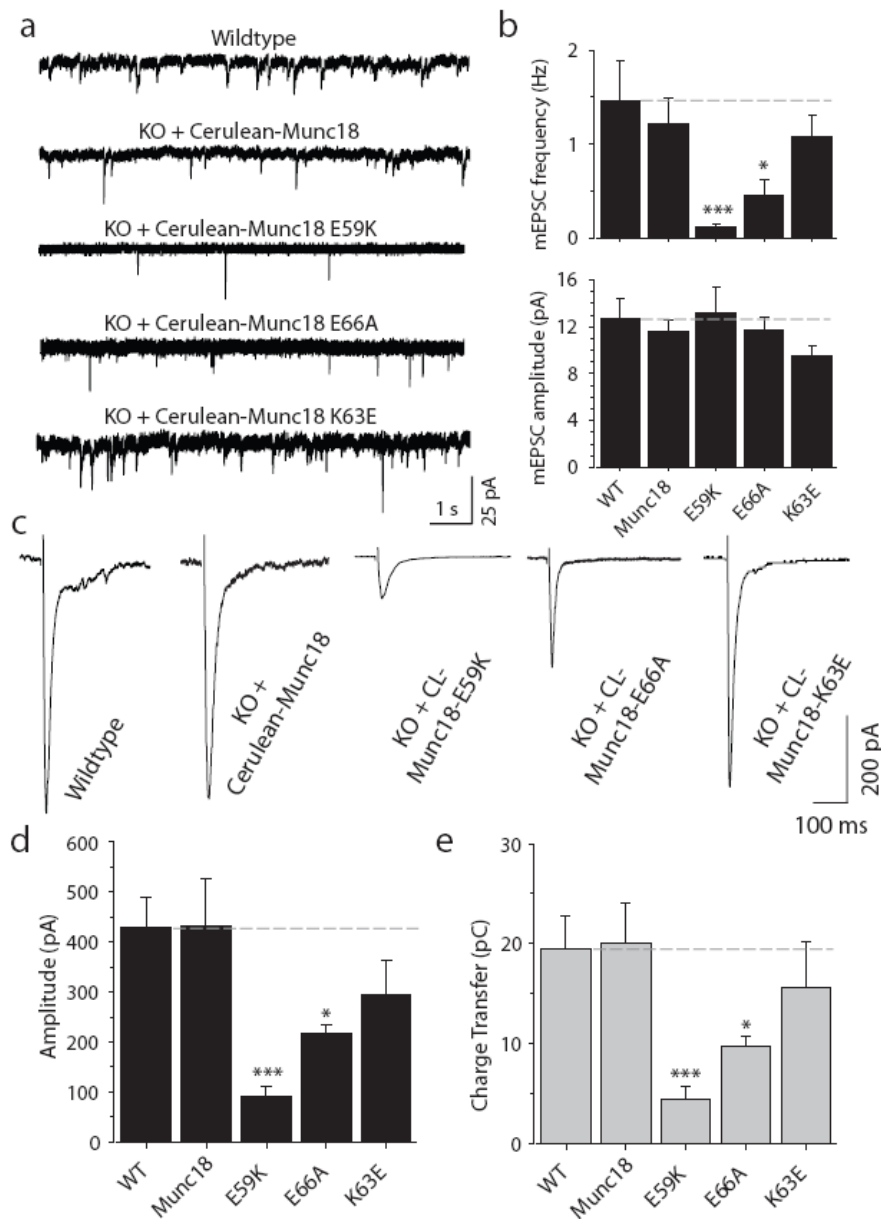


Figure 3-6 Synaptic release depends on Munc18-1 binding to the SNARE complex. (Data by Ferenc Deák)

(A) Analysis of spontaneous synaptic release upon rescue with WT and mutant Munc18-1s. Representative ten second segments from 10 minute-long traces of spontaneous excitatory synaptic activity, recorded at a holding potential of -70 mV in the presence of 1 μ M tetrodotoxin and 50 μ M picrotoxin. (B) Bar diagram describing the frequency (upper panel) and amplitude (lower panel) of spontaneous release (WT $n=13$; munc18 $n=19$, E59K $n=10$, K63E and E66A $n=9$). (C) Representative traces of field stimulation (at 0.4 Hz) evoked excitatory responses from neurons of WT ($n=14$) OR Munc18-1 KO infected with WT ($n=9$), E59K ($n=7$), E66A ($n=16$) or K63E ($n=11$) Munc18-1-24-cerulean. Note that only the first 400 ms of the traces are shown for clarity. (D) Bar diagram summarizing the amplitudes of evoked responses for cultures rescued with the WT Munc18-1 and different Munc18-1 mutants. (E) Synaptic responses characterized as the amount of transferred charge. Asterisks in the bar diagrams mark statistical significance of the

difference between the WT and mutant rescues (* $P < 0.05$; *** $P < 0.005$). (Figure from F. Deák et al., 2008, paper in preparation)

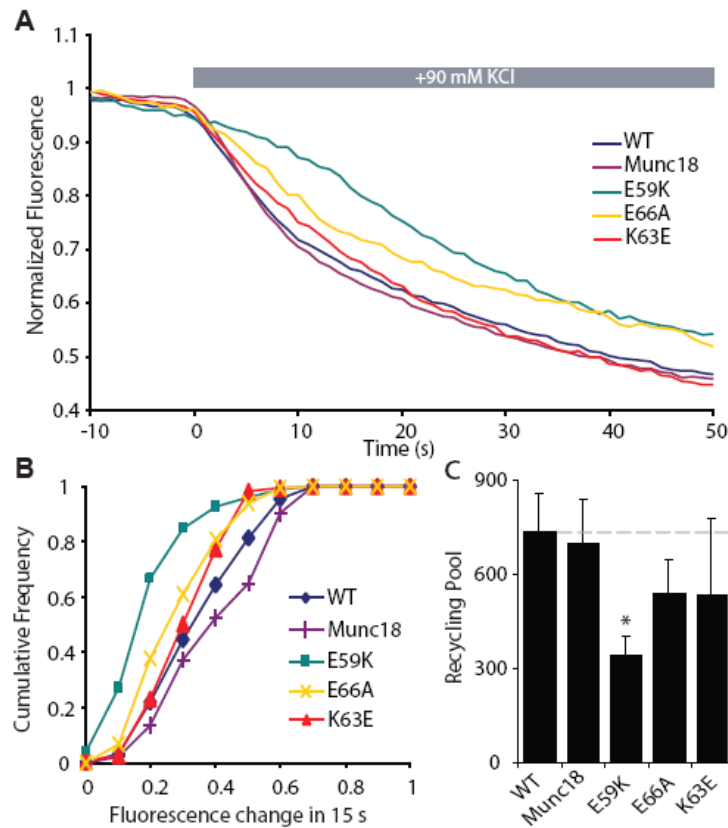


Figure 3-7 Munc18-1 binding to the SNARE complex is critical for release readiness of synaptic vesicles. (Data by Ferenc Deák)

(A)(B) Average destaining curves during depolarization (the fluorescence of FM2-10 dye was normalized to the beginning value right before the stimulation) (A) and cumulative diagram of the distribution of synaptic destaining kinetics (percent of fluorescence loss after 15 second of depolarization) (B). The data were obtained with WT neurons from littermate controls (WT \blacklozenge , $n=10$ cells, 719 synapses) of Munc18-1 KO neurons rescued with lentivirus expressing WT Munc18-1-24 cerulean (Munc18+, $n=10$ cells, 874 synapses) or Munc18-1-24-cerulean with the E59K (E59K \blacksquare , $n=6$ cells, 497 synapses), K63E (K63E \blacktriangle , $n=4$ cells, 287 synapses) or E66A (E66A \times , $n=5$ cells, 452 synapses) mutations. (C) Bar diagram depicting the difference in the size of recycling synaptic pools for synapses rescued with the WT and mutant Munc18-1s. (Figure from F. Deák et al., 2008, paper in preparation)

3.3.3 Mutations in Munc18-1 impair neurotransmitter release.

We next investigated the effects of the three mutations on Munc18-1 to its ability to rescue neurotransmitter release. For the spontaneous release, we found that the E59K-mutation on WT Munc18-1 dramatically decreased the frequency of minis, but has

no effect on their amplitude (Figure 3-6, A and B). The E66A-mutation also significantly decreased the mini frequency, but to a lesser extent than the E59K-mutation, whereas the K63E-mutation had no significant effect. Our observation showed that the impairment of the spontaneous release caused by the Munc18-1 mutations seems to correspond to their effects on Munc18-1 SNARE complex binding.

For the effects of the Munc18-1 mutations on evoked neurotransmitter release (Figure 3-6 C-E), again, the E59K-mutation severely impaired the release (~80%), the E66A-mutation had a more moderate impairment (~50%), and the K63E-mutation had no significant effect. Similar results were obtained from FM-dye labeling experiments (Figure 3-7, A-C).

3.3.4 Mutations in Munc18-1 decrease the readily-releasable pool size.

The decrease in evoked release caused by the mutations could in principle arise from a reduction in the size of the RRP of vesicles, and/or in the vesicular release probability. To distinguish between the two probabilities, we first analyzed evoked responses at 10 Hz stimulation frequency, in which a reduced release probability is expected to lead to synaptic facilitation. Second, we determined the size of the RRP of infected neurons by measuring synaptic response to hypertonic sucrose (0.5 M) application. The effects of the mutations on the amplitude of the first response of the train paralleled those observed at low frequency stimulation; however, all mutants exhibited a dramatic synaptic depression, not facilitation, during the stimulus train (data not shown). In hypertonic sucrose experiments, the E59K-mutation dramatically decreased the size of the RRP (~70% decrease), whereas the E66A-mutation had a smaller effect (~50%), and the K63E

mutation caused no significant effect (Figure 3-7, D-F). Thus, the effects of the mutations on the RRP correspond to those observed in the evoked responses by low and high frequency stimulation (Figure 3-6 and 3-7) and in the Munc18-1/SNARE complex binding experiments (Figure 3-3). These results suggest that the impairment in release caused by the Munc18-1 mutations occurs at the vesicle priming, and that formation of Munc18-1/SNARE complex assemblies is critical for this step.

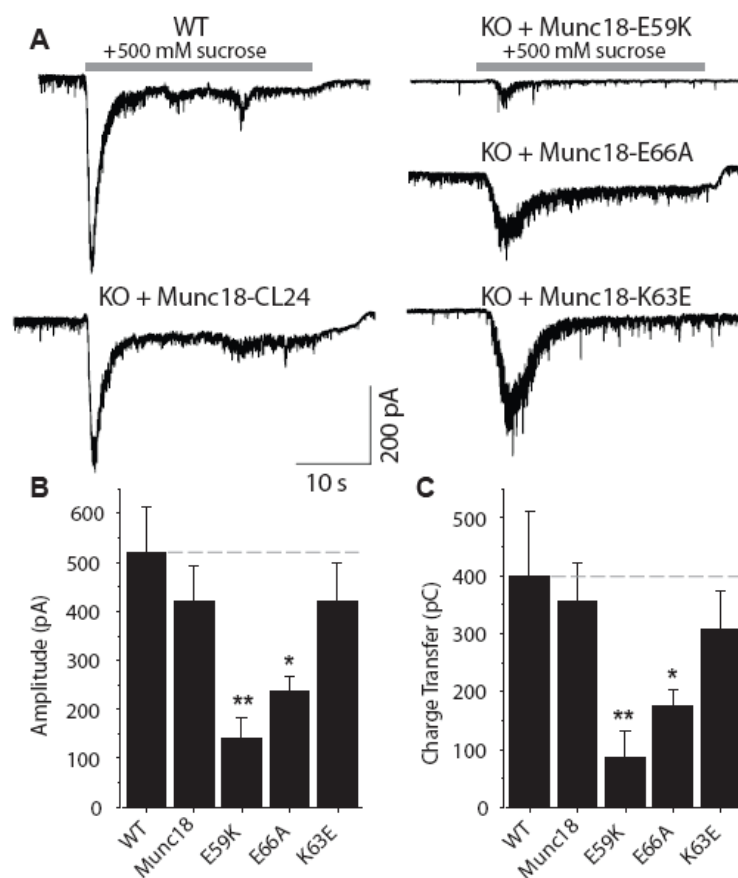


Figure 3-8 Munc18-1 mutations in SNARE binding reduce the size of readily releasable pool. (Data by Ferenc Deák)

(A) Representative traces of synaptic excitatory responses to hypertonic solution (+500 mM sucrose to the bath). (B) Bar diagram depicting the amplitudes of responses to the hypertonic solution for WT cultures or Munc18-1 knockout cultures rescued with the WT and mutant Munc18-1s (WT n=5; Munc18-1, K63E and E66A n=8; E59K n=5). (C) Readily releasable synaptic excitatory transmission characterized as the amount of transferred charge. Asterisks in the bar diagrams mark statistical significance of the difference between the WT and mutant rescues (*P<0.05; **P<0.01). (Figure from F. Deák et al., 2008, paper in preparation)

3.4 Discussion

The role of the SNAREs in membrane fusion was clearly demonstrated by their ability to form SNARE complexes that bridge the two membranes (T. Sollner et al., 1993; P. I. Hanson et al., 1997), but the role of SM proteins has been enigmatic. The early observation that Munc18-1 binds tightly to syntaxin-1 (Y. Hata et al., 1993), and the decrease in syntaxin-1 level observed in Munc18-1 knockout mice (M. Verhage et al., 2000), suggested that Munc18-1 is not essential for fusion, but its interaction with syntaxin-1 is physiologically relevant. However, new data revealed that Munc18-1 binding to SNARE, appears to be the general mode, as observed for most of SM proteins, and the Munc18-1/syntaxin-1 interaction is considered to be an atypical feature of Munc18-1 (C. M. Carr et al., 1999; R. Peng and D. Gallwitz, 2002; L. N. Carpp et al., 2006; C. Stroupe et al., 2006; I. Dulubova et al., 2007; C. F. Latham et al., 2007). Localization and functional data in various systems have provided evidence for the physiological relevance of Munc18-1/SNARE complex (C. M. Carr et al., 1999; E. Grote et al., 2000; L. Wang et al., 2002; T. Yamaguchi et al., 2002; K. M. Collins et al., 2005; M. Khvotchev et al., 2007; J. Shen et al., 2007), however, a clear correlation between formation of SM protein/SNARE complex assemblies and its function in living cells remains deficient. In addition, it is also important to characterize in which steps of neurotransmitter release involves the interaction of Munc18-1/SNARE complex. Our results now provide direct physiological evidence in living cells that syntaxin-1 binding is not sufficient for Munc18-1 function and that Munc18-1 binding to the SNARE complex serves a key component for synaptic vesicle priming.

To conduct structure function studies in living cultured neurons, we developed a

lentiviral infection system that overexpresses WT Munc18-1 in Munc18-1 deficient neurons to rescue neuron survival and neurotransmitter release phenotypes. We also designed a cerulean-tagged Munc18-1 fusion protein, with cerulean inserted in one of loops of Munc18-1, which fully rescues neuron survival and neurotransmission phenotypes indistinguishably from WT Munc18-1. The fluorescent tagged protein allows us to monitor the expression and localization of expressed proteins in cultured neurons. Our design for the mutations was based on the prediction that the interactions involving Munc18-1 residues that contact the H_{abc} domain/SNARE motif interface in the binary Munc18-1/syntaxin-1 complex are likely to be altered to some extent in the transition to the Munc18-1/SNARE complex assembly. Three mutations at N-terminal of Munc18-1 were selected for mutagenesis: E59K, which makes contact with the syntaxin-1 H_{abc} domain; K63E, which contacts the SNARE motif of syntaxin-1; and E66A, which contacts both motifs. All the three mutants retain high binding affinity to syntaxin-1, while E59K strongly impairs SNARE complex binding, E66A moderately impairs the binding, and K63E maintains its binding ability to SNARE. The fact that ITC experiments and the NMR experiment for the E59K mutant showed that none of the three mutations strongly reduced syntaxin-1 binding to Munc18-1 (Figure 3-2 and Figure 3-4) is not surprisingly for the uneven energetic distribution of interactions at protein-protein interfaces and the adaptability of these interfaces upon the introduction of point mutations, particularly for complexes of high affinity (S. Atwell et al., 1997).

The differential effects of the mutations on the two types of Munc18-1/SNARE interactions provided us the opportunity to study the functional importance of the Munc18-1/SNARE complex assembly without strongly perturbing the binary

Munc18-1/syntaxin-1 interaction. From our study, Munc18-1/syntaxin-1 is not important for neurotransmitter release, although one might argue that the defects in release caused by the E59K mutation could arise from the weakened Munc18-1/syntaxin-1 binding. However, the interaction remains strong for this mutant, and the weakened Munc18-1/syntaxin-1 binding was also induced by K63E and E66A. The former has a stronger effect and the latter exhibits a more moderate effect. Conversely, the K63E mutation does not perturb neurotransmitter release, whereas the E66A mutation impairs neurotransmitter release. Thus, defects in Munc18-1/syntaxin-1 binding are not main factors in impairing the vesicle fusion. In contrast, the effects of the three mutations on Munc18-1/SNARE complex binding exhibit a clear correlation with their impairment of release. The E59K mutation, which exhibits the strongest disruption of Munc18-1 binding to the SNARE complex (Figure 3-3), strongly impairs Ca^{2+} -triggered, hypotonic sucrose-induced, and spontaneous release (Figure 3-6, 3-7, and 3-8). The E66A mutation, which moderately decreases the affinity of the Munc18-1/SNARE complex interaction, impairs release to a smaller extent. Finally, the K63E mutation, which has no significant effect on SNARE complex binding, also displays no alteration in neurotransmitter release. These observations demonstrate that binding of Munc18-1 to the SNARE complex is critical for neurotransmitter release.

Earlier genetic study of Munc18-1 revealed that the docking of vesicles is normal in Munc18-1 deficient mice (M. Verhage et al., 2000), thus it is unlikely that impairment in Munc18-1/SNARE binding affects the docking step in membrane fusion. In contrast, two mutations that disrupt Munc18-1/SNARE complex binding appear to affect the spontaneous and hypertonic sucrose-induced release, suggesting that the impairment in

exocytosis arises from a defect in synaptic vesicle priming to a release-ready state. Our results show that binding of Munc18-1 to the SNARE complex is required for synaptic vesicle priming for both action potential-evoked release and spontaneous release. For future studies, since we cannot rule out the possibility that the Munc18-1/SNARE complex interaction might be important for events downstream of priming, further investigation in interaction of the complex with downstream factors (e.g. synaptotagmin 1 in Ca^{2+} -triggered step) (R. Fernandez-Chacon et al., 2001) will be necessary. In addition, the physiological relevance and significance of Munc18-1/syntaxin-1 interaction remains unclear and is needed to be addressed in future studies.

CHAPTER IV: E-SYTS, A FAMILY OF MEMBRANOUS CA²⁺-SENSOR PROTEINS WITH MULTIPLE C₂ DOMAINS

4.1 Introductions

In this study, we defined a family of homologous proteins referred as E-Syts. E-Syts were identified by databank searches for C₂ domain proteins that contain a TMR (O. H. Shin et al., 2005). Three evolutionarily conserved E-Syt proteins, E-Syt1, E-Syt2, and E-Syt3, were revealed by the analyses of vertebrate sequences. In order to assemble full-length sequences for the three E-Syt proteins, we sequenced multiple independent EST clones and verified their primary structures by comparing the resulting sequences with database entries.

We then investigated the phospholipids binding property and subcellular localization of these proteins. As a result, recombinant protein fragments of E-Syt2 that contain the first C₂ domain are capable of Ca²⁺-dependent phospholipids binding at micromolar level of free Ca²⁺, indicating that E-Syts bind to Ca²⁺ through their first C₂ domain in a phospholipids complex. In addition, expression of myc-tagged E-Syt proteins in transfected HEK293 cells demonstrated that E-Syt1 is localized to intracellular membranes, whereas E-Syt2 and E-Syt3 are localized to the plasma membrane. Finally, structure/function studies were conducted to uncover the unexpected membrane targeting mechanism of E-Syt2 and E-Syt3, which are directed to the plasma membrane by a mechanism mediated not by TMR, but instead, by their Ca²⁺-independent C₂C domain. All together, our findings suggest E-Syts represent a family of Ca²⁺-binding membrane

proteins that expand multiple C₂ domains trafficking proteins to a fourth class beyond synaptotagmins, ferlins, and MCTPs.

4.2 Materials and Methods

4.2.1 Cloning, sequence analyses, and data bank search

E-Syts were identified by databank searches of genomic and cDNA sequences. Their full-length human sequences were then assembled by sequencing of expressed-sequence tag clones, and submitted to GenBank (accession nos. DQ993200, DQ993201, and DQ993202).

4.2.2 Expression and purification of recombinant GST fusion proteins

The cDNA sequences encoding various domains of the human E-Syts were amplified by PCR, subcloned into pGEX-KG vector, and expressed and purified as recombinant GST fusion proteins essentially as described (V. Denis and M. S. Cyert, 2005). The following GST fusion proteins were produced: E-Syt1 X C₂AB (residues 91-600), E-Syt1 C₂A (residues 278-449), E-Syt1 C₂E (residues 918-1105), E-Syt2 XC₂AB (residues 147-658), E-Syt2 XC₂A (residues 147-511), E-Syt2 X (residues 147-387), E-Syt2 C₂A (residues 340-511), E-Syt2 C₂AB (residues 340-658), E-Syt2 C₂B (residues 500-658), and E-Syt2 C₂C (residues 736-922).

4.2.3 Construction and expression of vectors encoding various myc-tagged E-Syt fusion proteins

The following gene constructs were subcloned into pCMV vector with an

N-terminal myc-tag, and transfected into HEK293 cells for subcellular localization experiments: E-Syt1 full-length (residues 1-1105), E-Syt2 full-length (residues 1-922), E-Syt3 full-length (residues 1-887), E-Syt1 Δ TMR (residues 92-1105), E-Syt2 Δ TMR (residues 150-922), E-Syt3 Δ TMR (residues 73-887), E-Syt2 deletion constructs (residues 1-810, 1-458, 1-240, 240-922, 458-922, and 755-922), E-Syt1 deletion construct (residues 965-1105), and E-Syt3 deletion construct (residues 748-887).

Phospholipid binding assays were carried out with purified soluble GST fusion proteins in buffer A (50mM HEPES-NaOH, pH 6.8/0.1 M NaCl/4 mM sodium EGTA). The GST fusion C₂ domain proteins were incubated with liposomes of defined phospholipid composition in buffer A containing variable amounts of CaCl₂ or MgCl₂ to provide defined concentrations of free Ca²⁺ and Mg²⁺, respectively (calculated by using EqCal for Window software from biosoft, Ferguson, MO). After incubations, liposomes with bound C₂-domain proteins were isolated by centrifugation essentially as described (I. Fernandez et al., 2001; O. H. Shin et al., 2002) and bound proteins were precipitated, resuspended in 30 μ l of 2 \times SDS sample buffer, and analyzed by SDS/PAGE and Coomassie blue staining.

4.2.4 Immunostaining and confocal imaging

HEK293 cells plated on cover slips in 12-well plates were transfected with E-Syts expression and control vectors by using FuGENE (Roche Applied Science, Indianapolis, IN). Two days after transfection, cells were washed in PBS and fixed with 3.7% formaldehyde in PBS. After fixation, cells were blocked and non-permeabilized or permeabilized by 3% nonfat milk with 0.1% Nonidet P-40 in PBS. Cells were then

incubated with monoclonal antibodies against the myc epitope (SantaCruz Biotechnology, Santa Cruz, CA) and FITC-conjugated Phalloidin (Molecular Probes, Eugene, OR) for 1 h, washed three times with PBS, and reacted with Alexa Fluor 488-labeled secondary antibody (Invitrogen, Carlsbad, CA) for 1 h. After three washes with PBS, cells were briefly immersed in water, and mounted with Vectashield (Vector Laboratories, Burlingame, CA). Images were acquired on a TCS2 laser-scanning confocal microscope (Leica, Bannockburn, IL) using a magnification $\times 62$ oil objective.

4.2.5 Miscellaneous procedures

SDS/PAGE and immunoblotting were performed by using standard procedures (D. Bansal and K. P. Campbell, 2004; O. H. Shin et al., 2005). Immunoblots were developed by enhanced chemiluminescence (Amersham biosciences, Piscataway, NJ).

4.3 Results

4.3.1 Phospholipid binding by E-Syt2.

Because C₂A domain of E-Syts possess sequence motif that is essential for Ca²⁺-binding, we investigated their potential Ca²⁺-binding properties utilizing a series of GST fusion proteins of various fragments incubating with liposomes composed of 25% phosphatidylserine (PS)/75% phosphatidylcholine (PC) in the absence or presence of divalent cations, following by a sensitive centrifugation assay (Figure 4-1, A). No phospholipid binding in the absence of divalent cations or Mg²⁺ with any E-Syt2 fragments was observed. In contrast, fusion proteins of the C₂A domain, with either the X domain or the C₂B domain or both, displayed a Ca²⁺-specific liposome binding (Figure

4-1, A and B). It seems like the only denominator of these different E-Syt2 fragments was the presence of the C₂A domain, however, the isolated C₂A domain by itself only showed weak Ca²⁺-dependent binding to phospholipids (Figure 4-1, B). It is possible that the fragment used did not include the precise domain boundaries.

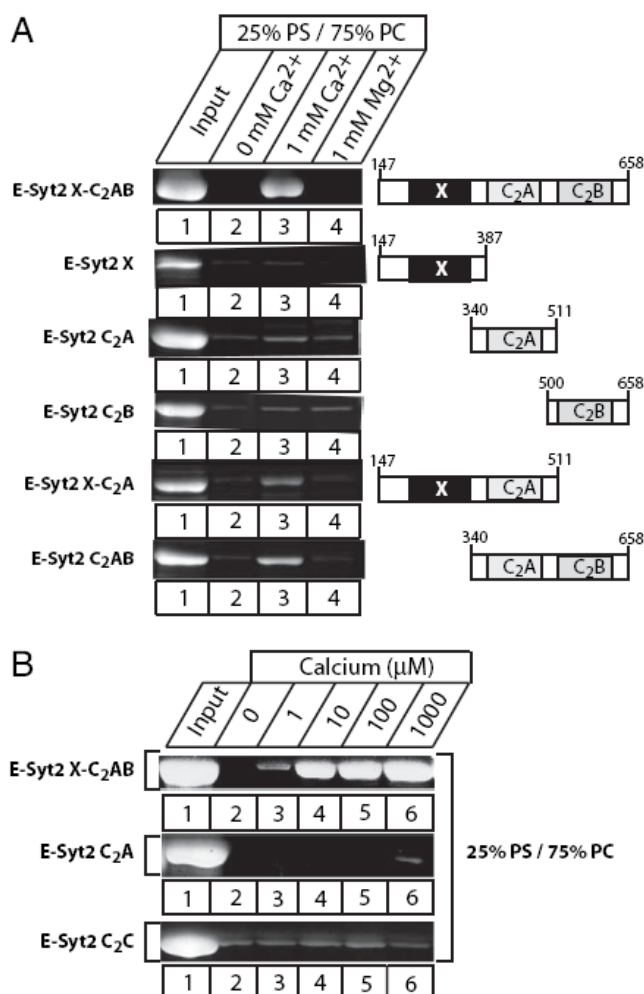


Figure 4-1 Ca²⁺- and phospholipids-dependent membrane binding by E-Syt2 C₂ domain.

(A) Recombinant GST-fusion proteins containing the E-Syt2 domains indicated on the right were used in phospholipids assays. Proteins were incubated in the absence of divalent cations, in 1 mM Ca²⁺, or in 1 mM Mg²⁺ with liposomes composed of 25% PS/75% PC (wt/wt). Liposomes were pelleted by centrifugation, and bound proteins were analyzed by SDS/PAGE and Coomassie staining. (B) Ca²⁺ dependent of phospholipids binding. Recombinant GST-fusion proteins containing either the E-Syt juxtamembranous X domain together with the C₂A and C₂B domains (XC₂AB), or only the C₂A or C₂C domain from E-Syt2, were incubated with liposomes composed of 25% PS/75% PC in the presence of the indicated concentrations of free Ca²⁺. Proteins bound to the liposomes were analyzed by centrifugation, followed by SDS/PAGE and Coomassie blue staining. (S. W. Min et al., 2007)

We next examined the Ca^{2+} affinity and phospholipid specificity of Ca^{2+} -dependent phospholipid binding by the E-Syt2 XC_2AB domain fragment (Figure 4-2). Binding to phospholipids at micromolar concentrations of free Ca^{2+} was observed, similar to that demonstrated for synaptotagmin-1 C_2 domains. In addition, Ca^{2+} -dependent phospholipid binding of E-Syt2 was not specific for negatively charged phospholipid but was also detected with liposomes composed of neutral phospholipids (PE and PC) (Figure 4-2), although negatively charged phospholipids exhibited a higher Ca^{2+} affinity.

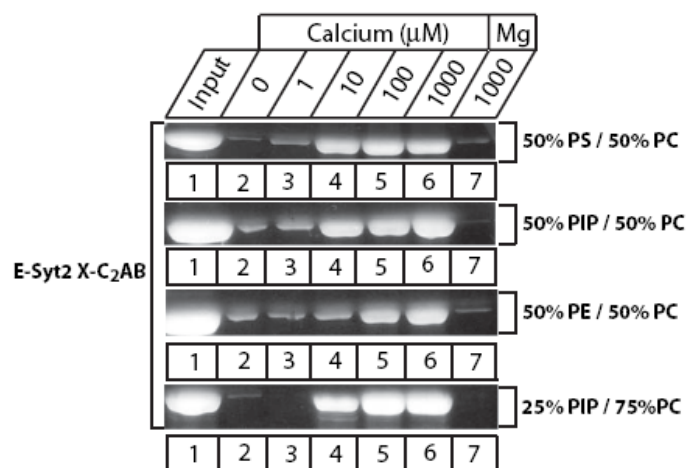


Figure 4-2 Phospholipid dependence of Ca^{2+} -dependent membrane binding of the E-Syt2 C_2AB domains.

Phospholipid binding of a GST fusion protein containing the E-Syt2 C_2AB domains was tested at the indicated Ca^{2+} concentrations and in the presence of 1 mM Mg^{2+} (as negative control) in liposomes with the four different phospholipid compositions shown on the right. (PIP, phosphatidylinositol phosphate; PE, phosphatidylethanolamine). (S. W. Min et al., 2007)

4.3.2 Subcellular localization of E-Syts.

To determine the subcellular localization of E-Syts, we constructed vectors that express N-terminal myc tag fusion of E-Syts, either as full-length proteins or as N-terminal TMR truncated proteins. The expression of these proteins from each of these

vectors was confirmed by immunoblotting in transfected HEK293 and COS cells.

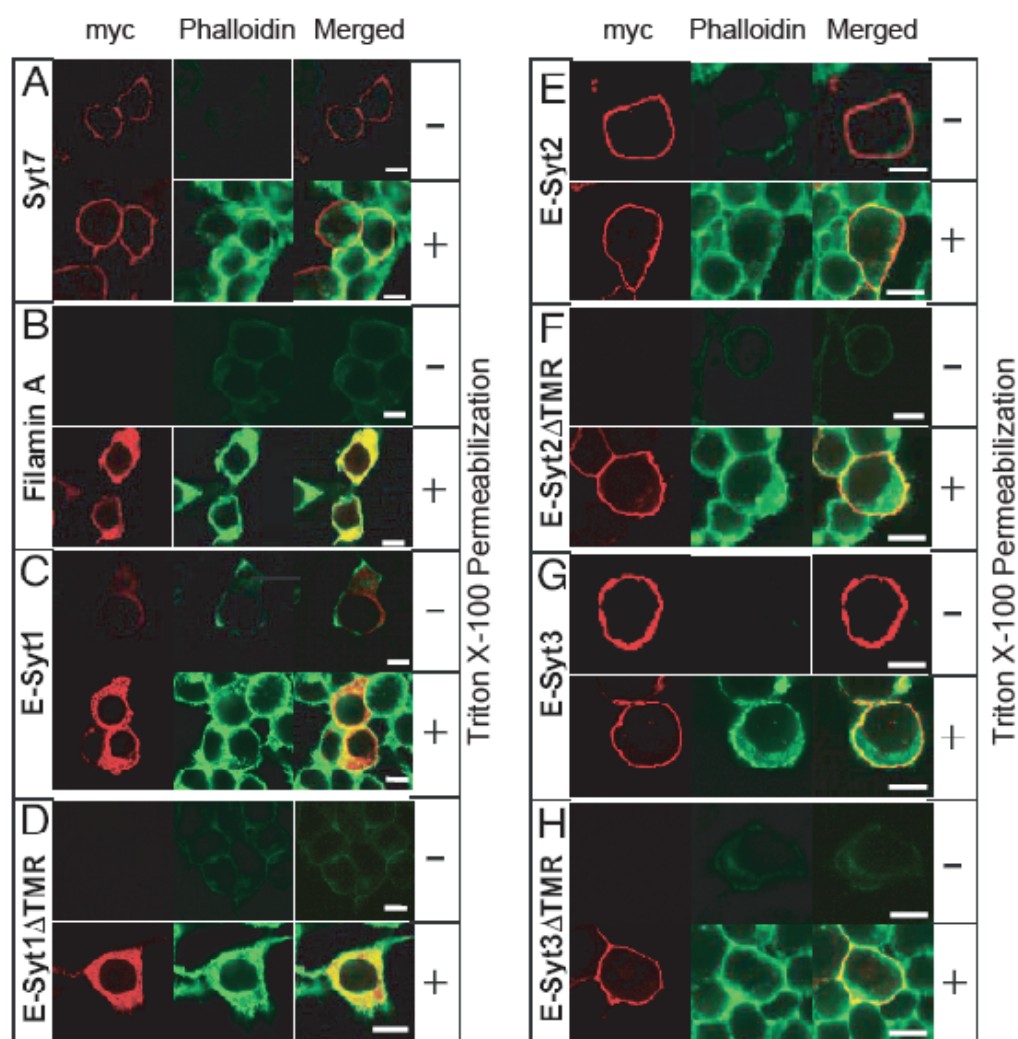


Figure 4-3 Subcellular localization of E-Syts in HEK293 cells. (Data by Sang-Won Min)

Confocal images of HEK293 cells transfected with various constructs expressing the proteins indicated on the left. (A) Synaptotagmin-7 (Syt-7). (B) Filamin-A. (C, E, and G) full-length E-Syt1, E-Syt2, or E-Syt3. (D, F, and H) truncated E-Syt1 (E-Syt1 Δ TMR), E-Syt2 (E-Syt2 Δ TMR), or E-Syt3 (E-Syt3 Δ TMR) lacking the N-terminal TMR. All proteins contained an N-terminal myc-epitope. Transfected cells were fixed and stained with anti-myc antibody (*Left*, red) and fluorescein-labeled phalloidin (*Center*, green). (*Right*, Merged images). Cells were analyzed either without detergent permeabilization to probe surface-exposed epitopes or after detergent solubilization with Triton X-100 as indicated on the right. (Scale bar: 5 μ m.) (S. W. Min et al., 2007)

In order to test whether E-Syts are plasma membrane proteins, we transfected the expression vectors to HEK293 cells, and immunostained the cells with anti-myc epitope

antibody either with or without membrane permeabilization. In the designed assay, plasma membrane localization of myc-tagged proteins would expose their N-terminal myc-tagged sequence on the cell surface and thus make them accessible to immunolabeling without permeabilization. We used N-terminal myc-tagged synaptotagmin-7, which has shown to be deposited into the plasma membrane (reference), as a positive control. As a negative control, we used N-terminal myc-tagged intracellular protein filamin A. Moreover, TMR truncated E-Syt proteins also served as further controls since they do not contain noncytoplasmic sequences and should not be localized to the cell surface. All cells are also probed with fluorescent phalloidin antibody to label the actin cytoskeleton.

Three principle observations were made: First, full-length E-Syt1 was not detected in unpermeabilized cells, but was detected in permeabilized cells with an unidentified intracellular compartment staining pattern that does not resemble staining of Golgi apparatus, endoplasmic reticulum, lysosomes, or mitochondria. Second, E-Syt2 and E-Syt3 are detected on cell surface of unpermeabilized transfected HEK293 cells. Furthermore, because staining of permeabilized cells does not reveal additional staining of these E-Syts, suggesting that they are completely inserted into plasma membrane. Finally, the removal of TMR from E-Syt2 and E-Syt3 does not change their associated localizations. Although E-Syt2 and E-Syt3 without TMR can no longer be detected on the cell surface of unpermeabilized cells, they were still found to be associated to plasma membrane in permeabilized cells. Therefore, TMR is not the essential domain for localizing E-Syt2 and E-Syt3 into close proximity to the plasma membrane.

4.3.3 Plasma membrane targeting of E-Syt2 and E-Syt3 is mediated by its C-terminal C₂ domain.

We next investigated which sequence domain is responsible for targeting E-Syt2 and E-Syt3 to the plasma membrane even in the absence of TMR. We generated E-Syt2 deletion constructs that contained an N-terminal myc epitope and analyzed localization of the proteins by transfecting these vectors into HEK293 cells. We found that the plasma membrane localization of E-Syt2 can be completely abolished by deleting its C₂C domain. In contrast, partial or complete deletion of the TMR, X domain, and/or the C₂A domain had no effect on the plasma membrane localization of E-Syt2.

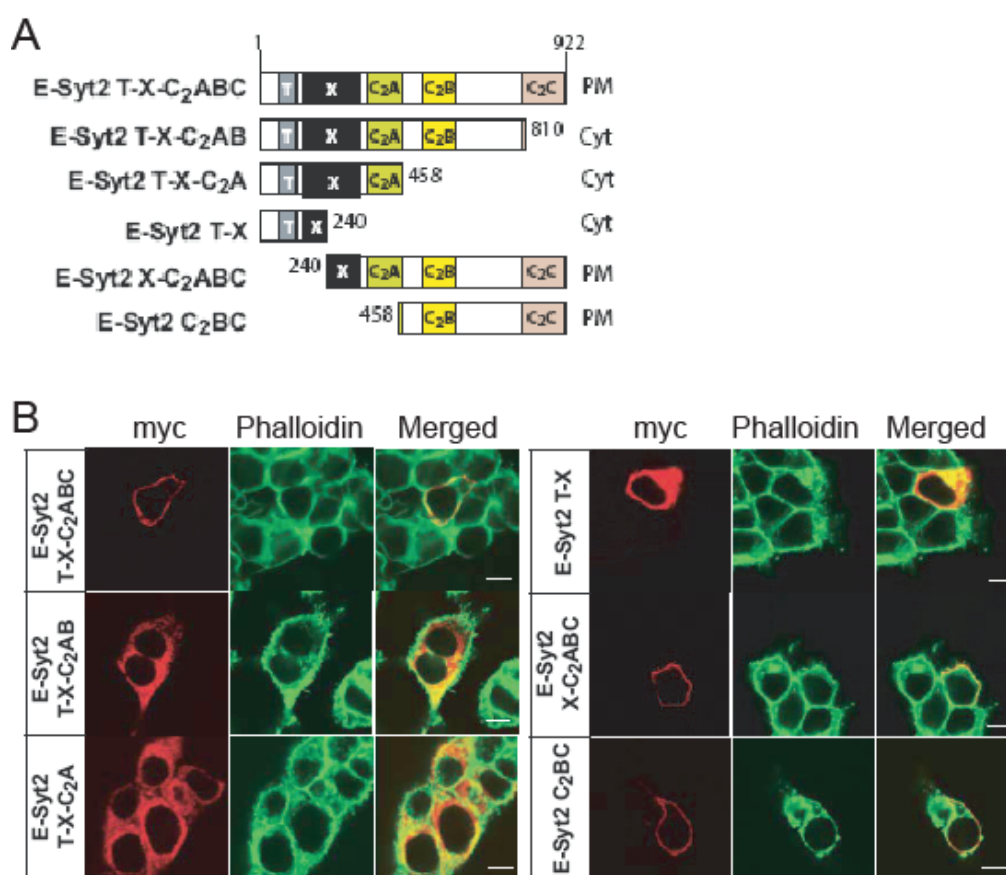


Figure 4-4 Transmembrane Region of E-Syt2 does not mediate plasma membrane targeting. (Data by Sang-Won Min)

(A) Schematic diagram of the E-Syt2 deletion constructs and summary of their subcellular localization in

transfected HEK293 cells (on right; PM, plasma membrane; Cyt, cytoplasmic). Numbers display residue numbers at the N and C termini of the various fragments. (B) Confocal images of HEK 293 cells transfected with various constructs as indicated on the left, permeabilized, and stained with myc antibodies (red) and fluorescent phalloidin (green); merged images are depicted on the right (yellow indicates red/green overlap). (Scale bar, 5 μm .) (S. W. Min et al., 2007)

To test whether the C₂C domain of E-Syt2 is sufficient for its plasma membrane localization and whether the C-terminal C₂ domains of other E-Syts shares the same property, we examined the localization of isolated C-terminal C₂ domains in transfected HEK293 cells. C₂C domains of both E-Syt2 and E-Syt3 were localized to the plasma membrane, while the E-Syt1 C₂E domain was not, upon which their localizations reflect the localization of the full-length proteins. It is interesting that although C-terminal domains of E-Syt1, E-Syt2, and E-Syt3 are highly homologous to each other, only C₂C domains of E-Syt2 and E-Syt3 contain targeting information that is sufficient to direct them to the intracellular surface of plasma membrane.

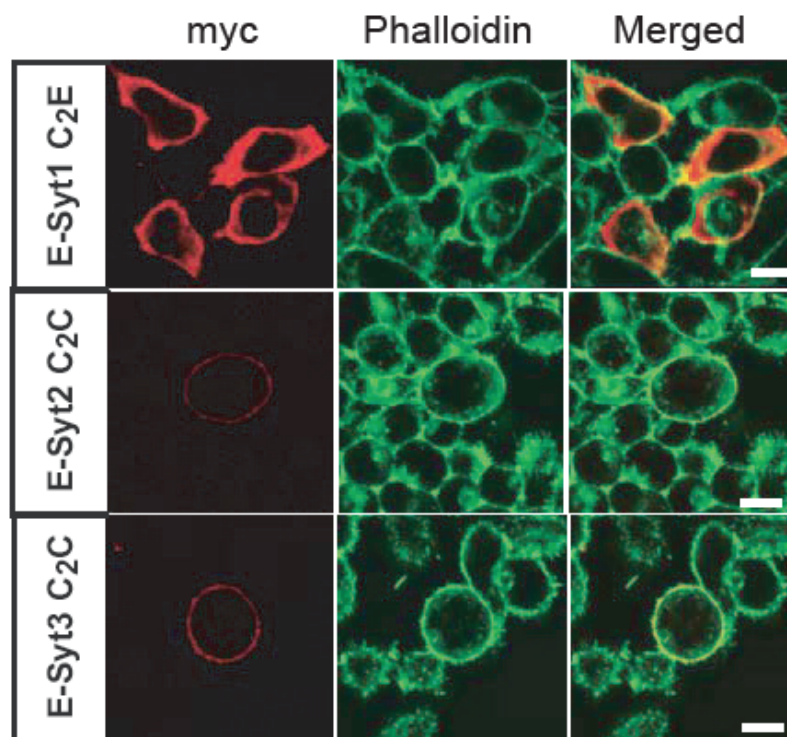


Figure 4-5 The C-terminal C₂ domain of E-Syt2 and E-Syt3 but not E-Syt1 direct plasma membrane

localization. (Data by Sang-Won Min)

Confocal images of HEK293 cell transfected with myc-tagged C-terminal C₂ domains of E-Syt1, E-Syt2, and E-Syt3, permeabilized, and stained with myc antibodies (red) and fluorescent phalloidin (green); merged images are depicted on the right (yellow indicates red/green overlap). (Scale bar, 5 μ m.) (S. W. Min et al., 2007)

Further biochemical study using E-Syt C₂BC domain fragment was conducted to unravel potential mechanisms underlying membrane targeting property of the C₂C domain, which reveals that E-SytC₂BC is detergent insoluble, and thus excludes the possibility that C₂C domain binds to phospholipids and anchors the protein to plasma membrane. Moreover, disrupting the actin cytoskeleton with latrunculin or the microtubule cytoskeleton with nocodazole does not alter the plasma membrane localization. Thus, the domain fragment of E-Syt2 is also not anchored to the plasma membrane by the cortical skeleton.

4.4 Discussion

In our study, we describe a family of membrane proteins with multiple C₂ domains and a TMR, referred as E-Syts. Together with E-Syts, four families of evolutionarily conserved Ca²⁺-binding membrane proteins have been defined: synaptotagmins, ferlins, MCTPs, and E-Syts (M. S. Perin et al., 1990; D. Bansal and K. P. Campbell, 2004; O. H. Shin et al., 2005). One common feature for these proteins is that they all include a single TMR and multiple C₂ domains. Additionally, E-Syts share other properties with synaptotagmins, ferlins, and MCTPs: as some synaptotagmins and ferlins isoforms, two of three E-Syt isoforms are localized to the plasma membrane, and all three isoforms of E-Syt are ubiquitously expressed with enrichment in brain. However, E-Syts and synaptotagmins have an N-terminal TMR, whereas ferlins and MCTPs contain a

C-terminal TMR. Further, examination of E-Syts in this study has demonstrated at least three main properties of E-Syts that are distinct from other protein families with multiple C₂ domains: First, E-Syts are the only proteins out of four families that have evolutionarily conserved homolog in yeast, where they are related to tricalbins, although in tricalbins, none of C₂ domains have Ca²⁺-binding motif, making it highly unlikely for Ca²⁺-binding. Second, the C₂A domain of E-Syt2 appears to mediate Ca²⁺-dependent phospholipid binding, however, the binding properties are unusual. The phospholipid binding specificity of E-Syt2 does not require negatively charged phospholipids, but also works with neutral phospholipids. In addition, the C₂A domain does not display efficient Ca²⁺-dependent phospholipid binding unless expressed in juxtaposition with either the X domain or the C₂B domain. Finally, our characterization of E-Syts suggests that they are Ca²⁺-regulated membrane proteins, but their physiological roles remain unclear at this point. E-Syts seem to have an important role since they are evolutionarily conserved and their yeast homolog is essential for survival (C. E. Creutz et al., 2004). Besides, the distinct localization of E-Syt1, E-Syt2, and E-Syt3, as well as the differences in their domain structure imply divergent functions for the three isoforms. However, further genetic and cell-biological studies will be needed to determine functions of E-Syts.

One of interesting observations we made in this study is the unexpected membrane targeting function of C₂C domains of E-Syt2 and E-Syt3. E-Syt1 was shown to localize to intracellular membranes, whereas E-Syt2 and E-Syt3 were localized to the plasma membrane. Nevertheless, the intracellular vesicular localization of E-Syt1, and the plasma membrane localization of E-Syt2 and E-Syt3 are independent of their TMRs, yet the C₂C domains were shown to be sufficient to deposit them into plasma membrane.

The facts that the E-Syt2 C₂BC domain fragment is detergent-insoluble and thus not phospholipids-bound, and that drugs disrupting either the action or the microtubule cytoskeleton did not change the plasma membrane localization or insolubility of E-Syt2 C₂BC, suggesting that the C-terminal C₂C domains might bind to and anchored to plasma membrane by some unidentified membrane components.

BIBLIOGRAPHY

- Antonin W, Fasshauer D, Becker S, Jahn R, Schneider TR (2002) Crystal structure of the endosomal SNARE complex reveals common structural principles of all SNAREs. *Nat Struct Biol* 9:107-111.
- Arac D, Murphy T, Rizo J (2003) Facile detection of protein-protein interactions by one-dimensional NMR spectroscopy. *Biochemistry* 42:2774-2780.
- Atluri PP, Regehr WG (1998) Delayed release of neurotransmitter from cerebellar granule cells. *J Neurosci* 18:8214-8227.
- Atwell S, Ultsch M, De Vos AM, Wells JA (1997) Structural plasticity in a remodeled protein-protein interface. *Science* 278:1125-1128.
- Bajjalieh SM, Peterson K, Shinghal R, Scheller RH (1992) SV2, a brain synaptic vesicle protein homologous to bacterial transporters. *Science* 257:1271-1273.
- Bajjalieh SM, Peterson K, Linial M, Scheller RH (1993) Brain contains two forms of synaptic vesicle protein 2. *Proc Natl Acad Sci U S A* 90:2150-2154.
- Bajjalieh SM, Frantz GD, Weimann JM, McConnell SK, Scheller RH (1994) Differential expression of synaptic vesicle protein 2 (SV2) isoforms. *J Neurosci* 14:5223-5235.
- Bansal D, Campbell KP (2004) Dysferlin and the plasma membrane repair in muscular dystrophy. *Trends Cell Biol* 14:206-213.
- Barrett EF, Stevens CF (1972) The kinetics of transmitter release at the frog neuromuscular junction. *J Physiol* 227:691-708.
- Benfenati F, Greengard P, Brunner J, Bahler M (1989) Electrostatic and hydrophobic interactions of synapsin I and synapsin I fragments with phospholipid bilayers. *J Cell Biol* 108:1851-1862.
- Betz A, Okamoto M, Benseler F, Brose N (1997) Direct interaction of the rat unc-13 homologue Munc13-1 with the N terminus of syntaxin. *J Biol Chem* 272:2520-2526.

- Biederer T, Sudhof TC (2000) Mints as adaptors. Direct binding to neuexins and recruitment of munc18. *J Biol Chem* 275:39803-39806.
- Bracher A, Weissenhorn W (2002) Structural basis for the Golgi membrane recruitment of Sly1p by Sed5p. *EMBO J* 21:6114-6124.
- Brenner S (1974) The genetics of *Caenorhabditis elegans*. *Genetics* 77:71-94.
- Buckley K, Kelly RB (1985) Identification of a transmembrane glycoprotein specific for secretory vesicles of neural and endocrine cells. *J Cell Biol* 100:1284-1294.
- Carpp LN, Ciufo LF, Shanks SG, Boyd A, Bryant NJ (2006) The Sec1p/Munc18 protein Vps45p binds its cognate SNARE proteins via two distinct modes. *J Cell Biol* 173:927-936.
- Carr CM, Grote E, Munson M, Hughson FM, Novick PJ (1999) Sec1p binds to SNARE complexes and concentrates at sites of secretion. *J Cell Biol* 146:333-344.
- Chapman ER, Jahn R (1994) Calcium-dependent interaction of the cytoplasmic region of synaptotagmin with membranes. Autonomous function of a single C2-homologous domain. *J Biol Chem* 269:5735-5741.
- Chen X, Tomchick DR, Kovrigin E, Arac D, Machius M, Sudhof TC, Rizo J (2002) Three-dimensional structure of the complexin/SNARE complex. *Neuron* 33:397-409.
- Ciufo LF, Barclay JW, Burgoyne RD, Morgan A (2005) Munc18-1 regulates early and late stages of exocytosis via syntaxin-independent protein interactions. *Mol Biol Cell* 16:470-482.
- Collins KM, Thorngren NL, Fratti RA, Wickner WT (2005) Sec17p and HOPS, in distinct SNARE complexes, mediate SNARE complex disruption or assembly for fusion. *EMBO J* 24:1775-1786.
- Connell E, Darios F, Broersen K, Gatsby N, Peak-Chew SY, Rickman C, Davletov B (2007) Mechanism of arachidonic acid action on syntaxin-Munc18. *EMBO Rep* 8:414-419.
- Connors BW, Long MA (2004) Electrical synapses in the mammalian brain. *Annu Rev Neurosci* 27:393-418.
- Coppola T, Frantz C, Perret-Menoud V, Gattesco S, Hirling H, Regazzi R (2002)

- Pancreatic beta-cell protein granuphilin binds Rab3 and Munc-18 and controls exocytosis. *Mol Biol Cell* 13:1906-1915.
- Coussens L, Parker PJ, Rhee L, Yang-Feng TL, Chen E, Waterfield MD, Francke U, Ullrich A (1986) Multiple, distinct forms of bovine and human protein kinase C suggest diversity in cellular signaling pathways. *Science* 233:859-866.
- Creutz CE, Snyder SL, Schulz TA (2004) Characterization of the yeast tricalbins: membrane-bound multi-C2-domain proteins that form complexes involved in membrane trafficking. *Cell Mol Life Sci* 61:1208-1220.
- Crowder KM, Gunther JM, Jones TA, Hale BD, Zhang HZ, Peterson MR, Scheller RH, Chavkin C, Bajjalieh SM (1999) Abnormal neurotransmission in mice lacking synaptic vesicle protein 2A (SV2A). *Proc Natl Acad Sci U S A* 96:15268-15273.
- Custer KL, Austin NS, Sullivan JM, Bajjalieh SM (2006) Synaptic vesicle protein 2 enhances release probability at quiescent synapses. *J Neurosci* 26:1303-1313.
- Dai H, Shin OH, Machius M, Tomchick DR, Sudhof TC, Rizo J (2004) Structural basis for the evolutionary inactivation of Ca²⁺ binding to synaptotagmin 4. *Nat Struct Mol Biol* 11:844-849.
- Dai H, Tomchick DR, Garcia J, Sudhof TC, Machius M, Rizo J (2005) Crystal structure of the RIM2 C2A-domain at 1.4 Å resolution. *Biochemistry* 44:13533-13542.
- Dascher C, Ossig R, Gallwitz D, Schmitt HD (1991) Identification and structure of four yeast genes (SLY) that are able to suppress the functional loss of YPT1, a member of the RAS superfamily. *Mol Cell Biol* 11:872-885.
- Davletov BA, Sudhof TC (1993) A single C2 domain from synaptotagmin I is sufficient for high affinity Ca²⁺/phospholipid binding. *J Biol Chem* 268:26386-26390.
- Deak F, Shin OH, Kavalali ET, Sudhof TC (2006) Structural determinants of synaptobrevin 2 function in synaptic vesicle fusion. *J Neurosci* 26:6668-6676.
- Denis V, Cyert MS (2005) Molecular analysis reveals localization of *Saccharomyces cerevisiae* protein kinase C to sites of polarized growth and Pkc1p targeting to the nucleus and mitotic spindle. *Eukaryot Cell* 4:36-45.
- Dong M, Yeh F, Tepp WH, Dean C, Johnson EA, Janz R, Chapman ER (2006) SV2 is the protein receptor for botulinum neurotoxin A. *Science* 312:592-596.

- Dulubova I, Khvotchev M, Liu S, Huryeva I, Sudhof TC, Rizo J (2007) Munc18-1 binds directly to the neuronal SNARE complex. *Proc Natl Acad Sci U S A* 104:2697-2702.
- Dulubova I, Sugita S, Hill S, Hosaka M, Fernandez I, Sudhof TC, Rizo J (1999) A conformational switch in syntaxin during exocytosis: role of munc18. *Embo J* 18:4372-4382.
- Dulubova I, Yamaguchi T, Gao Y, Min SW, Huryeva I, Sudhof TC, Rizo J (2002) How Tlg2p/syntaxin 16 'snares' Vps45. *EMBO J* 21:3620-3631.
- Fasshauer D, Sutton RB, Brunger AT, Jahn R (1998) Conserved structural features of the synaptic fusion complex: SNARE proteins reclassified as Q- and R-SNAREs. *Proc Natl Acad Sci U S A* 95:15781-15786.
- Feany MB, Lee S, Edwards RH, Buckley KM (1992) The synaptic vesicle protein SV2 is a novel type of transmembrane transporter. *Cell* 70:861-867.
- Fernandez-Chacon R, Konigstorfer A, Gerber SH, Garcia J, Matos MF, Stevens CF, Brose N, Rizo J, Rosenmund C, Sudhof TC (2001) Synaptotagmin I functions as a calcium regulator of release probability. *Nature* 410:41-49.
- Fernandez I, Ubach J, Dulubova I, Zhang X, Sudhof TC, Rizo J (1998) Three-dimensional structure of an evolutionarily conserved N-terminal domain of syntaxin 1A. *Cell* 94:841-849.
- Fernandez I, Arac D, Ubach J, Gerber SH, Shin O, Gao Y, Anderson RG, Sudhof TC, Rizo J (2001) Three-dimensional structure of the synaptotagmin 1 C2B-domain: synaptotagmin 1 as a phospholipid binding machine. *Neuron* 32:1057-1069.
- Fiebig KM, Rice LM, Pollock E, Brunger AT (1999) Folding intermediates of SNARE complex assembly. *Nat Struct Biol* 6:117-123.
- Fukuda M, Kanno E, Saegusa C, Ogata Y, Kuroda TS (2002) Slp4-a/granophilin-a regulates dense-core vesicle exocytosis in PC12 cells. *J Biol Chem* 277:39673-39678.
- Geppert M, Goda Y, Hammer RE, Li C, Rosahl TW, Stevens CF, Sudhof TC (1994) Synaptotagmin I: a major Ca²⁺ sensor for transmitter release at a central synapse. *Cell* 79:717-727.
- Gerber SH, Sudhof TC (2002) Molecular determinants of regulated exocytosis. *Diabetes*

51 Suppl 1:S3-11.

- Gingrich JA, Andersen PH, Tiberi M, el Mestikawy S, Jorgensen PN, Fremeau RT, Jr., Caron MG (1992) Identification, characterization, and molecular cloning of a novel transporter-like protein localized to the central nervous system. *FEBS Lett* 312:115-122.
- Giorgione JR, Lin JH, McCammon JA, Newton AC (2006) Increased membrane affinity of the C1 domain of protein kinase Cdelta compensates for the lack of involvement of its C2 domain in membrane recruitment. *J Biol Chem* 281:1660-1669.
- Goda Y, Stevens CF (1994) Two components of transmitter release at a central synapse. *Proc Natl Acad Sci U S A* 91:12942-12946.
- Grote E, Carr CM, Novick PJ (2000) Ordering the final events in yeast exocytosis. *J Cell Biol* 151:439-452.
- Hanson PI, Roth R, Morisaki H, Jahn R, Heuser JE (1997) Structure and conformational changes in NSF and its membrane receptor complexes visualized by quick-freeze/deep-etch electron microscopy. *Cell* 90:523-535.
- Harrison SD, Broadie K, van de Goor J, Rubin GM (1994) Mutations in the *Drosophila* Rop gene suggest a function in general secretion and synaptic transmission. *Neuron* 13:555-566.
- Hata Y, Slaughter CA, Sudhof TC (1993) Synaptic vesicle fusion complex contains unc-18 homologue bound to syntaxin. *Nature* 366:347-351.
- Heinemann C, Chow RH, Neher E, Zucker RS (1994) Kinetics of the secretory response in bovine chromaffin cells following flash photolysis of caged Ca²⁺. *Biophys J* 67:2546-2557.
- Hosono R, Hekimi S, Kamiya Y, Sassa T, Murakami S, Nishiwaki K, Miwa J, Taketo A, Kodaira KI (1992) The unc-18 gene encodes a novel protein affecting the kinetics of acetylcholine metabolism in the nematode *Caenorhabditis elegans*. *J Neurochem* 58:1517-1525.
- Hu SH, Latham CF, Gee CL, James DE, Martin JL (2007) Structure of the Munc18c/Syntaxin4 N-peptide complex defines universal features of the N-peptide binding mode of Sec1/Munc18 proteins. *Proc Natl Acad Sci U S A* 104:8773-8778.

- Jahn R, Südhof TC (1993) Synaptic vesicle traffic: rush hour in the nerve terminal. *J Neurochem* 61:12-21.
- Jahn R, Südhof TC (1999) Membrane fusion and exocytosis. *Annu Rev Biochem* 68:863-911.
- Jahn R, Scheller RH (2006) SNAREs--engines for membrane fusion. *Nat Rev Mol Cell Biol* 7:631-643.
- Jahn R, Lang T, Südhof TC (2003) Membrane fusion. *Cell* 112:519-533.
- Janz R, Südhof TC (1999) SV2C is a synaptic vesicle protein with an unusually restricted localization: anatomy of a synaptic vesicle protein family. *Neuroscience* 94:1279-1290.
- Janz R, Hofmann K, Südhof TC (1998) SVOP, an evolutionarily conserved synaptic vesicle protein, suggests novel transport functions of synaptic vesicles. *J Neurosci* 18:9269-9281.
- Janz R, Goda Y, Geppert M, Missler M, Südhof TC (1999) SV2A and SV2B function as redundant Ca²⁺ regulators in neurotransmitter release. *Neuron* 24:1003-1016.
- Kandel ER, Schwartz. J.H., and Jessell, T.M. (2000) *Principle of Neural Science*, 4th Edition.
- Katz B, Miledi R (1967a) The timing of calcium action during neuromuscular transmission. *J Physiol* 189:535-544.
- Katz B, Miledi R (1967b) A study of synaptic transmission in the absence of nerve impulses. *J Physiol* 192:407-436.
- Katz B, Miledi R (1967c) Ionic requirements of synaptic transmitter release. *Nature* 215:651.
- Khvotchev M, Dulubova I, Sun J, Dai H, Rizo J, Südhof TC (2007) Dual modes of Munc18-1/SNARE interactions are coupled by functionally critical binding to syntaxin-1 N terminus. *J Neurosci* 27:12147-12155.
- Laemmli UK (1970) Cleavage of structural proteins during the assembly of the head of bacteriophage T4. *Nature* 227:680-685.

- Latham CF, Osborne SL, Cryle MJ, Meunier FA (2007) Arachidonic acid potentiates exocytosis and allows neuronal SNARE complex to interact with Munc18a. *J Neurochem* 100:1543-1554.
- Lazzell DR, Belizaire R, Thakur P, Sherry DM, Janz R (2004) SV2B regulates synaptotagmin 1 by direct interaction. *J Biol Chem* 279:52124-52131.
- Lee HY, Park JB, Jang IH, Chae YC, Kim JH, Kim IS, Suh PG, Ryu SH (2004) Munc-18-1 inhibits phospholipase D activity by direct interaction in an epidermal growth factor-reversible manner. *J Biol Chem* 279:16339-16348.
- Lee JO, Yang H, Georgescu MM, Di Cristofano A, Maehama T, Shi Y, Dixon JE, Pandolfi P, Pavletich NP (1999) Crystal structure of the PTEN tumor suppressor: implications for its phosphoinositide phosphatase activity and membrane association. *Cell* 99:323-334.
- Lu J, Machius M, Dulubova I, Dai H, Sudhof TC, Tomchick DR, Rizo J (2006) Structural basis for a Munc13-1 homodimer to Munc13-1/RIM heterodimer switch. *PLoS Biol* 4:e192.
- Lynch BA, Lambeng N, Nocka K, Kensel-Hammes P, Bajjalieh SM, Matagne A, Fuks B (2004) The synaptic vesicle protein SV2A is the binding site for the antiepileptic drug levetiracetam. *Proc Natl Acad Sci U S A* 101:9861-9866.
- Mahrhold S, Rummel A, Bigalke H, Davletov B, Binz T (2006) The synaptic vesicle protein 2C mediates the uptake of botulinum neurotoxin A into phrenic nerves. *FEBS Lett* 580:2011-2014.
- Maximov A, Sudhof TC (2005) Autonomous function of synaptotagmin 1 in triggering synchronous release independent of asynchronous release. *Neuron* 48:547-554.
- Maximov A, Pang ZP, Tervo DG, Sudhof TC (2007) Monitoring synaptic transmission in primary neuronal cultures using local extracellular stimulation. *J Neurosci Methods* 161:75-87.
- McNew JA, Parlati F, Fukuda R, Johnston RJ, Paz K, Paumet F, Sollner TH, Rothman JE (2000) Compartmental specificity of cellular membrane fusion encoded in SNARE proteins. *Nature* 407:153-159.
- Meinrenken CJ, Borst JG, Sakmann B (2003) Local routes revisited: the space and time dependence of the Ca²⁺ signal for phasic transmitter release at the rat calyx of Held. *J Physiol* 547:665-689.

- Min SW, Chang WP, Sudhof TC (2007) E-Syts, a family of membranous Ca²⁺-sensor proteins with multiple C2 domains. *Proc Natl Acad Sci U S A* 104:3823-3828.
- Misura KM, Scheller RH, Weis WI (2000) Three-dimensional structure of the neuronal-Sec1-syntaxin 1a complex. *Nature* 404:355-362.
- Morris NJ, Ross SA, Neveu JM, Lane WS, Lienhard GE (1999) Cloning and preliminary characterization of a 121 kDa protein with multiple predicted C2 domains. *Biochim Biophys Acta* 1431:525-530.
- Murthy VN, Stevens CF (1999) Reversal of synaptic vesicle docking at central synapses. *Nat Neurosci* 2:503-507.
- Nicholson KL, Munson M, Miller RB, Filip TJ, Fairman R, Hughson FM (1998) Regulation of SNARE complex assembly by an N-terminal domain of the t-SNARE Sso1p. *Nat Struct Biol* 5:793-802.
- Novick P, Schekman R (1979) Secretion and cell-surface growth are blocked in a temperature-sensitive mutant of *Saccharomyces cerevisiae*. *Proc Natl Acad Sci U S A* 76:1858-1862.
- Novick P, Field C, Schekman R (1980) Identification of 23 complementation groups required for post-translational events in the yeast secretory pathway. *Cell* 21:205-215.
- Okamoto M, Sudhof TC (1997) Mints, Munc18-interacting proteins in synaptic vesicle exocytosis. *J Biol Chem* 272:31459-31464.
- Oyler GA, Higgins GA, Hart RA, Battenberg E, Billingsley M, Bloom FE, Wilson MC (1989) The identification of a novel synaptosomal-associated protein, SNAP-25, differentially expressed by neuronal subpopulations. *J Cell Biol* 109:3039-3052.
- Pang ZP, Shin OH, Meyer AC, Rosenmund C, Sudhof TC (2006) A gain-of-function mutation in synaptotagmin-1 reveals a critical role of Ca²⁺-dependent soluble N-ethylmaleimide-sensitive factor attachment protein receptor complex binding in synaptic exocytosis. *J Neurosci* 26:12556-12565.
- Parlati F, Varlamov O, Paz K, McNew JA, Hurtado D, Sollner TH, Rothman JE (2002) Distinct SNARE complexes mediating membrane fusion in Golgi transport based on combinatorial specificity. *Proc Natl Acad Sci U S A* 99:5424-5429.
- Paumet F, Brugger B, Parlati F, McNew JA, Sollner TH, Rothman JE (2001) A t-SNARE

- of the endocytic pathway must be activated for fusion. *J Cell Biol* 155:961-968.
- Peng R, Gallwitz D (2002) Sly1 protein bound to Golgi syntaxin Sed5p allows assembly and contributes to specificity of SNARE fusion complexes. *J Cell Biol* 157:645-655.
- Perin MS, Fried VA, Mignery GA, Jahn R, Südhof TC (1990) Phospholipid binding by a synaptic vesicle protein homologous to the regulatory region of protein kinase C. *Nature* 345:260-263.
- Pyle RA, Schivell AE, Hidaka H, Bajjalieh SM (2000) Phosphorylation of synaptic vesicle protein 2 modulates binding to synaptotagmin. *J Biol Chem* 275:17195-17200.
- Ramón y Cajal S (1937) *Recuerdos de mi Vida*. Cambridge.
- Reigada D, Diez-Perez I, Gorostiza P, Verdaguer A, Gomez de Aranda I, Pineda O, Vilarrasa J, Marsal J, Blasi J, Aleu J, Solsona C (2003) Control of neurotransmitter release by an internal gel matrix in synaptic vesicles. *Proc Natl Acad Sci U S A* 100:3485-3490.
- Richards DA, Guatimosim C, Rizzoli SO, Betz WJ (2003) Synaptic vesicle pools at the frog neuromuscular junction. *Neuron* 39:529-541.
- Rickman C, Medine CN, Bergmann A, Duncan RR (2007) Functionally and spatially distinct modes of munc18-syntaxin 1 interaction. *J Biol Chem* 282:12097-12103.
- Rizo J, Südhof TC (1998) C2-domains, structure and function of a universal Ca²⁺-binding domain. *J Biol Chem* 273:15879-15882.
- Rizo J, Südhof TC (2002) Snares and Munc18 in synaptic vesicle fusion. *Nat Rev Neurosci* 3:641-653.
- Rizo J, Chen X, Arac D (2006) Unraveling the mechanisms of synaptotagmin and SNARE function in neurotransmitter release. *Trends Cell Biol* 16:339-350.
- Rosenmund C, Stevens CF (1996) Definition of the readily releasable pool of vesicles at hippocampal synapses. *Neuron* 16:1197-1207.
- Rosenmund C, Stevens CF (1997) The rate of aldehyde fixation of the exocytotic machinery in cultured hippocampal synapses. *J Neurosci Methods* 76:1-5.

- Südhof TC (2000) The synaptic vesicle cycle revisited. *Neuron* 28:317-320.
- Südhof TC (2002) Synaptotagmins: why so many? *J Biol Chem* 277:7629-7632.
- Südhof TC (2004) The synaptic vesicle cycle. *Annu Rev Neurosci* 27:509-547.
- Südhof TC, Baumert M, Perin MS, Jahn R (1989) A synaptic vesicle membrane protein is conserved from mammals to *Drosophila*. *Neuron* 2:1475-1481.
- Südhof TC, and Scheller, R.H. (2000) Mechanism and Regulation of Neurotransmitter Release. In: *Synapse*. Baltimore: The John Hopkins University Press.
- Sabatini BL, Regehr WG (1996) Timing of neurotransmission at fast synapses in the mammalian brain. *Nature* 384:170-172.
- Sassa T, Harada S, Ogawa H, Rand JB, Maruyama IN, Hosono R (1999) Regulation of the UNC-18-Caenorhabditis elegans syntaxin complex by UNC-13. *J Neurosci* 19:4772-4777.
- Satzler K, Sohl LF, Bollmann JH, Borst JG, Frotscher M, Sakmann B, Lubke JH (2002) Three-dimensional reconstruction of a calyx of Held and its postsynaptic principal neuron in the medial nucleus of the trapezoid body. *J Neurosci* 22:10567-10579.
- Schikorski T, Stevens CF (2001) Morphological correlates of functionally defined synaptic vesicle populations. *Nat Neurosci* 4:391-395.
- Schivell AE, Batchelor RH, Bajjalieh SM (1996) Isoform-specific, calcium-regulated interaction of the synaptic vesicle proteins SV2 and synaptotagmin. *J Biol Chem* 271:27770-27775.
- Schivell AE, Mochida S, Kensel-Hammes P, Custer KL, Bajjalieh SM (2005) SV2A and SV2C contain a unique synaptotagmin-binding site. *Mol Cell Neurosci* 29:56-64.
- Schneggenburger R, Meyer AC, Neher E (1999) Released fraction and total size of a pool of immediately available transmitter quanta at a calyx synapse. *Neuron* 23:399-409.
- Scranton TW, Iwata M, Carlson SS (1993) The SV2 protein of synaptic vesicles is a keratan sulfate proteoglycan. *J Neurochem* 61:29-44.
- Shen J, Tareste DC, Paumet F, Rothman JE, Melia TJ (2007) Selective activation of

- cognate SNAREpins by Sec1/Munc18 proteins. *Cell* 128:183-195.
- Shin OH, Rizo J, Sudhof TC (2002) Synaptotagmin function in dense core vesicle exocytosis studied in cracked PC12 cells. *Nat Neurosci* 5:649-656.
- Shin OH, Han W, Wang Y, Sudhof TC (2005) Evolutionarily conserved multiple C2 domain proteins with two transmembrane regions (MCTPs) and unusual Ca²⁺ binding properties. *J Biol Chem* 280:1641-1651.
- Sollner T, Bennett MK, Whiteheart SW, Scheller RH, Rothman JE (1993) A protein assembly-disassembly pathway in vitro that may correspond to sequential steps of synaptic vesicle docking, activation, and fusion. *Cell* 75:409-418.
- Stahl B, Chou JH, Li C, Sudhof TC, Jahn R (1996) Rab3 reversibly recruits rabphilin to synaptic vesicles by a mechanism analogous to raf recruitment by ras. *EMBO J* 15:1799-1809.
- Stevens CF, Tsujimoto T (1995) Estimates for the pool size of releasable quanta at a single central synapse and for the time required to refill the pool. *Proc Natl Acad Sci U S A* 92:846-849.
- Stroupe C, Collins KM, Fratti RA, Wickner W (2006) Purification of active HOPS complex reveals its affinities for phosphoinositides and the SNARE Vam7p. *EMBO J* 25:1579-1589.
- Sun J, Pang ZP, Qin D, Fahim AT, Adachi R, Sudhof TC (2007) A dual-Ca²⁺-sensor model for neurotransmitter release in a central synapse. *Nature* 450:676-682.
- Sutton RB, Fasshauer D, Jahn R, Brunger AT (1998) Crystal structure of a SNARE complex involved in synaptic exocytosis at 2.4 Å resolution. *Nature* 395:347-353.
- Sutton RB, Davletov BA, Berghuis AM, Sudhof TC, Sprang SR (1995) Structure of the first C2 domain of synaptotagmin I: a novel Ca²⁺/phospholipid-binding fold. *Cell* 80:929-938.
- Tang J, Maximov A, Shin OH, Dai H, Rizo J, Sudhof TC (2006) A complexin/synaptotagmin 1 switch controls fast synaptic vesicle exocytosis. *Cell* 126:1175-1187.
- Toonen RF, Verhage M (2007) Munc18-1 in secretion: lonely Munc joins SNARE team and takes control. *Trends Neurosci* 30:564-572.

- Trimble WS, Cowan DM, Scheller RH (1988) VAMP-1: a synaptic vesicle-associated integral membrane protein. *Proc Natl Acad Sci U S A* 85:4538-4542.
- Tsuboi T, Fukuda M (2006) The Slp4-a linker domain controls exocytosis through interaction with Munc18-1.syntaxin-1a complex. *Mol Biol Cell* 17:2101-2112.
- Ubach J, Zhang X, Shao X, Sudhof TC, Rizo J (1998) Ca²⁺ binding to synaptotagmin: how many Ca²⁺ ions bind to the tip of a C2-domain? *EMBO J* 17:3921-3930.
- Ubach J, Garcia J, Nittler MP, Sudhof TC, Rizo J (1999) Structure of the Janus-faced C2B domain of rabphilin. *Nat Cell Biol* 1:106-112.
- Verhage M, de Vries KJ, Roshol H, Burbach JP, Gispen WH, Sudhof TC (1997) DOC2 proteins in rat brain: complementary distribution and proposed function as vesicular adapter proteins in early stages of secretion. *Neuron* 18:453-461.
- Verhage M, Maia AS, Plomp JJ, Brussaard AB, Heeroma JH, Vermeer H, Toonen RF, Hammer RE, van den Berg TK, Missler M, Geuze HJ, Sudhof TC (2000) Synaptic assembly of the brain in the absence of neurotransmitter secretion. *Science* 287:864-869.
- Voets T, Toonen RF, Brian EC, de Wit H, Moser T, Rettig J, Sudhof TC, Neher E, Verhage M (2001) Munc18-1 promotes large dense-core vesicle docking. *Neuron* 31:581-591.
- Wang L, Seeley ES, Wickner W, Merz AJ (2002) Vacuole fusion at a ring of vertex docking sites leaves membrane fragments within the organelle. *Cell* 108:357-369.
- Weber T, Zemelman BV, McNew JA, Westermann B, Gmachl M, Parlati F, Sollner TH, Rothman JE (1998) SNAREpins: minimal machinery for membrane fusion. *Cell* 92:759-772.
- Wu MN, Fergestad T, Lloyd TE, He Y, Broadie K, Bellen HJ (1999) Syntaxin 1A interacts with multiple exocytic proteins to regulate neurotransmitter release in vivo. *Neuron* 23:593-605.
- Xu T, Bajjalieh SM (2001) SV2 modulates the size of the readily releasable pool of secretory vesicles. *Nat Cell Biol* 3:691-698.
- Yamaguchi T, Dulubova I, Min SW, Chen X, Rizo J, Sudhof TC (2002) Sly1 binds to Golgi and ER syntaxins via a conserved N-terminal peptide motif. *Dev Cell* 2:295-305.